INFORMATION TO USERS

This manuscript has been reproduced from the microfilm master. UMI films the text directly from the original or copy submitted. Thus, some thesis and dissertation copies are in typewriter face, while others may be from any type of computer printer.

The quality of this reproduction is dependent upon the quality of the copy submitted. Broken or indistinct print, colored or poor quality illustrations and photographs, print bleedthrough, substandard margins, and improper alignment can adversely affect reproduction.

In the unlikely event that the author did not send UMI a complete manuscript and there are missing pages, these will be noted. Also, if unauthorized copyright material had to be removed, a note will indicate the deletion.

Oversize materials (e.g., maps, drawings, charts) are reproduced by sectioning the original, beginning at the upper left-hand corner and continuing from left to right in equal sections with small overlaps.

ProQuest Information and Learning
300 North Zeeb Road, Ann Arbor, MI 48106-1346 USA
800-521-0600

Detection of Oligonucleotide Sequences on Diazonium Modified Silicon Substrates Through Electrical Impedance Measurements

Ann Wing Hien Mak

A Thesis

In

The Department

Of

Chemistry and Biochemistry

Presented in Partial Fulfillment of the Requirements
for the Degree of Master of Science at
Concordia University
Montreal, Quebec, Canada

August 2002

Abstract

Detection of Oligonucleotide Sequences on Diazonium Modified Silicon Substrates Through Electrical Impedance Measurements

Ann Wing Hien Mak

4-nitrobenzenediazonium modified silicon substrates were used in the detection of immobilized 20-mer homo-oligonucleotides through electrical impedance measurement. The silicon (100) and (111) substrates were functionalized with the diazonium through cyclic voltammetry and the nitro group was subsequently reduced to an amino group by cyclic voltammetry. The functionalized substrates were activated with glutaraldehyde and the oligo-20mer with an amino-linker was immobilized onto the surface. Electrical impedance shows a negative shift in the flat-band potential upon immobilization of the oligo probe layer following glutaraldehyde treatment. Upon hybridization with the complementary oligo-20mer sequence, a positive shift in the flat-band potential was observed. A comparison between the immobilized oligo$(dT)_{20}$ and that of the oligo$(dA)_{20}$ demonstrated that the use of the oligo$(dT)_{20}$ as a probe layer is better than that of the oligo$(dA)_{20}$. The results also show that the Si(100) oriented substrates performed better than the Si(111) substrates under the same conditions. Qualitative verification of the various modification steps up to glutaraldehyde treatment has been performed by X-ray photoelectron spectroscopy (XPS) and through Fourier transform infrared spectroscopy (FT-IR). Shifts in the flat-band potentials are observed following the various modification steps and these results show that the immobilization of the oligo$(dT)_{20}$ probe layer on the Si(100) substrates using a diazonium moiety is rapid and reproducible.

Acknowledgments

I would like to express my gratitude and appreciation for my supervisor, Dr. Marcus F. Lawrence for his precious guidance, encouragement and support throughout the course of this work.

I would also like to thank my research committee members, Dr. Joanne Turnbull and Dr. Cameron Skinner for their advice and helpful consultations.

To my colleagues, Dr. Christophe Marquette and Alvira Macanovic for their valuable help and insights with this project. As well as Bernard, Marika and all the other members of the Chemistry and Biochemistry faculty for their help and support and for the fond memories.

Lastly, I would like to dedicate this to my family and friends who have been supportive of my endeavors throughout the years.

Table of Contents

3. Experimental

4. Results and Discussion

List of Figures

List of Tables

List of Symbols

A	Surface area of working electrode
d	Thickness of dielectric
E_F	Fermi energy
E_G	Band-gap energy
f	Frequency
I	Current (dc)
$\tilde{I}$	Current (ac)
$\tilde{I}_i$	In-phase Current
$\tilde{I}_r$	Out-of-phase Current
T_m	Melting Temperature
V	Voltage (dc)
$\tilde{V}$	Voltage (ac)
V_{fb}	Flat-band potential
V_i	In-phase voltage
V_r	Out-of-phase voltage
Z	Impedance
Z_i	In-phase impedance
Z_r	Out-of-phase impedance
Z_{sc}	Impedance of semiconductor
Ω	Ohms
ε	Permittivity of free space

ε_o Permittivity of dielectric material

ω Angular frequency ($2\pi f$)

1. Overview

1.1 Biosensors

What makes biosensor technology so important? With the increase of AIDS, cancer, diabetes and other diseases, there has been a growing need to determine which individuals are at risk of developing health problems. For instance, the anthrax cases of recent months have demonstrated the need to develop biosensors which provide rapid results. The design of an optimal biosensor has remained one of the greatest challenges in the field of biotechnology. Traditional methods of identification involving fluorescent or radioactive labeled probes [1-4] are tedious and time consuming, which prevents real time and in-situ monitoring. Recent studies have proposed the use of biosensors, which do not require labeling.

A biosensor is composed of two elements – a biological component and a transducer. The biological components, such as enzymes, single strand DNA, or antibodies, are used as the probe layer. The transducer has two major functions - namely to provide a support for immobilization of the biological component and a means of converting the biological activity into a measurable signal, for example, an electrical one. Optical fibers [5-7], surface plasmon resonance devices [8-9], piezoelectric devices [10-12] and various types of materials such as metal or semiconductor electrodes [13-17] have been used as transducers. In order to immobilize a probe layer to the transducer, the surface usually needs to be functionalized. Self-assembled monolayer films [18-19], organosilane chemistry [20-23] and other types of chemical modifications [24-30] have been used to functionalize these surfaces. The detection of the biological activity is observed through optical, acoustic, or electrical means [31-40]. In general, the fundamental limitation with all

biosensors lies in the reproducibility of creating a well-ordered surface for the immobilization of the probe layer.

In this research, a silicon semiconductor was functionalized with a diazonium moiety for the immobilization of single stranded DNA as the probe and electrical impedance measurements were used for detection of complementary strands in a liquid media. The advantage with the impedance method is that it is rapid and easy to use as silicon semiconductor technology is well developed, their surfaces are well characterized and lend themselves well to functionalization and the substrates are cost-effective since they can be manufactured on a large scale. Also, miniaturization becomes possible to produce high-density arrays. Electrochemical modification of silicon surfaces with a diazonium moiety is proven to be more rapid compared to commonly used silane chemistry and gives more reproducible and well ordered probe layers.

1.2 Deoxyribonucleic Acid (DNA)

DNA, is the genetic material that organisms inherit from their parents. The DNA molecule varies in length and consists of thousands of genes, each occupying a specific position along a single molecule. The DNA molecule is comprised of four types of building blocks – purines, pyrimidines, furanose sugars and phosphate groups. The four nitrogenous bases that make up the nucleic acids are adenine, thymine, cytosine, and guanine (Figure 1.1). These nitrogenous bases can be classified into two groups: purines, such as adenine and guanine with two rings and pyrimidines, such as thymine and cytosine, which has one ring.

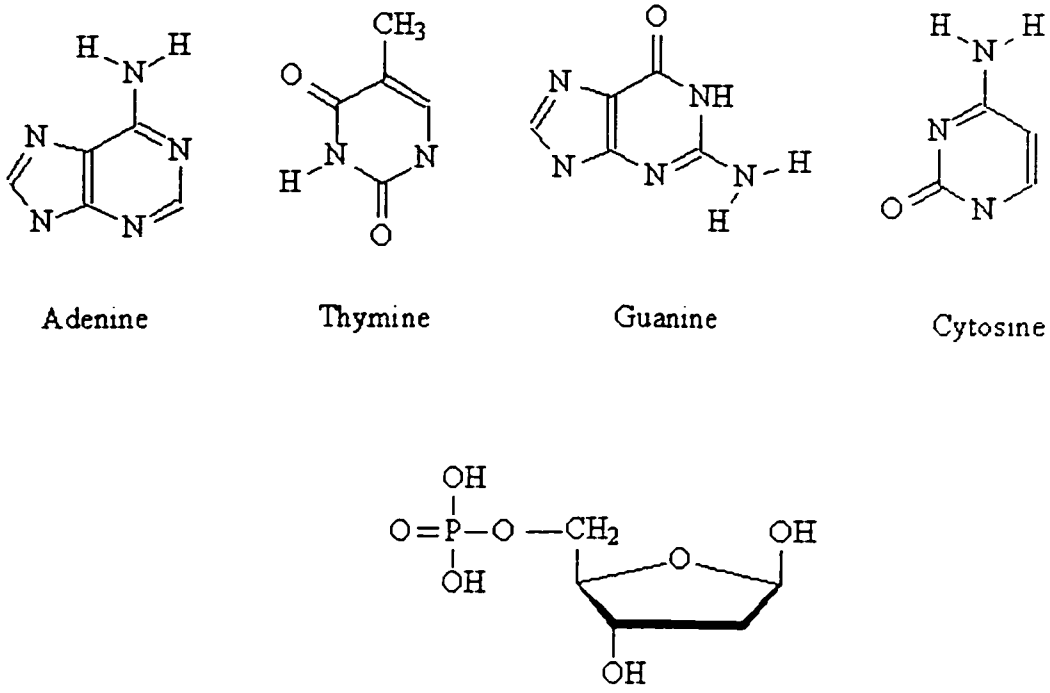

Figure 1.1 The four bases and the deoxyribose sugar with a phosphate group.

Each nucleotide is itself composed of three parts: a nitrogenous base, which is joined to a pentose (five-carbon sugar), which in turn is bonded to a phosphate group. The nucleic acids are covalently linked together through phosphodiester bonds, which links the phosphate of one nucleotide to the sugar of the next monomer. As a result, it forms an alternating sugar-phosphate backbone with the nitrogenous bases oriented towards the interior (Figure 1.2). It should be noted that the structure of the DNA has one less hydroxyl group at the 2' carbon compared to that of the RNA (ribonucleic acid) which is found in protein synthesis.[41]

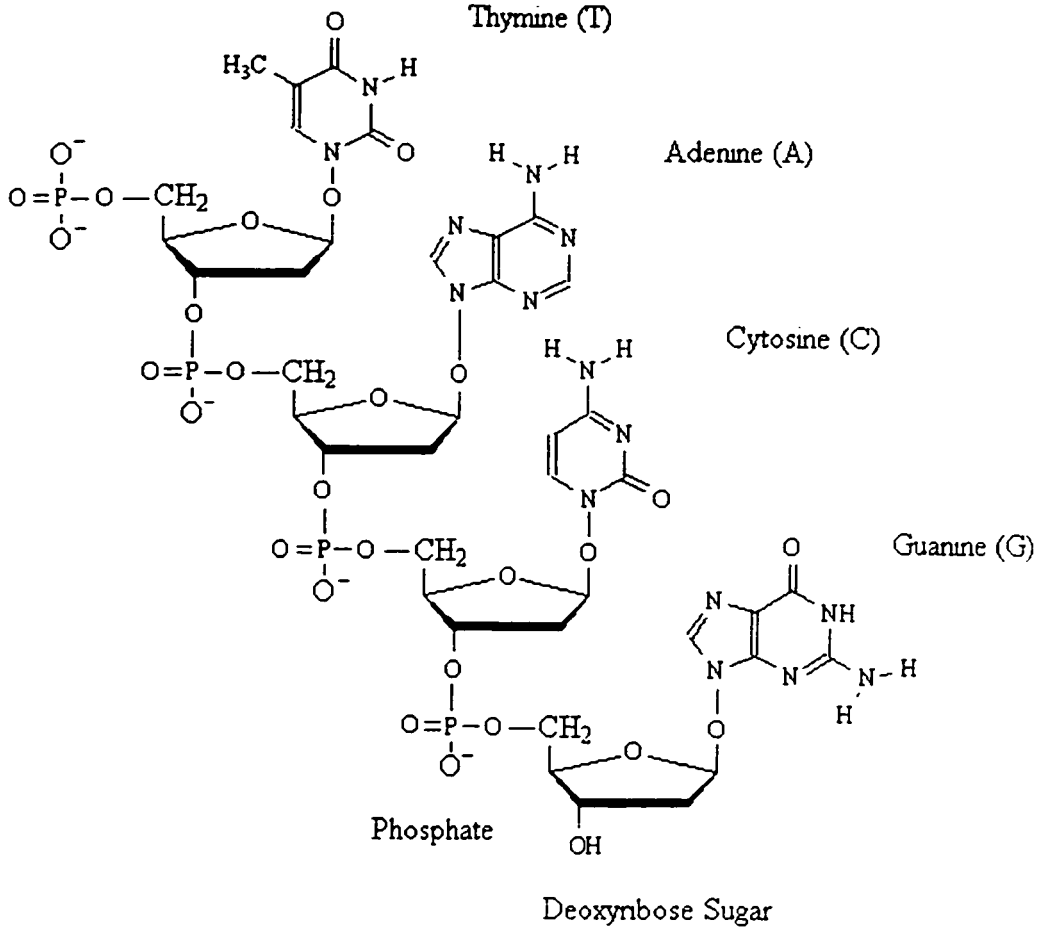

Figure 1.2 The chemical structure of the DNA strand.

The DNA's base composition is governed by Chargaff's rules (named after American biologist Erwin Chargaff), which states that the total number of purine bases is equal to the total number of pyrimidine bases; that is, A + G = T + C. Each of the purine-pyrimidine base pairs couples together to form hydrogen bonds with a specific partner: adenine with thymine forming two hydrogen bonds and cytosine with guanine forming three hydrogen bonds (Figure 1.3). [42]

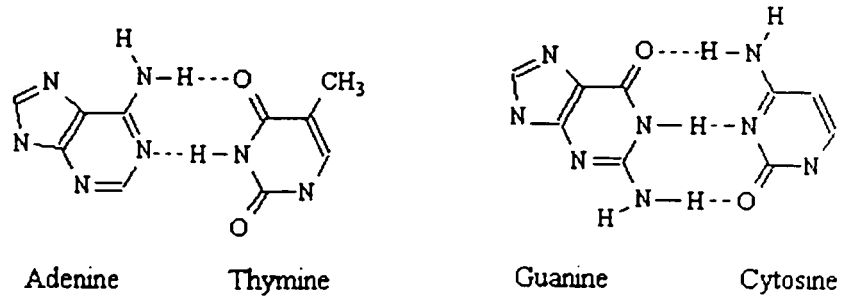

Figure 1.3 Hydrogen bonding between the base pairs: adenine with thymine and guanine with cytosine.

James Watson and Francis Crick formulated the double helical structure for the DNA molecule in 1953. Under ideal conditions, the complimentary strands bind together (hybridize) to form the DNA double helix. The two complementary strands are held together through hydrogen bonding between the base pairs located at the interior of the helix. Inside the double helix, Van der Waals interactions between the stacked base pairs gives a rise of 0.34 nm and there are ten base pairs per turn, thus giving a pitch (height) of 3.4 nm and a radius of 1 nm from the central axis (Figure 1.4). [41]

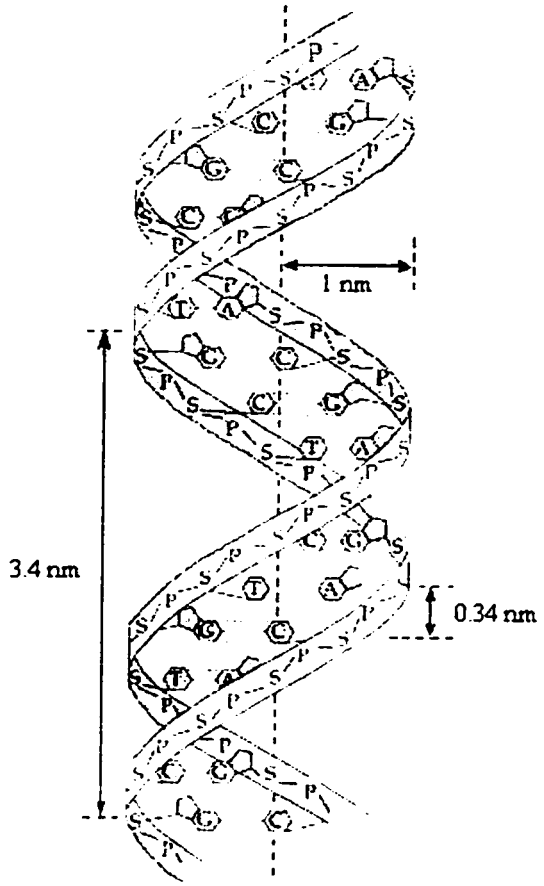

Figure 1.4 The structure of the DNA helix.

It is this specific affinity between the bases pairs which researchers use in the development of DNA biosensors. By knowing the sequence of the DNA probe, the sequence of the complementary strand (the sample DNA target) can be determined.

1.3 Previous Research

Previous research in this lab focused on the functionalization of Si/SiO_2 silicon substrates with an oxide layer that was 150Å thick. The surface was hydroxylated with sulfochromic acid and was functionalized with silanization agents such as 3-aminopropyltriethoxysilane (APTS) or 3-glycidoxypropyltrimethoxysilane (GPTS). In the APTS method, oligonucleotides with a bromine linker at the 5' end were immobilized as the probe layer onto the surface whereas the GPTS method used oligonucleotides with an amino-link for the immobilization. Of the two methods, the GPTS/amine (epoxy-amine coupling reaction) method was shown to be more effective compared to the APTS/bromine method because the APTS silanization conditions may provoke APTS polymerization in solution and adsorption on the surface rather than creating covalent bonding with the silica. Furthermore, interactions between the primary amine moiety of the APTS and the silica surface silanols may decrease the amount to oligonucleotides immobilized onto the surface. As well, the bromine on the oligonucleotide (being less accessible) prevents it from reacting easily with the amine moiety of the silane, which leads to a lack of reproducibility in the immobilization of the probe layer. [43-47]

The silanization modification steps are long and even once the surface has been silanized, the coverage may not be adequate. As a result, this leads to variations in the density for the immobilization of the probe layer. A new method proposed in this research uses a diazonium moiety instead of a silane layer, and oxide-free silicon substrates.

1.4 Scope of Research

The transducer used is a silicon semiconductor that is modified with a diazonium moiety and amino-linked homo-oligonucleotide 20mer as the probe layer. The advantage of using a silicon semiconductor is that it is a well characterized material, affordable, can be chemically modified and integrated with microelectronics, thus allowing miniaturization. Functionalization with a diazonium moiety is similar to creating an insulating layer on the semiconductor, thus forming a semiconductor/ insulator/electrolyte interface, which is monitored through impedance measurements. The modifications performed on the semiconductor surface results in changes in accumulated charge at the dielectric layer surface, causing shifts in the impedance measurements. The results will show that the diazonium approach is rapid while giving reproducible results.

2. Theory

2.1 The EIS Structure

The main feature of the detection system that allows impedance measurements to be obtained is the electrolyte/insulator/semiconductor interface (EIS). The semiconductor is the transducer which converts the biological signal into an electrical one and it also acts as the substrate onto which the chemical modifications are performed. The diazonium moiety, glutaraldehyde and the single-strand DNA probe layer that are immobilized onto its surface behave like an insulator and prevent the passage of current from the semiconductor to the electrolyte solution. The purpose of the electrolyte is to allow the passage of current (albeit an a.c. current) from the working electrode to the counter electrode within the bulk of the solution.

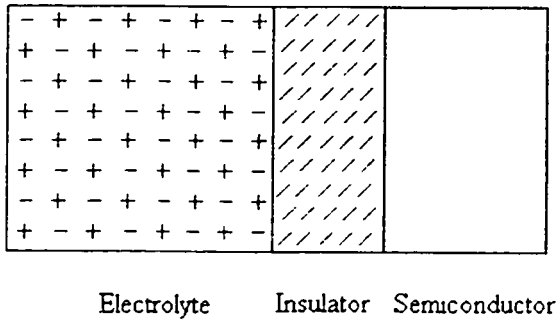

Figure 2.1 The EIS structure.

2.2 Semiconductors

A semiconductor is defined as a material with a conductivity between that of a conductor, which readily permits the passage of current through its structure, and an insulator, which prevents the passage of current. There are basically three types of semiconductors: intrinsic, n-type and p-type. Each of them are characterized by their purity and their Fermi energy (E_F) levels.

Conduction occurs when electrons in the filled valence band are excited into the empty conduction band. Upon excitation, an unoccupied vacancy (a hole) is left in the valence band. A hole is a positively charged entity that occupies the same space as an electron. The holes and excited electrons can move in response to an applied electric field and so permit the passage of current.

Figure 2.2 shows the structure of silicon as an intrinsic semiconductor with its band-gap diagram. The valence band corresponds to filled bonding orbitals and is lower in energy than that of the conduction band, which is higher in energy and corresponds to anti-bonding orbitals. The difference in energy between the valence band and the conduction band is defined as the band-gap energy. The Fermi energy, E_F, is defined as the energy level for which the probability of occupation by electrons is equal to 0.5. It corresponds to the average energy of the electrical species that are mobile, which are the electrons and holes.[42, 48]

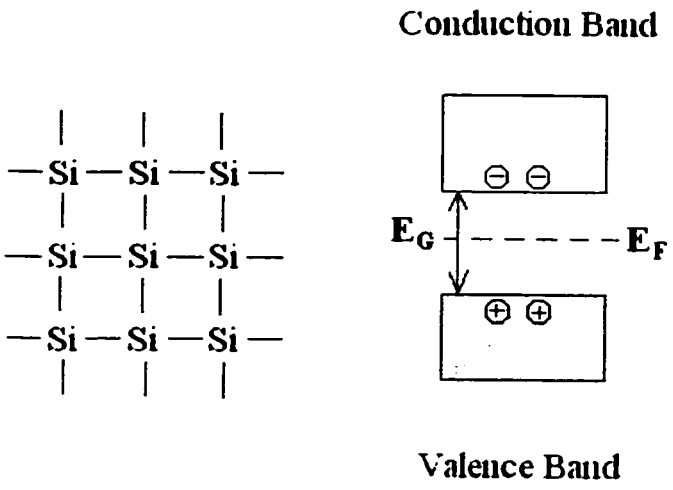

Figure 2.2 Crystal structure of an intrinsic semiconductor with the corresponding band diagram. The (-) and (+) denotes electrons and holes respectively.

With the addition of an impurity, or dopant, the conductivity of the intrinsic semiconductor can be enhanced. By introducing an atom that has one valence electron less than its host silicon lattice, such as a boron atom, a p-type (positive-type) semiconductor (Figure 2.3) is formed. For conduction to occur, a valence electron gets trapped by the boron atom. The vacancy created at that silicon atom can then be filled by an electron from a neighboring silicon atom, and so on so forth. As a result, excess holes form the majority of the charge carriers, thus lowering the Fermi energy closer to the valence band. Impurities that are electron deficient are called acceptor impurities because they accept electrons from neighboring atoms.[42]

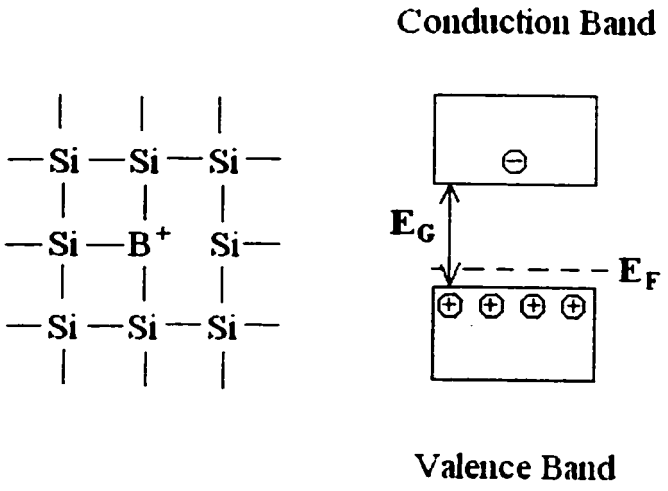

Figure 2.3 Crystal structure of a p-type semiconductor with its band diagram.

Similarly, introduction of a dopant with one valence electron more than that of its host silicon lattice, such as a phosphorous atom, will create an n-type (negative type) semiconductor (Figure 2.4). Since the phosphorous has one more valence electron than silicon, there is a weakly bound valence electron that is left over as four of them are used to form covalent bonds with valence electrons of the neighboring silicon atoms. As a result, the excess electrons form the majority of charge carriers that can easily contribute to conduction, thus raising the Fermi energy closer to the conduction band. Impurities that are electron abundant are called donor impurities because they have excess electrons which contributes to conduction. [42]

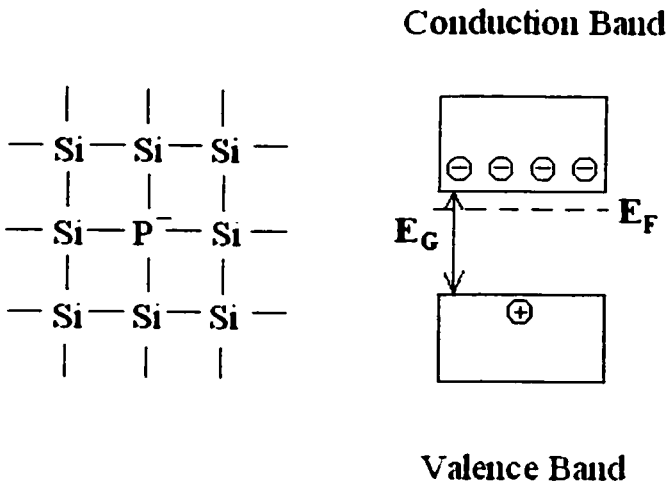

Figure 2.4 Crystal structure of an n-type semiconductor with its band diagram.

2.3 Impedance Measurements

2.3.1 What is Impedance?

In an electrical system where a direct voltage (dc voltage) is applied, the voltage (V), resistance (R) and current (I) are related by Ohm's Law

$$V = RI \qquad (1)$$

When an alternating voltage (ac voltage) is applied, each of the variables takes on a complex form and the resistance in Ohm's Law is replaced by impedance, Z, as shown below

$$\tilde{V} = Z\tilde{I} \qquad (2)$$

The (~) on the V and I denotes that we are dealing with alternating voltage and current.

The overall impedance, Z, is made up of two components: an in-phase and an out-of-phase component. Equation 2 becomes

$$\tilde{V} = (Z_r + iZ_i)\tilde{I} \qquad (3)$$

The in-phase component is denoted with an r and out-of-phase component is denoted with an i. The voltage and the current are also complex.

$$\tilde{V} = V_r + iV_i \quad \text{and} \quad \tilde{I} = I_r + iI_i \qquad (4)$$

By substituting the individual real and imaginary components into Equation 3, the real and imaginary parts of the overall impedance can be expressed as:

$$Z_r = \frac{V_r I_r + V_i I_i}{I_r^2 + I_i^2} \quad \text{and} \quad Z_i = \frac{V_i I_r - V_r I_i}{I_r^2 + I_i^2} \qquad (5)$$

The EIS structure is basically made up of three electrical components: the resistance of the electrolyte, capacitance of the insulator, and the impedance of the semiconductor.

Thus EIS structure can be represented by the following equivalent electronic circuit (Figure 2.5), where Z_{sc} is the impedance of the semiconductor, C is the capacitance of the dielectric layer and R is the resistance due to the electrolyte solution and the ohmic contacts of the electrode.

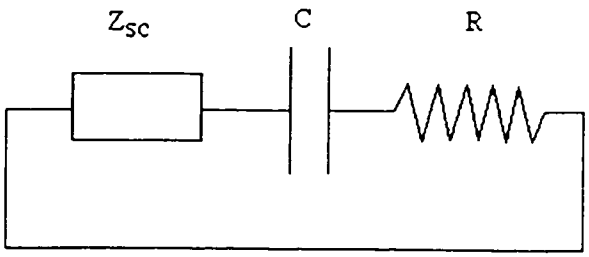

Figure 2.5 Equivalent circuit of the EIS structure.

Each modification of the semiconductor's surface changes the thickness of the dielectric layer and its dielectric constant, thus leading to changes in the capacitance

$$C = (\varepsilon_o \varepsilon A)/d \qquad (6)$$

where C is the capacitance

ε_o is the permittivity of free space

ε is the permittivity of the dielectric material

A is the surface area of the working electrode

d is the thickness of the dielectric

The changes in the capacitance are then reflected by the changes in the out-of-phase impedance according to

$$Z_i = 1/\omega C \qquad (7)$$

where ω is the angular frequency ($2\pi f$) of the applied ac potential. It should be noted that the impedance is frequency dependent, thus, at a lower frequency, the impedance would be higher, while a higher frequency results in a lower impedance.[49]

2.3.2 Impedance Curve Profile

In this electrochemical system, an ac potential at a frequency of 100kHz with a 10mV amplitude is superimposed onto the dc potential applied. When the silicon semiconductor is placed in contact with an electrolyte, it compensates for the changes at the electrolyte/insulator interface by changing the charge distribution at the semiconductor/insulator interface. As the applied dc potential is varied (keeping the ac voltage constant at 10mV), the semiconductor continuously compensates for the changes by changing its charge distribution, and hence, changes in the capacitance. As a result, an impedance curve with the following profile (Figure 2.6) is generated, which shows three regions corresponding to accumulation, depletion and inversion.

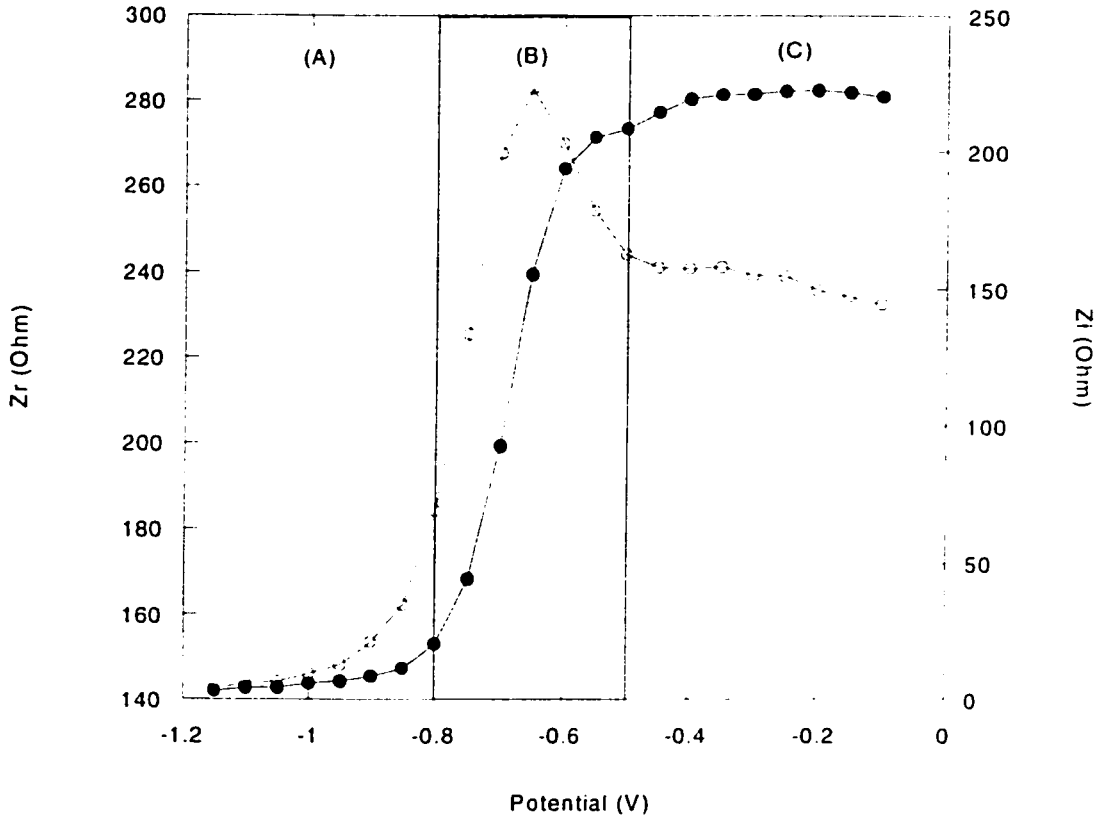

Figure 2.6 Impedance curve of Z_r (o) and Z_i (•) as a function of DC potential vs. SCE where (A), (B) and (C) represents the accumulation, depletion and inversion regimes.

In the accumulation region (at more negative dc potentials), the majority charge carriers (the electrons) accumulate at the semiconductor/insulator interface (Figure 2.7A). As the dc potential becomes more positive, the fermi level moves downward toward the edge of the valence band causing the bands to flatten out (giving the flat-band potential) (Figure 2.7B). This is referred to as the depletion regime. At even more positive dc potentials, the bands gradually bend upwards so that holes accumulate at the semiconductor/insulator interface. This is known as the inversion region (Figure 2.7C).

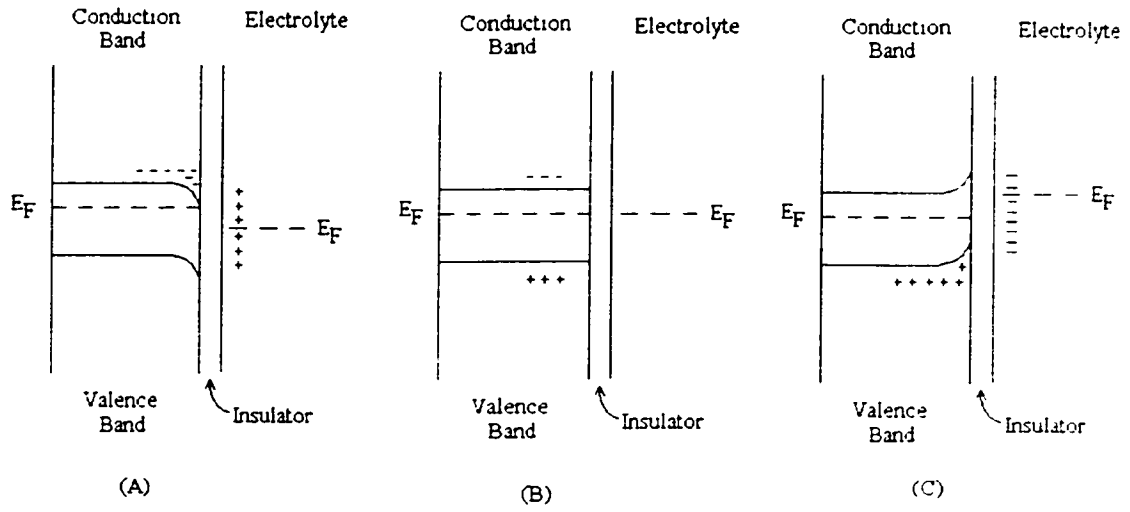

Figure 2.7 Flat-band diagrams for the accumulation (A), depletion (B) and inversion (C) regimes for an n-type semiconductor.

2.3.3 Flat-Band Potential

The impedance curve that provides information about the changes on the surface of the electrolyte/insulator interface is the out-of-phase or imaginary curve, Z_i. The flat-band potential is the experimental potential value that must be applied externally in order to cancel out the band bending in the semiconductor. Any chemical modifications performed on the semiconductor surface changes the overall capacitance of the system and this is reflected in the horizontal displacement of the Z_i curve along the potential axis (i.e. changes in the flat-band potential).

The capacitance, C, of the depletion layer formed in the semiconductor is analogous to that of a parallel plate capacitor as given by Equation 6.

The distance separating the parallel plates, d, also corresponds to the width, W, of the semiconductor's depletion layer: [50]

$$W = \left[\frac{2 \varepsilon \varepsilon_o (V - V_{fb} - kT/q)}{q N_D} \right]^{0.5} \qquad (8)$$

where V is the applied dc potential

V_{fb} is the flat-band potential

k is the Boltzman constant

T is the absolute temperature

q is the elementary charge

N_D is the dopant density per unit area

The combination of the Equations (6) and (8) is the relationship between the total capacitance of the EIS structure and the dc potential applied: [50]

$$1/C^2 = \frac{2}{\varepsilon \varepsilon_o q N_D A^2} (V - V_{fb} - kT/q) \qquad (9)$$

This is known as the Mott-Schottky relation.

A linear plot of $1/C^2$ versus the applied potential, V, permits the extrapolation of the slope in the depletion regime to the applied potential axis by which the intercept yields the flat-band potential, V_{fb}.

2.4 Cyclic Voltammetry

Cyclic voltammetry involves the variation of the dc potential applied to the working electrode as a function of time and a measurement of the dc current. Figure 2.8A illustrates the variation in potential as a function of time where a linear sweep begins at a potential, E_1 and varies until it reaches E_2. At this point, the direction of the sweep is reversed and the electrode potential is scanned back to its initial potential at E_1.

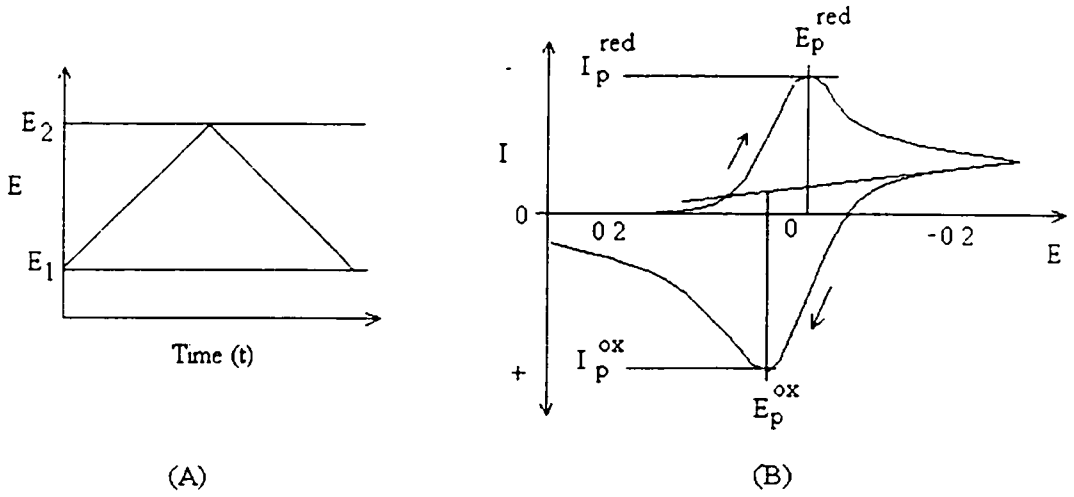

Figure 2.8 Variation of the applied potential as a function of time (A) and a cyclic voltammogram for a reversible electron transfer reaction (B).

By plotting the measured current as a function of the potential, a cyclic voltammogram is produced and this is used as a means to characterize the redox behavior of a compound. Figure 2.8B is a typical cyclic voltammogram of a reversible electron transfer reaction. Upon a forward scan (towards a more negative potential), the redox species is reduced while on the reverse scan (towards a more positive potential) the redox species is being oxidized. The redox potential of the two species in solution is given by the value between these two maxima. [51]

Cyclic voltammetry was used as a method of functionalizing the substrate by electrochemically reducing the 4-nitrobenzenediazonium onto the substrate's etched surface. It was done using the standard 3-electrode cell as shown in Figure 2.9.

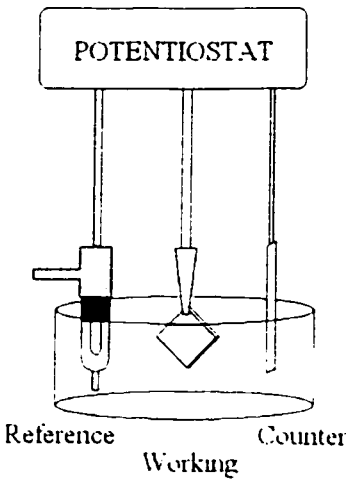

Figure 2.9 Electrochemical setup for the functionalization of the substrate.

2.5 Reaction Mechanisms

The silicon substrates are first prepared by cleaning them to remove surface contaminants. Following the cleaning, the substrates are then etched to remove any oxide present and this produces a H-terminated surface (Reaction (I)), which is subsequently functionalized with the diazonium:

$$-Si-Si- \; + \; HF \; + \; NH_4F \longrightarrow \; -\overset{H}{\underset{|}{Si}}-\overset{H}{\underset{|}{Si}}- \qquad (I)$$

The substrates were then functionalized through electrochemical reduction of the diazonium moiety in the following manner:

$$\overset{+}{N}\equiv N-Ar-NO_2 + e^- \longrightarrow {}^{\bullet}Ar-NO_2 + N_2 \qquad (II)$$

$$Si-H + {}^{\bullet}Ar-NO_2 \longrightarrow Si^{\bullet} + H-Ar-NO_2 \qquad (III)$$

$$Si^{\bullet} + {}^{\bullet}Ar-NO_2 \longrightarrow Si-Ar-NO_2 \qquad (IV)$$

$$Si-H + H_2O + e^- \longrightarrow Si^{\bullet} + H_2 + OH^- \qquad (V)$$

$$Si^{\bullet} + H_2O + e^- \longrightarrow Si-H + OH^- \qquad (VI)$$

$$Si-Ar-NO_2 + 6e^- + 6H^+ \longrightarrow Si-Ar-NH_2 + 2H_2O \qquad (VII)$$

Reaction (II) shows the generation of the nitrobenzene radical in an acidic aqueous media. In this case, the acidic aqueous media contains hydrofluoric acid and sulfuric acid and they also act as the background electrolyte to prevent polarization effects. In a protic solution, the formation of a second layer seems very unlikely since the NO_2 on top of the aryl group will not be easily removed from the ring. In Reaction (III), a radical first abstracts the H atom from the surface of the substrate leaving behind a surface radical which may react with a second aryl radical to generate a covalent bond between the silicon substrate and the nitrobenzene, as shown in Reaction (IV). It should also be noted that the products formed in Reaction (III) might be responsible for the inhibition of the surface upon prolonged cathodic polarization in the diazonium solution since nitrobenzene is poorly soluble in aqueous solutions. Reactions (V) and (VI) accounts for the cathodic evolution of molecular hydrogen, seen as the evolution bubbles on the surface of the H-terminated silicon upon electrochemical reduction. Reactions (II) to (VI) shows that two electrons are necessary to bind an aryl group to the surface of the substrate and that some of the aryl radicals that are generated are used up in secondary

reactions. Reaction (VII) corresponds to the electrochemical reduction of the nitro group to form an amino group in a protic solution.[52-53]

Following the functionalization of the substrate with the aryl diazonium, the surface needs to be treated with glutaraldehyde, as the amino linked single-strand DNA will not bind directly to the amino groups on the surface. The glutaraldehyde acts as a link between the surface of the modified substrate and the C_6H_{10} amino linker on the DNA. It also acts as a spacer between the two functional groups which allows more mobility for the DNA to subsequently hybridize.

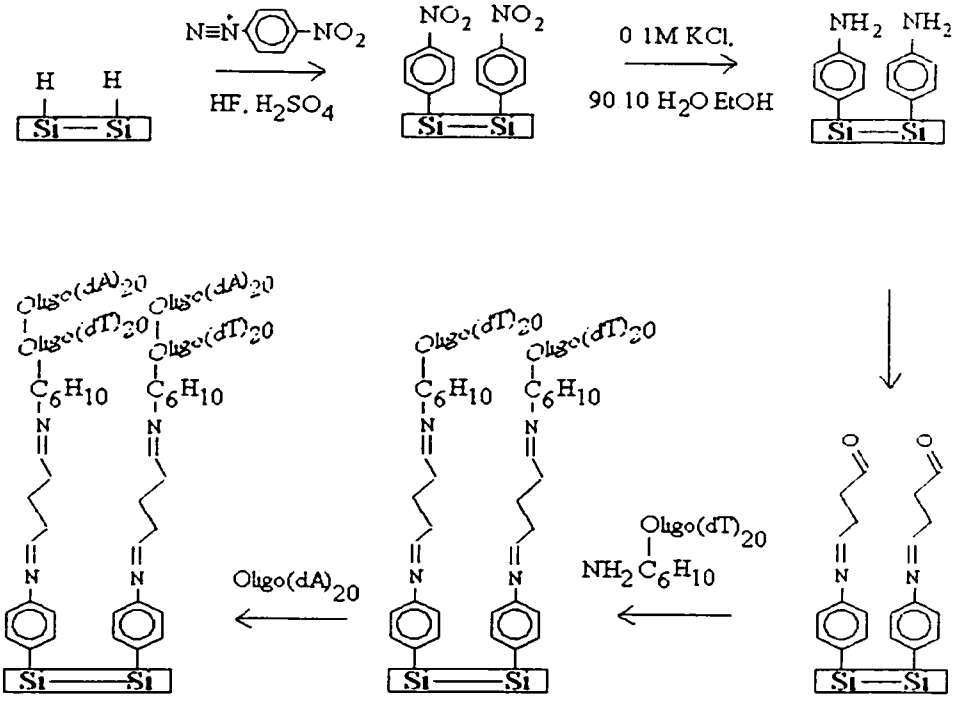

Figure 2.11 A schematic illustration of the various modification steps involved.

2.6 Characterization of the Substrates

2.6.1 X-Ray Photoelectron Spectroscopy (XPS)

X-ray photoelectron spectroscopy is a technique used to determine the structural and oxidation state of the compounds in the sample by giving information on the atomic binding energy between atoms. [49] Figure 2.11 shows a schematic representation of how XPS works. A monochromatic beam of x-rays with a known amount of energy is used to excite an electron in the core shell. As a result, the electron is removed from the core shell and travels to a detector. The detector measures the kinetic energy of the electron and determines the binding energy, which is the difference in energy between the x-ray beam and the kinetic energy of the electron that is ejected.

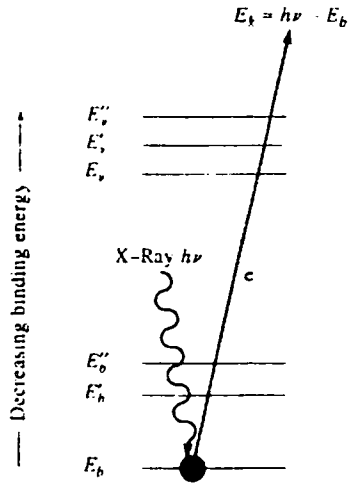

Figure 2.11 A schematic representation of the XPS process where E_b represents the core shell and E_v represents the valence shells.

3. Experimental

3.1 Reagents

Table 3.1 is a list of all the reagents used. The reagents were used as received and were stored at room temperature, except for the 4-nitrobenzenediazonium tetrafluororborate and glutaraldehyde, which were stored at 5°C and the oligonucleotides at –20°C. All solutions were prepared in distilled-deionized water.

Reagent	Source	Purity
Trichloroethylene	Fisher	Technical Grade
Acetone	Fisher	Reagent Grade
Methanol	Fisher	HPLC Grade
Hydrofluoric Acid	Fisher	48-50%
Buffered Ammonium Fluoride	J.T. Baker	Electronic Grade, Low Sodium MOS
Glutaraldehyde	J.B.Em Services	25% solution
Ethyl Alcohol	Sigma-Aldrich	HPLC Grade
Sulfuric Acid	J.T. Baker	Reagent Grade
Nitrogen Gas	PraxAir	Ultra High Purity (UHP)
4-Nitrobenzenediazonium Tetrafluoroborate	Aldrich	97%
Sodium Chloride	EM Sciences	Reagent Grade
Potassium Chloride	Fisher	Reagent Grade
Sodium Citrate Dihydrate	Fisher	Reagent Grade
Sodium Bicarbonate	Sigma	99.50%
Oligo $(dT)_{20}$ am	BioCorp Inc.	Standard
Oligo $(dA)_{20}$ am	BioCorp Inc.	Standard
Oligo $(dT)_{20}$	BioCorp Inc.	Standard
Oligo $(dA)_{20}$	BioCorp Inc.	Standard

Table 3.1 List of the reagents used.

3.2 Impedance Measurements

Impedance measurements were taken after each modification step using a three electrode setup with the silicon substrate acting as the working electrode, a platinum foil as the counter electrode, and a saturated calomel electrode (SCE) as the reference. All measurements were performed in a "dark-box" to prevent the generation of photocurrents, which would also affect the impedance measurements (Figure 3.1). The electrolyte used for the impedance measurements was 0.01M NaCl. Measurements were taken at 50mV increments at applied dc voltages varying between −1.2 to 0.2V, with a superimposed 10mV amplitude ac voltage at a frequency of 100 kHz. A VoltaLab40 PGZ301 Radiometer Analytical workstation, coupled to an IBM PC was used to perform the experiments. The impedance data was obtained and processed using the VoltaMaster 4.0 Electrochemical Software (Version 3.0) and the subsequent data analyses were done using KaleidaGraph (Version 3.5) software.

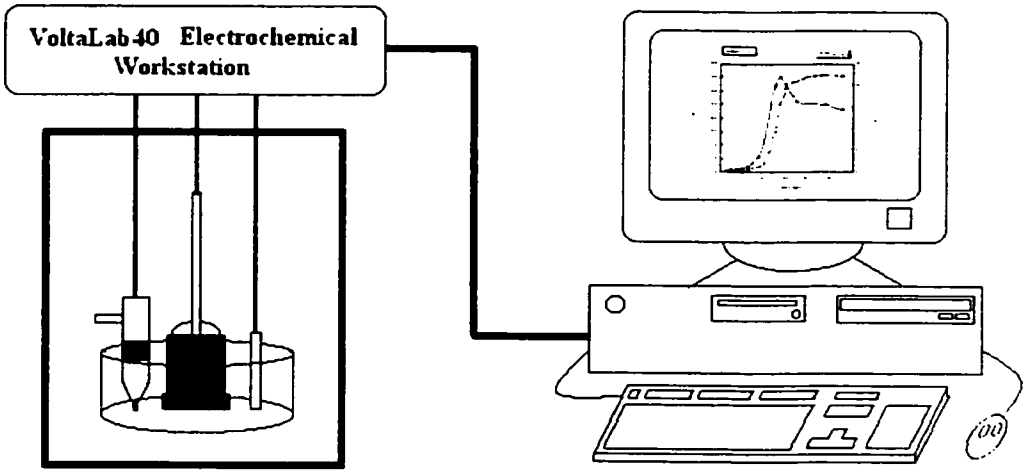

Figure 3.1 Diagram of the electrochemical workstation.

3.3 Substrates

The n-type silicon (100) substrates (Silicon Valley Microelectronics, USA) were doped with phosphorous to a density of 10^{15} atoms/cm^3 to give a resistivity of 5-10 Ω/cm. The silicon layer was 300 μm thick and chromium/gold layers were vacuum evaporated onto the backside to provide an ohmic contact. The silicon substrates were polished and the wafers were diced to give 1 cm^2 chips.

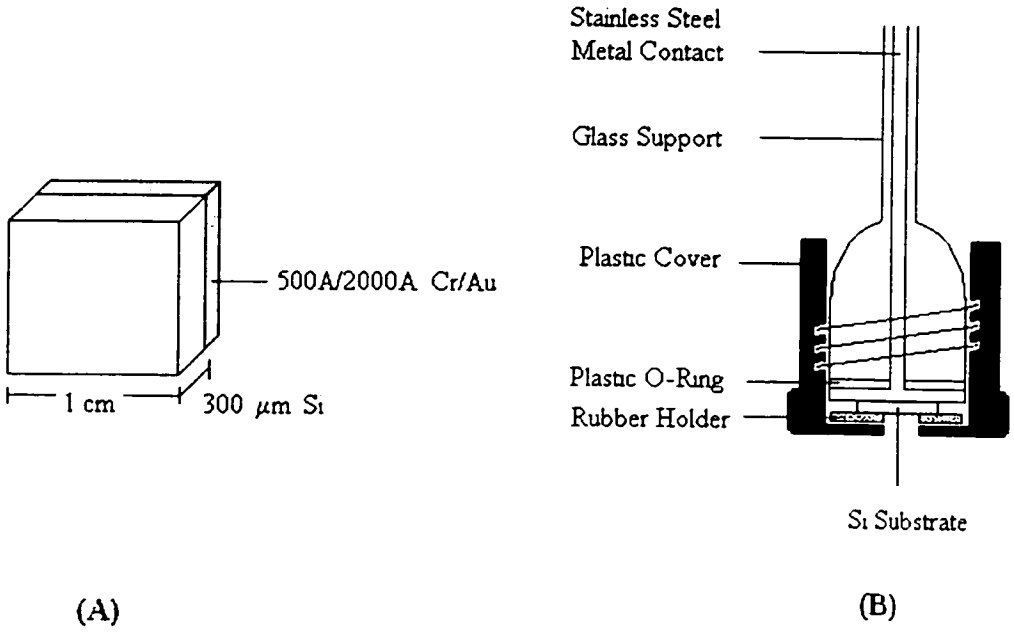

Figure 3.2 Diagram of the silicon substrate (A) and the working electrode (B).

3.4 Substrate Preparation

3.4.1. Cleaning and Etching

Surface contaminants such as grease, dust and other organic substances were removed by immersing the substrates in organic solvents. Each beaker contained 15 mL of trichloroethylene, acetone and methanol and the substrates were immersed into each solvent for 1 minute each. They were then etched in a 48-50% HF solution (15mL in a plastic beaker) for 1 minute followed by a 6 minute treatment in a 40% buffered NH_4F solution (15mL in a plastic beaker) to provide a hydrogen-terminated silicon surface.[54-55] The substrates were rinsed for 30 seconds with deionized-distilled water and dried under a gentle stream of nitrogen gas following each modification step.

3.4.2. Functionalization of the Substrate

A 2mM solution of 4-nitrobenzenediazonium tetrafluoroborate with 2% HF and 0.1M H_2SO_4 as supporting electrolytes was deoxygenated by bubbling nitrogen gas into it for 20 minutes. The etched substrates were then functionalized by electrochemically reducing the diazonium solution through cyclic voltammetry within a range of –0.4V to –1.7V (vs. SCE) at a scan rate of 20 mV/sec. The current range was set at 10 mA and three scans were performed to ensure surface passivation. [52]

Following this initial modification, the nitro group of the diazonium moiety is reduced to an amino group in a 90:10 water-ethanol solution containing 0.1M KCl through cyclic voltammetry within a range of –0.4V to –1.7V (vs. SCE) at a scan rate of 100 mV/sec, and a current range of 100 mA. Three scans were also performed to ensure reduction of the nitro groups. [53]

3.4.3. Glutaraldehyde Treatment

The functionalized substrates were then immersed in a 5% solution of glutaraldehyde (200μL of 25% stock solution with 800μL distilled water) in a test tube for 30 minutes at room temperature. They were subsequently rinsed for 30 seconds with distilled-deionized water and dried with a gentle stream of nitrogen gas. The glutaraldehyde acts as a cross linker between the amino groups on the substrate and the C_6H_{10} aminolinker on the oligo$(dT)_{20}$ or oligo$(dA)_{20}$ being used as the probe layer.

3.4.4. Immobilization

The oligo$(dT)_{20}$ and oligo$(dA)_{20}$ with a C_6H_{10} amino-linker at the 5' end and the complementary oligomers (oligo$(dT)_{20}$ and oligo$(dA)_{20}$) were prepared by diluting it with 600μL of 1.0M $NaHCO_3$ to give a concentration of 2.0μg/μL and was stored at -20°C for later use. 5μL of the amino-linked oligomer was diluted in 500μL of 3mM $NaHCO_3$ solution and 40μL of this solution was deposited onto the surface of the substrate and left for 45 minutes in a moist environment (Petri dish with a moistened Kimwipe) to prevent it from drying. A blank was also made by depositing the 3mM $NaHCO_3$ solution (no oligo$(dT)_{20}$ or oligo$(dA)_{20}$) onto the surface to determine the effects due to adsorbed electrolytes from the solution itself. The substrates were then rinsed with distilled-deionized water for 30 seconds to remove any unbound DNA and the electrolyte.

3.4.5. Hybridization

The complementary oligomers (oligo$(dA)_{20}$ and oligo$(dT)_{20}$) were prepared in the same manner as the amino-linked oligomers and also had a concentration of 2.0μg/μL.

Following the immobilization of the amino-linked oligomer probe layer, the substrates were immersed in a test tube containing 1 mL solution of 0.001M sodium citrate dihydrate with 10μL of the complementary oligomer to be hybridized for 2 hours at 26°C in a water bath. A blank for the hybridization was also done by immersing a substrate with an immobilized oligomer probe layer in 1 mL of the 0.001M sodium citrate solution. The substrates were then rinsed for 30 seconds to remove any unbound DNA and electrolyte from the surface and were dried with nitrogen.

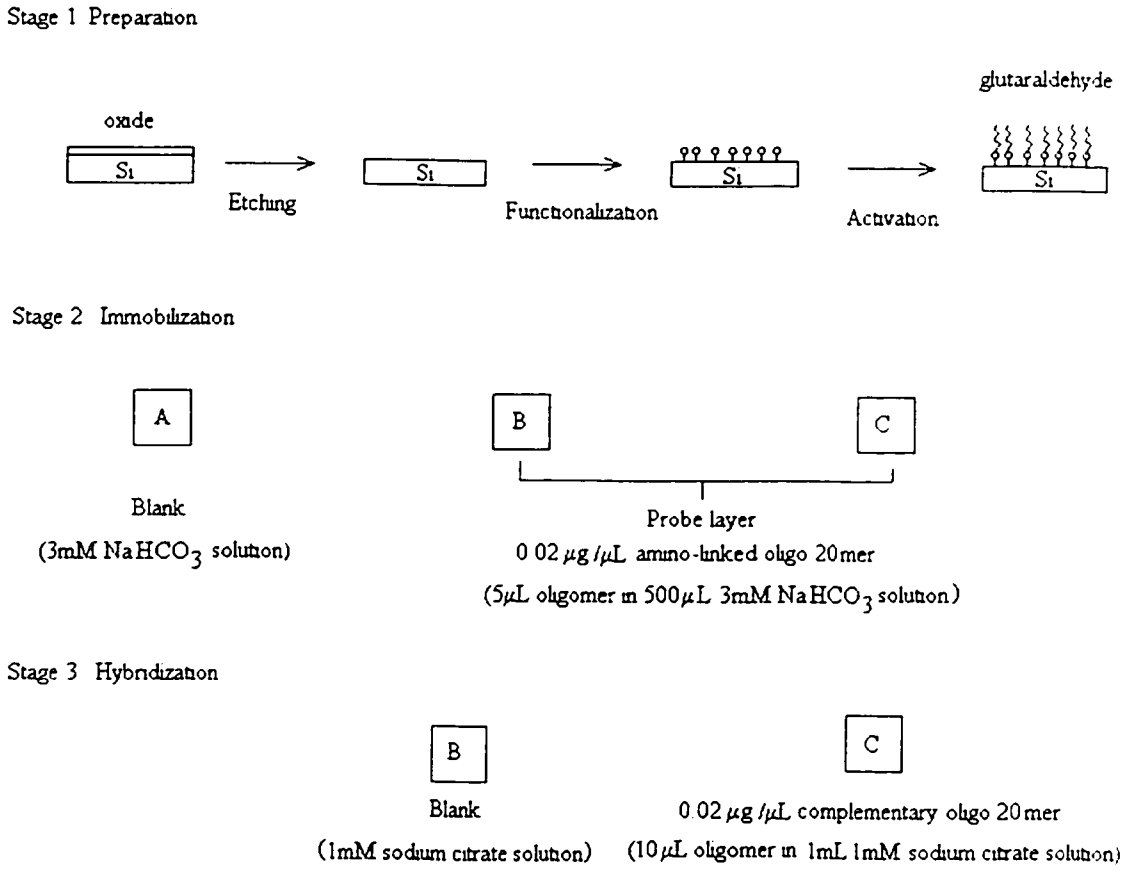

Figure 3.3 Flow chart for the various modification a substrate undergoes.

Figure 3.3 is a pictorial version of the various modifications that a substrate goes through. All of the substrates must undergo Stage 1, before they undergo the different treatments in Stage 2. In Stage 2, there are at least three substrates, as two of them are then used in Stage 3 for hybridization. Stage 3 is the hybridization phase where the probe layer is hybridized with the complementary strand. As illustrated, one of the substrates from Stage 2 is used as a blank (or reference) for the hybridization. The amount of oligomer used for the hybridization is the same as the amount used in the immobilization.

3.5 Other Measurements

3.5.1 X-Ray Photoelectron Spectroscopy

The substrates were analyzed using the EscaLab 220iXL spectrometer using Al K_α X-ray source at 1486.6 eV. Pressure of the analysis chamber was 10^{-9} torr. The data was collected and analyzed using CasaXPS.

3.5.2 FT-IR Measurements

Diffuse reflectance infrared transmission (DRIFT) was used to determine the various types of functional groups on the surface of the substrates. The substrates were analyzed using a Spectra-Tech ABB Bomem MB Series Fourier transform infrared spectroscope and the data was collected and analyzed using Bomem Grams/32 software.

3.5.3 Melting Point Temperature (T_m) Ramps

Melting point temperature ramps (T_m) were performed to determine the melting point of a hybridized DNA duplex. The setup used is the same as that of the impedance

measurements except that a thermocouple was inserted into the electrolyte to monitor temperature changes and two tubes were inserted as well to allow fluid circulation to and from the thermopump. The pump was set to +1 with reverse flow rate of 75mL/min for the fluid circulation. The temperature was set to increase from room temperature (approximately 24°C) to 65°C in 20 minutes (ramp time) and was left for 15 minutes (soak time) at 65°C to allow the measurements to stabilize. Temperature changes were measured at one minute intervals and corresponding imaginary impedance values were acquired. The potential value at the mid-point of the depletion region (Z_i vs. V curves) was used as the measuring point to monitor changes in the imaginary impedance. The time at which the impedance changed throughout the duration of the temperature measurements was noted. The results from the temperature-impedance curves were plotted simultaneously on a double y-axis with respect to time represented on the x-axis. The melting temperature is taken to be the point at which the impedance levels off and does not change significantly.

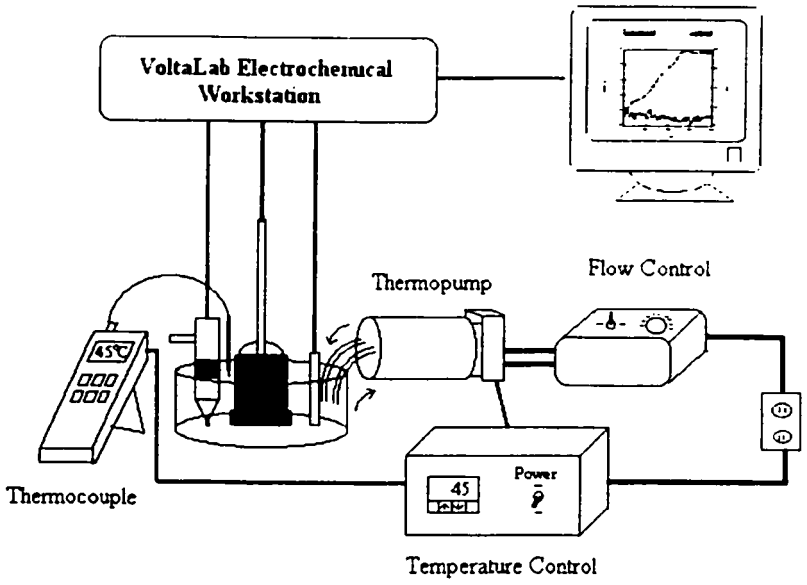

Figure 3.4 Diagram of the melting temperature analysis set-up.

4. Results/Discussion

The results illustrated for 4.1, 4.2 and 4.3 are for the Si(100) oriented substrates.

4.1 Cyclic Voltammetry

Cyclic voltammetry was used to modify the substrate's surface by reducing the diazonium functional group into 4-nitrobenzene. Figure 4.1 shows a typical cyclic voltammogram generated during the functionalization of the silicon substrate. The first curve (bold line) corresponds to the initial reduction cycle while the second curve (dotted line) corresponds to a second cycle performed immediately after the first one. The initial downward wave beginning at –0.8V (going from more positive to more negative potentials) corresponds to the electrochemical reduction of water into H^+ and OH^- ions (theoretically at –0.83V). [56] This leads to the formation of bubbles (~0.1 to 1 mm in diameter) on the surface of the substrate at more negative potentials during the electrochemical deposition. The formation of these bubbles may have blocked other sites on the substrate, thus preventing them from being functionalized. The cathodic reduction continues and at approximately -1.0 V there is a sharp drop in the curve and this corresponds to the removal of the diazo group of the 4-nitrobenzenediazonium into 4-nitrobenzene. [52] The cyclic voltammogram shows that the electrochemical reduction process is practically complete after the first cycle since the current intensity decreases significantly. There is practically no change observed upon a third cycle (data not shown).

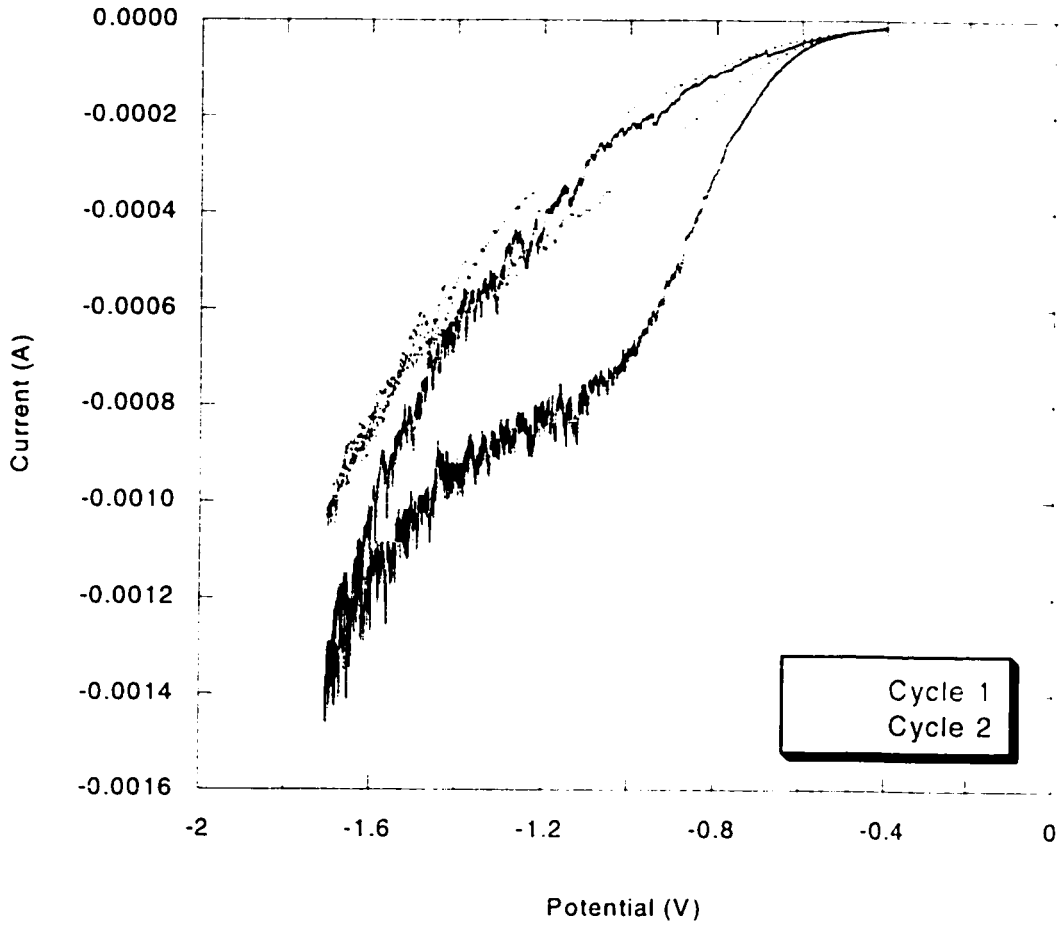

Figure 4.1 Cyclic voltammogram for the electrochemical deposition of the 4-nitrobenzene diazonium.

Figure 4.2 shows two consecutive cyclic voltammograms for the reduction of the nitrobenzene into the aniline moiety. The reduction curves occur at –1.1V and is within a smaller current range compared to that of the initial electrochemical deposition of the 4-nitrobenzene diazonium, which may suggest that the conversion of the nitro groups into amino groups is not complete.[52-53] A smaller current range is also to be expected since the resistance (R) is higher after the functionalization with the nitro groups.

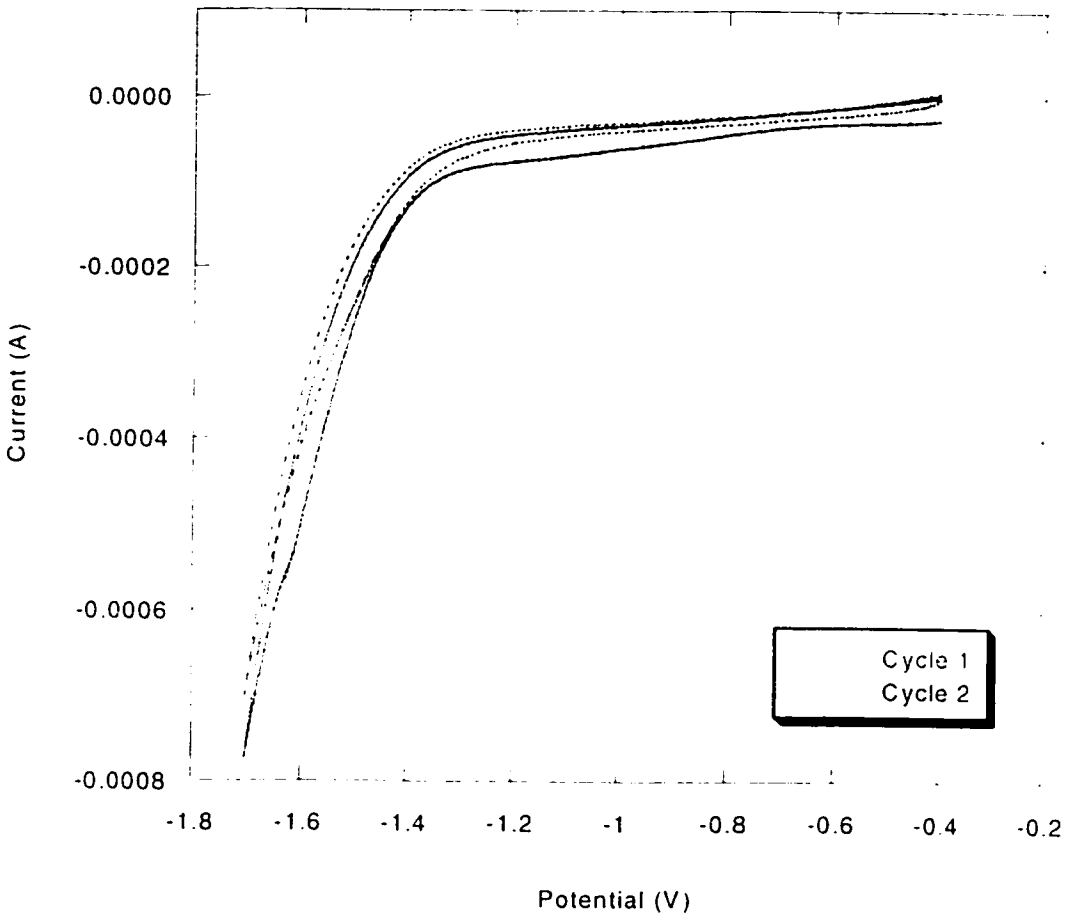

Figure 4.2 Cyclic voltammogram for the reduction of the nitro group into an amino group following the functionalization of the substrate.

4.2 X-Ray Photoelectron Spectroscopy (XPS) Results

X-ray photoelectron spectroscopy scans were used to obtain qualitative and quantitative information from the binding energies of the Si 2p, N 1s, O 1s and C 1s peaks following these modifications. Figures 4.3 to 4.6 correspond to the complete XPS scans of cleaned, etched, and the functionalized substrates with the nitro and amino groups respectively. The XPS scan for the cleaned substrates (Figure 4.3) shows the binding energy of the O 1s peak at 533.95 eV and a Si 2p peak at 104.35 eV, which is characteristic for the SiO_2 species (O 1s at 533.0 eV and Si 2p at 103.6 eV) [57-59] indicating that there is an oxide present.

Upon etching (Figure 4.4), the O 1s peak height has decreased to approximately half its value after cleaning. The Si 2p and Si 2s peaks are more prominent and the Si 2p peak has shifted to a lower binding energy of 99.4 eV which corresponds to the value for clean Si surface of 99.3 eV [58]. It can be inferred that some of the oxide has been removed during this process.

The scan of the functionalized substrate with the 4-nitrobenzene diazonium (Figure 4.5) shows a double nitrogen peak at 406.1 eV and a larger carbon peak at 284.9 eV, while the intensity of the oxygen and silicon peaks are slightly smaller. The theoretical peak values for nitrobenzene are 284.5 for C 1s and 405.7 for N 1s. [59] The scan of the functionalized substrate with the reduction of the nitrobenzene into an aniline moiety (Figure 4.6) shows peak heights similar to those in Figure 4.5. The double nitrogen peak at 406.3 eV and the carbon peak at 285.1 eV are similar to that of the theoretical peak values for aniline at 405.5 eV and 284.6 eV for the N 1s and C 1s peaks respectively. [59] A comparison of the N 1s peaks (Figure 4.7) from these two

modifications shows some changes in the peak intensities as well as the binding energies. For the N 1s of the 4-nitrobenzene modified substrate (Figure 4.7A), the double peaks have different intensities, where one is at 11.2 kCPS (kilo counts per second) at 406 eV and the other is at 9.6 kCPS at 400.9 eV. On the other hand, the double N 1s peaks following the reduction of the nitro group into an amino group (Figure 4.7B) are similar in intensity with one peak at 10.3 kCPS at 406.1 eV and the other at 10 kCPS at 400.6 eV. Although the peak intensities are different, the binding energies of the peaks are similar, making it difficult to distinguish between the nitro groups and amino groups. Further clarification on this point was sought using FT-IR.

Table 4.1 presents the atomic percentage of the elements probed by the XPS. Prior to etching of the substrates, the amounts (atomic percentages) of oxygen and silicon present were 56.35% and 33.45% respectively, which corresponds to the presence of an oxide layer. Once the substrate has been etched, most of the oxide layer is removed and more of the silicon is exposed giving atomic percentages of 7.59% and 89.31% for oxygen and silicon respectively. After the substrates were functionalized, the atomic percentage of silicon and oxygen decreased while that of the carbon and nitrogen peaks increased, which corresponds to the nitrobenzene and aniline functionalization of the substrates. Following the glutaraldehyde treatment (XPS is similar to functionalized ones), there is slightly less silicon detected and more carbon and oxygen. There is a general decrease in the atomic percentage in the silicon peaks as the functionalization progresses (i.e. more layers are added to the surface). In contrast, there is an increase in the atomic percentage for carbon following each modification.

Treatment	Atomic %			
Peak Assignment	Si 2p	C 1s	N 1s	O 1s
Clean	33.45	9.18	0.39	56.35
Etched	89.31	2.23	0.87	7.59
Functionalized with NO_2	19.69	57.53	7.83	14.94
Reduction of NO_2 to NH_2	16.99	58.83	6.82	17.36
Glutaraldehyde	12.12	62.77	5.28	19.83

Table 4.1 Quantitative analysis of each peak for different modifications.

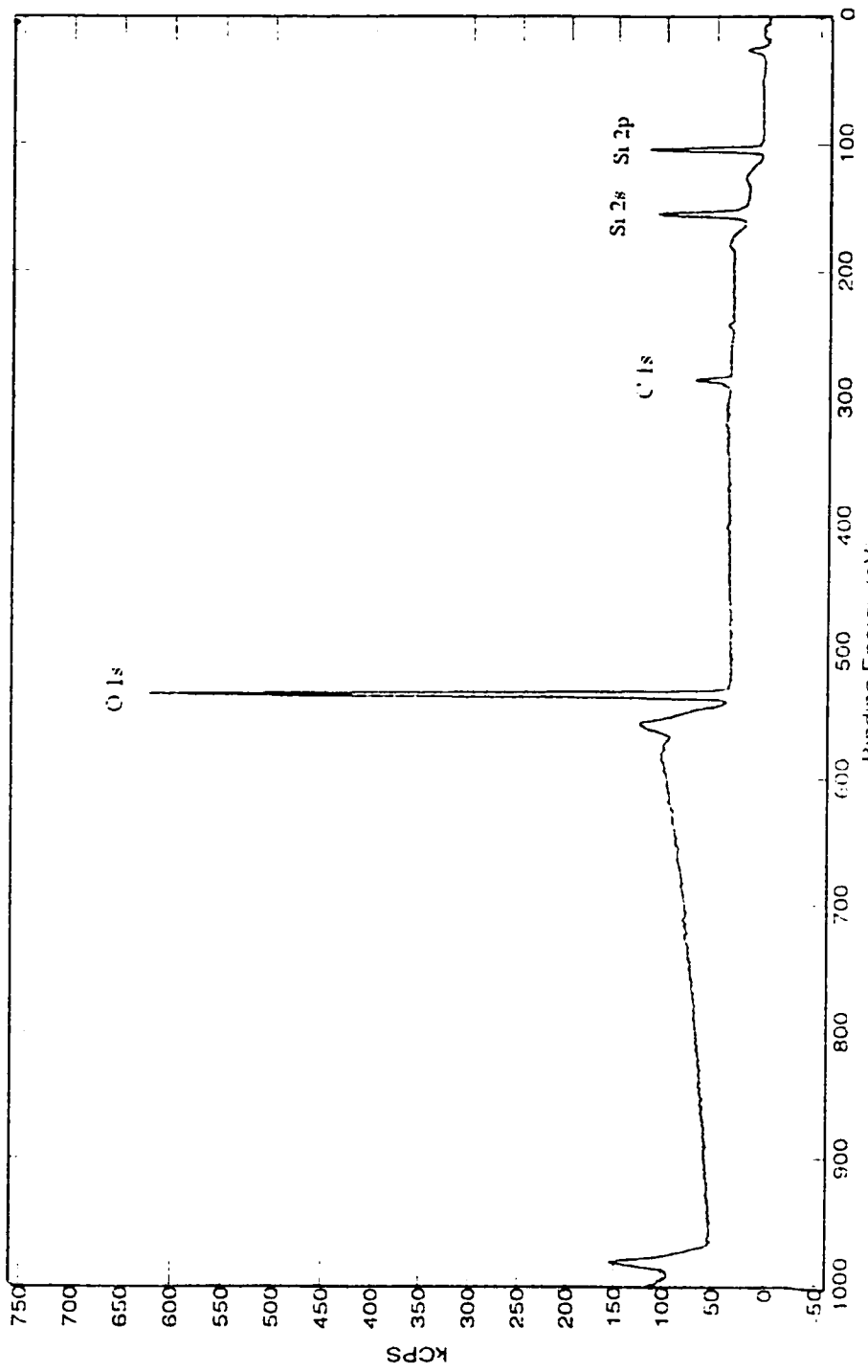

Figure 4.3 XPS of a cleaned substrate.

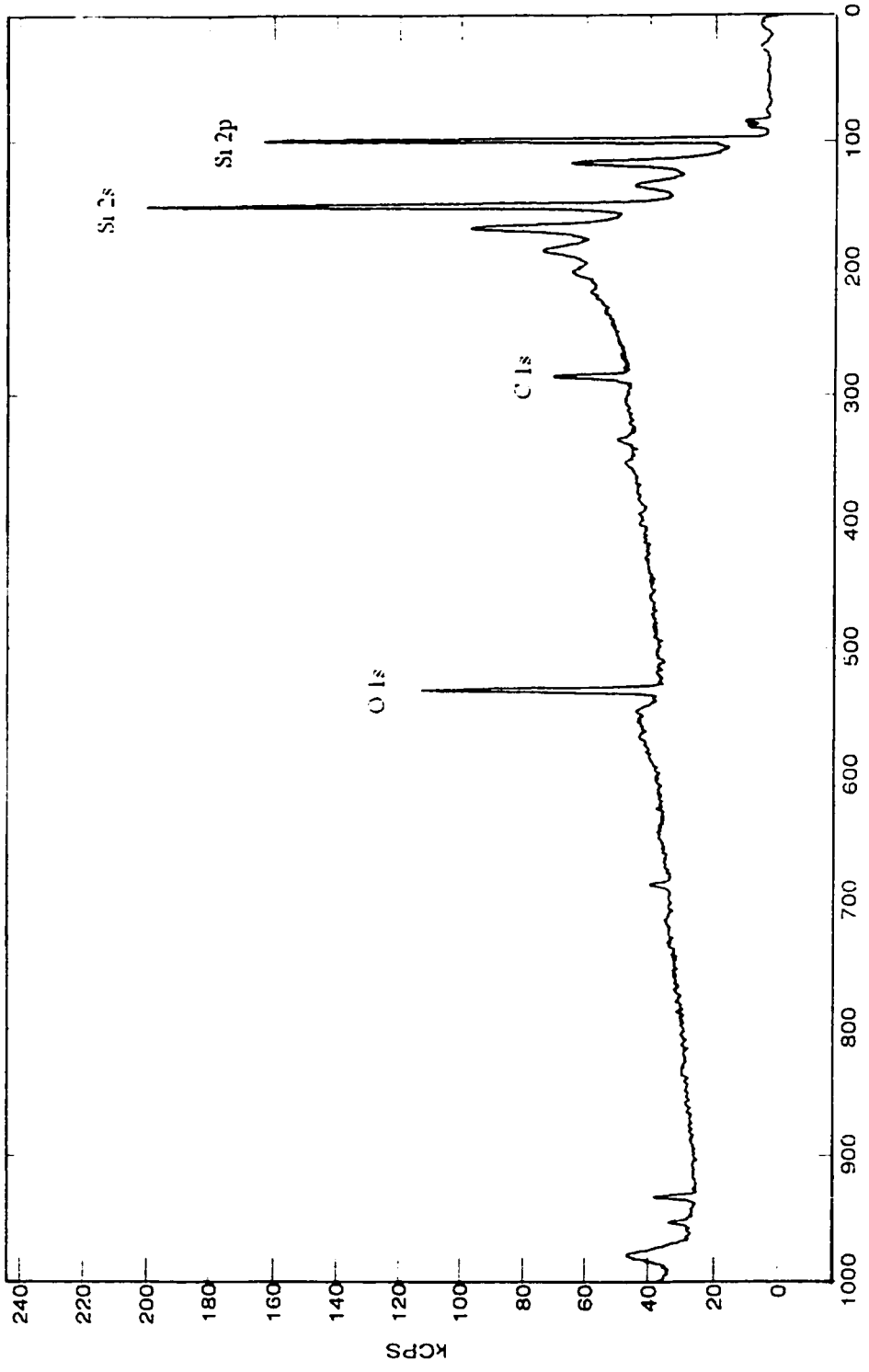

Figure 4.4 XPS of an etched substrate.

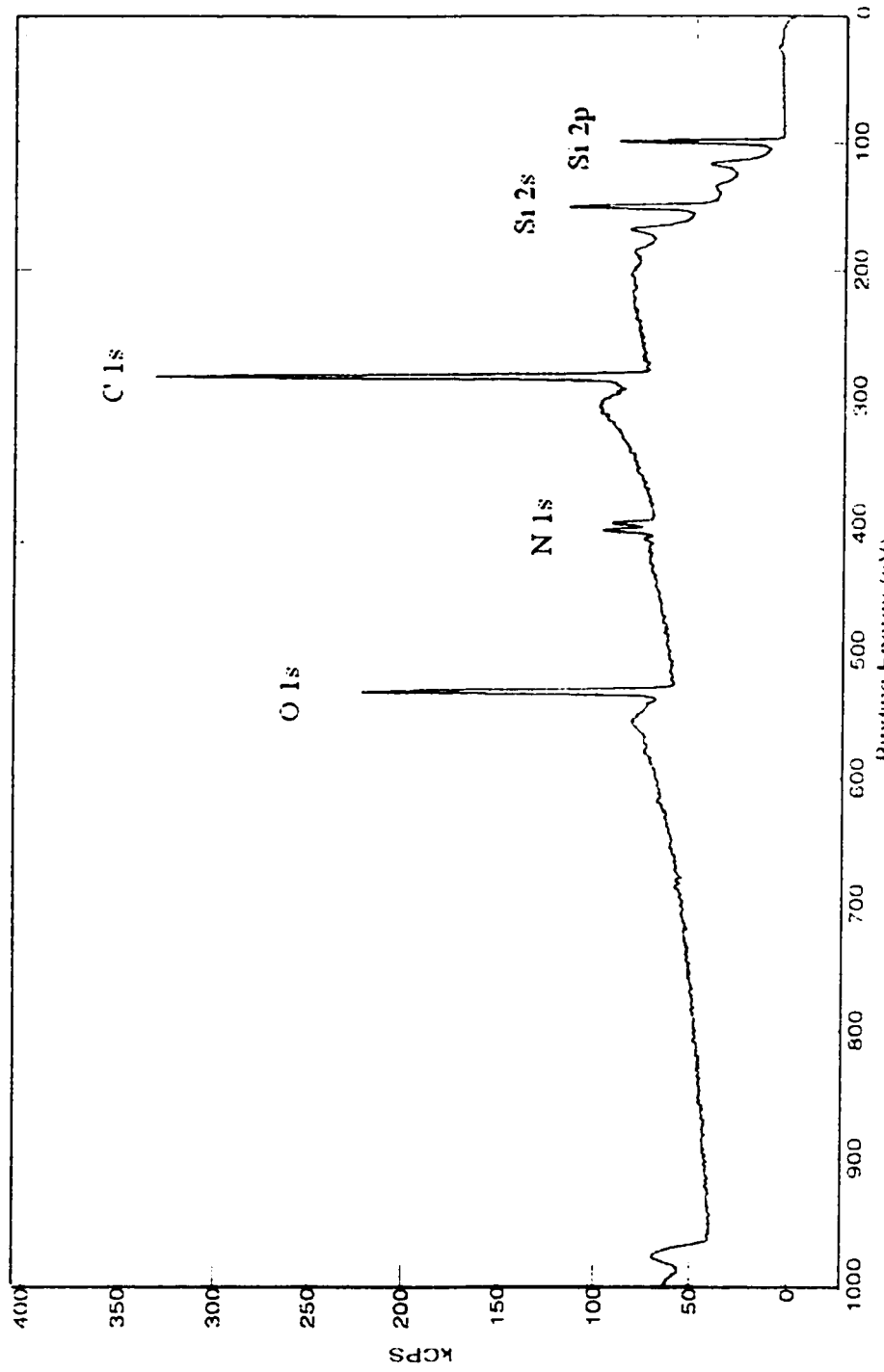

Figure 4.5 XPS of a 4-nitrobenzene functionalized substrate.

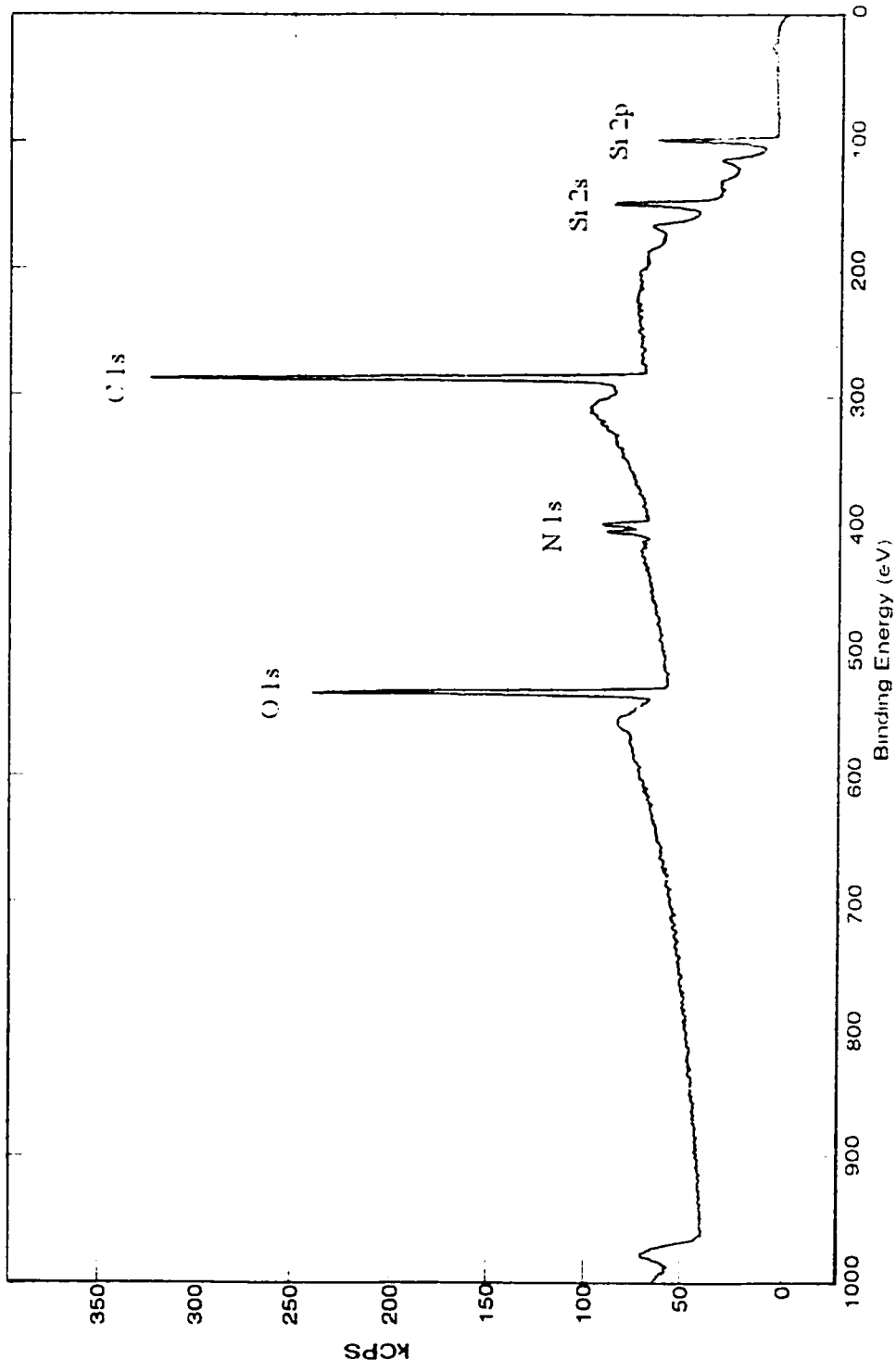

Figure 4.6 XPS of substrate following reduction of nitro group into an amino group.

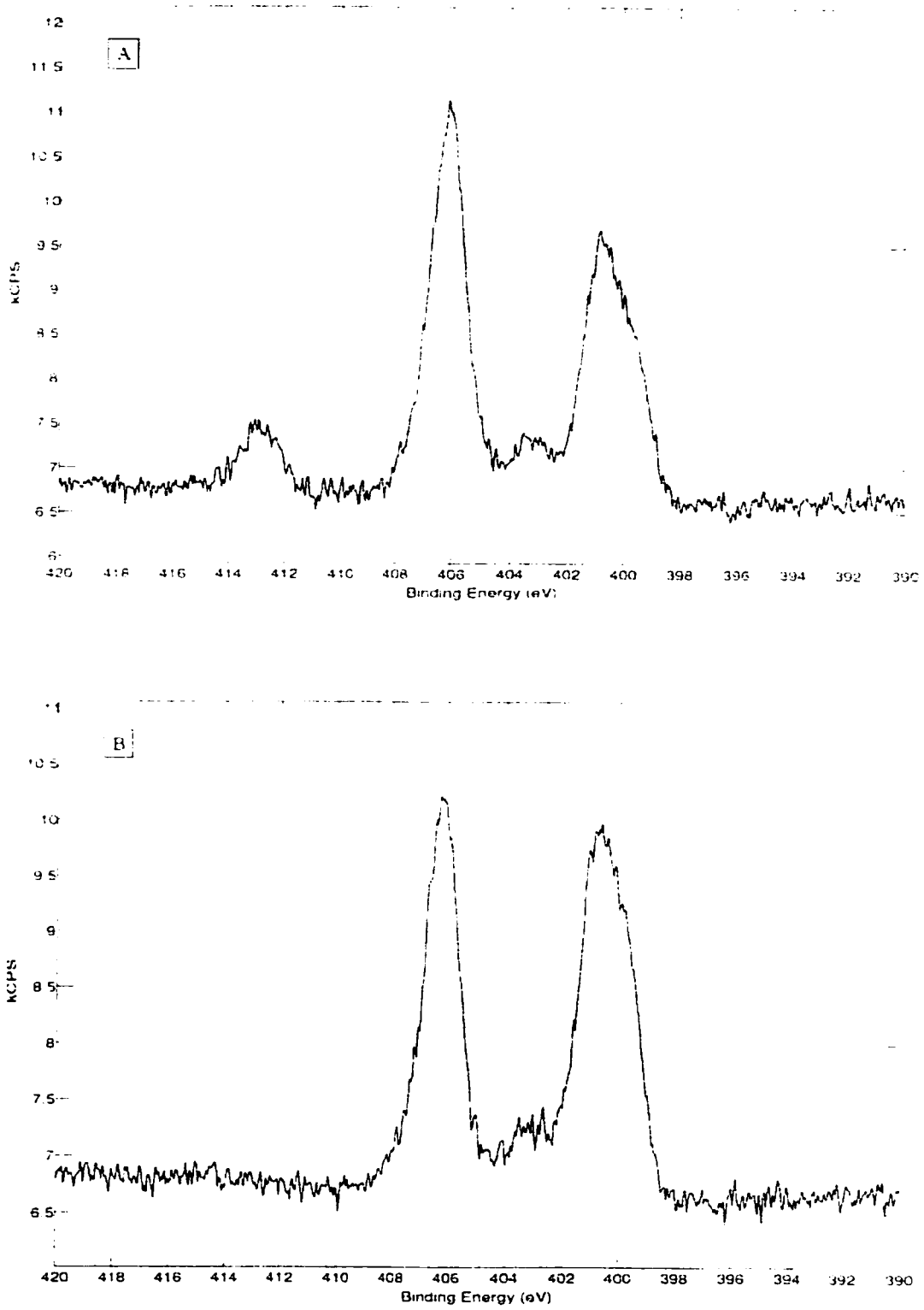

Figure 4.7 Comparison of N1s peaks for a nitro group (A) and an amino group (B).

4.3 Fourier Transform Infrared Spectroscopy (FT-IR) Results

As mentioned earlier (in section 4.2), the XPS N 1s peaks are very similar for the nitrobenzene and aniline modifications, so Fourier Transform infrared spectroscopy was performed to determine if there were any differences. Figures 4.8 and 4.9 represents the FT-IR for the 4-nitrobenzene functionalized substrate and the FT-IR following the reduction of the nitro group into an amino group. A visual analysis shows that the two scans are similar and there is very little difference between the two. In both cases, the peaks of interest are the Si-benzene at 1110 cm^{-1}, Si-H at 800-950 cm^{-1} and C-N at 1028-1190 cm^{-1}. The characteristic peaks for the aryl-NO_2 and aryl-NH_2 are at 1320-1675 cm^{-1} and 1250-1350 cm^{-1} respectively [60]. Table 4.2 is a summary of the different types of peaks which may be present and their peak intensities. [49, 60-62]

Peak Assignment	Wavelength (cm^{-1})	Intensity
Si-H	800-950	
	2170-2300	
Si-benzene	700-1100	medium
	1420-1450	strong
Aryl-NO_2	1320-1370	
	1350-1675	
	1500-1540	
	2300	
C-N	1028-1190	medium
C-NO	1540	strong
Aryl-NH_2	1250-1350	
	1320-1350	
N-H	3430-3450	sharp, medium
C-NH_2	3300-3500	medium

Table 4.2 Summary of the IR peaks and their intensities.

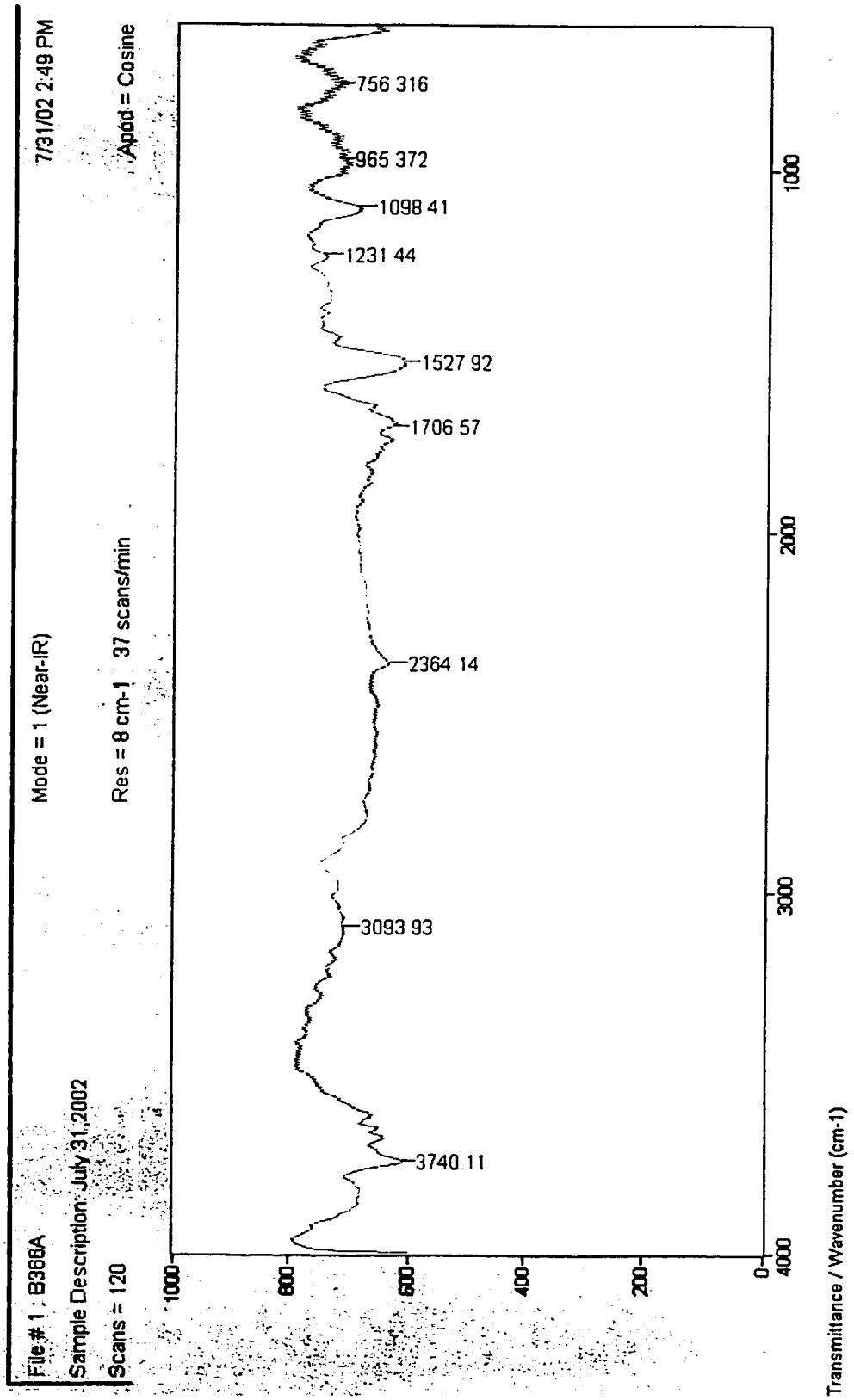

Figure 4.8 FT-IR of a substrate functionalized with 4-nitrobenzene.

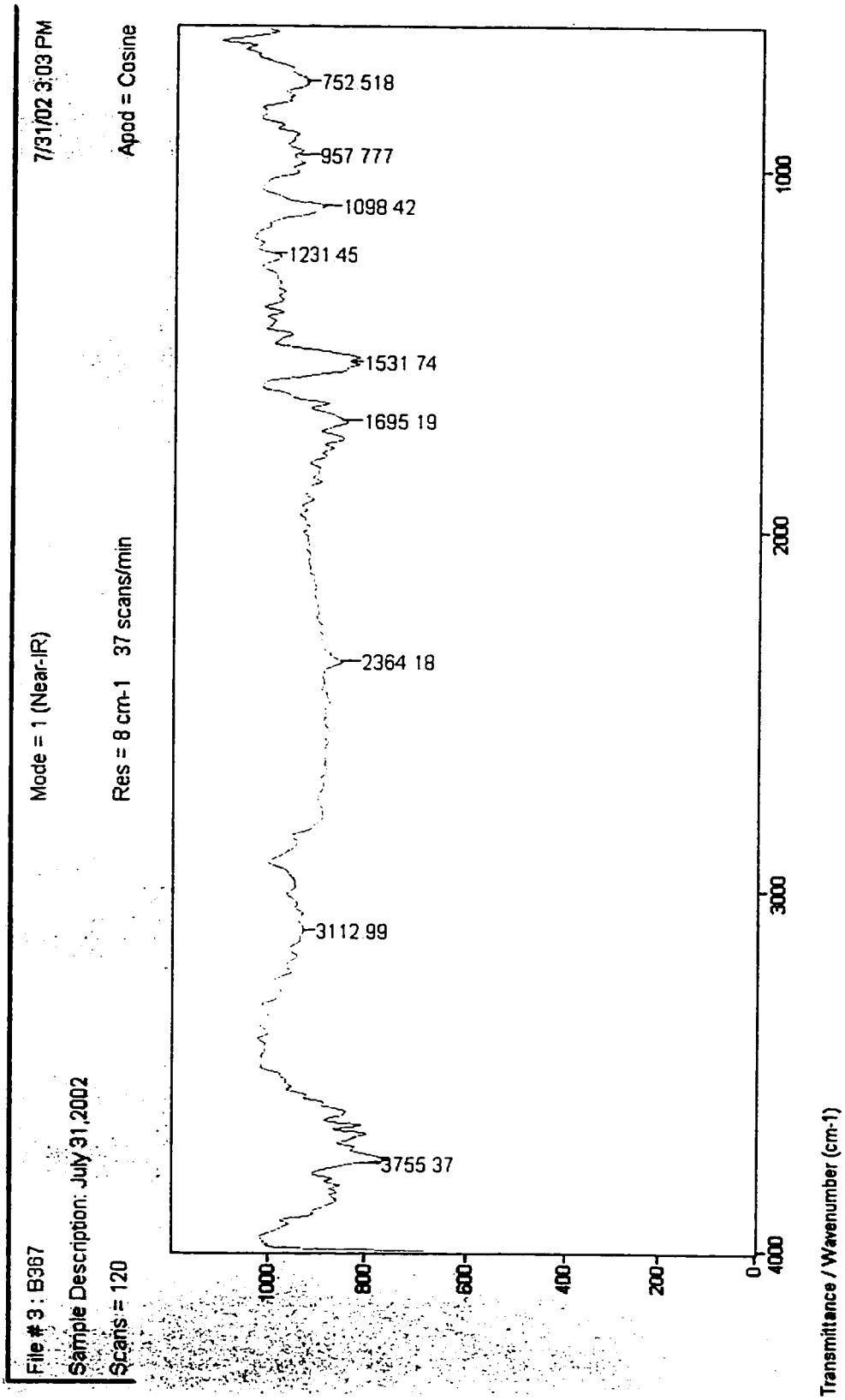

Figure 4.9 FT-IR if a substrate following the reduction of the nitro group into an amino group.

Due to the similarities in the FT-IR scans, it can be inferred that either there is a mix of both nitro and amino groups present on both substrates, or the FT-IR technique is simply not sensitive enough to show the distinction.

4.4.1 Impedance Results for Si (100)

Two basic types of substrates were studied in order to determine which type would provide a better surface for the immobilization of the probe layer. Figure 4.10 shows three different types of crystal orientation associated to. [63] The results for the Si(100) substrates will be discussed in this section while the results for the Si(111) substrates will be discussed in section 4.4.2.

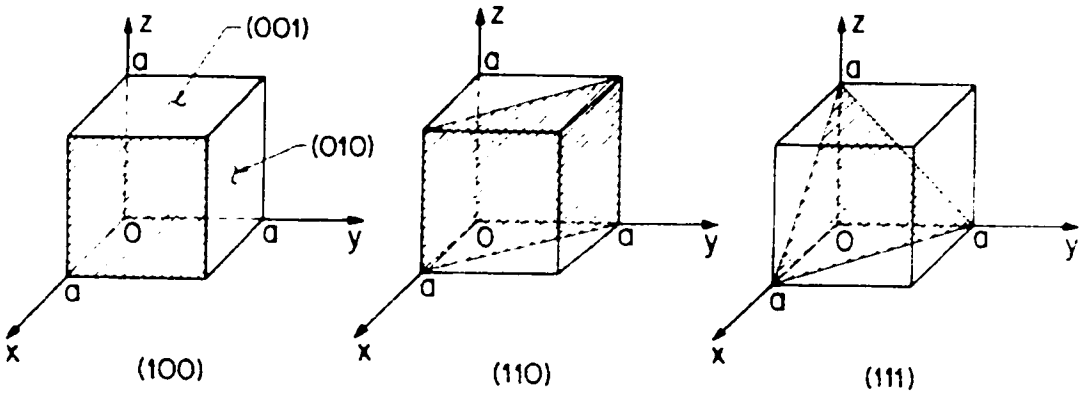

Figure 4.10 Different types of crystal orientations.

The difference in the crystal orientation results in the difference in the number of available bond sites per unit area of the silicon surface, as shown in Table 4.3 [63]. It is apparent that the (111) surface has the largest number of available bonds per centimeter

squared while the (100) has the smallest. Thus, this difference may be reflected in the electrochemical responses observed during the modification steps.

Orientation	Plane Area of Unit Cell (cm^2)	Atoms in Area	Available Bonds in Area	Atoms/cm^2	Available Bonds/cm^2
111	$\sqrt{3}a/2$	2	3	7.85×10^{14}	11.8×10^{14}
110	$\sqrt{2}a^2$	4	4	9.6×10^{14}	9.6×10^{14}
100	a^2	2	2	6.8×10^{14}	6.8×10^{14}

Table 4.3 Properties of silicon crystal planes.

4.4.1.1 Determination of Flat-Band Potential (V_{fb})

Impedance measurements were used to provide direct information on the capacitance of the EIS structure through each modification step. This capacitance is monitored through changes in the flat-band potential of the semiconductor (V_{fb}) which is determined by extrapolating the slope of the Z_i curve in the depletion region to the x-axis, as in Figure 4.11.

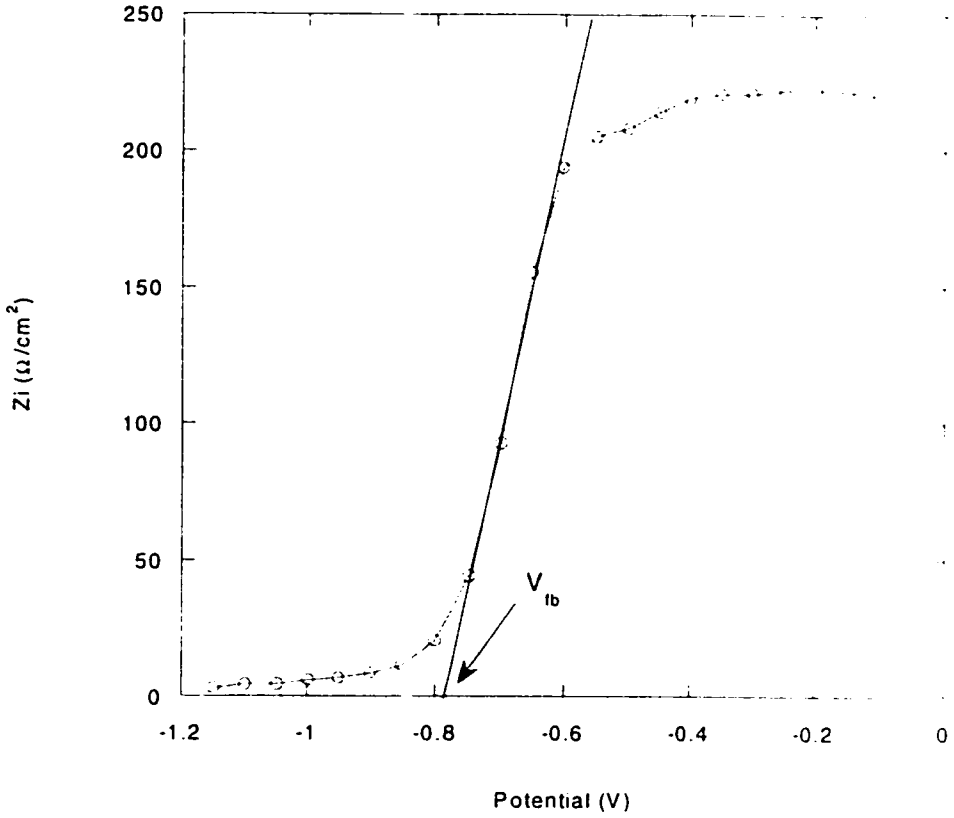

Figure 4.11 Determination of V_{fb} from the Z_i impedance curve.

4.4.1.2 Stability Measurements

Figure 4.12 shows how the substrate's flat-band potential changes following the initial impedance measurement. In most cases, there is either a slight or no shift observed following the very first measurement. This is the result of equilibration of the system with the ions in the electrolyte solution (0.01M NaCl) being adsorbed onto the substrate's surface. It was determined that as the concentration of the electrolyte was increased to 0.05M NaCl (in Tris-HCl) and 0.10M NaCl (in phosphate buffer saline solution), the initial shifts due to equilibration in the flat-band potential also increased. Therefore, the concentration of the electrolyte had to be kept low (0.01M NaCl) in order to keep these

shifts to a minimum with little or no shifts upon further scanning. All subsequent measurements were taken after this initial equilibration.

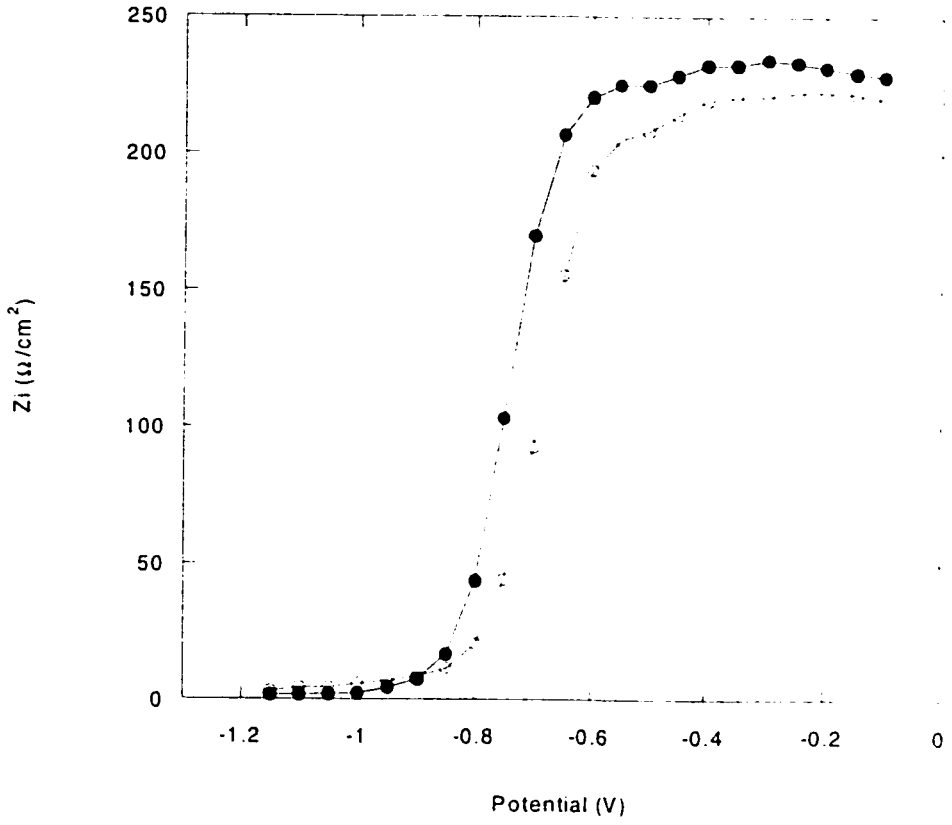

Figure 4.12 Two successive runs (Run 1 (o) and Run 2 (•)) to determine shifts due to equilibration of the EIS structure.

The stability of the system was determined by taking many consecutive scans to determine how much effect the electrolyte had on the substrate. As an example, a functionalized substrate following the reduction of the nitro group into an amino group (Figure 4.13) is used. As illustrated in the figure, the impedance curves are reproducible and there is very little shift exhibited.

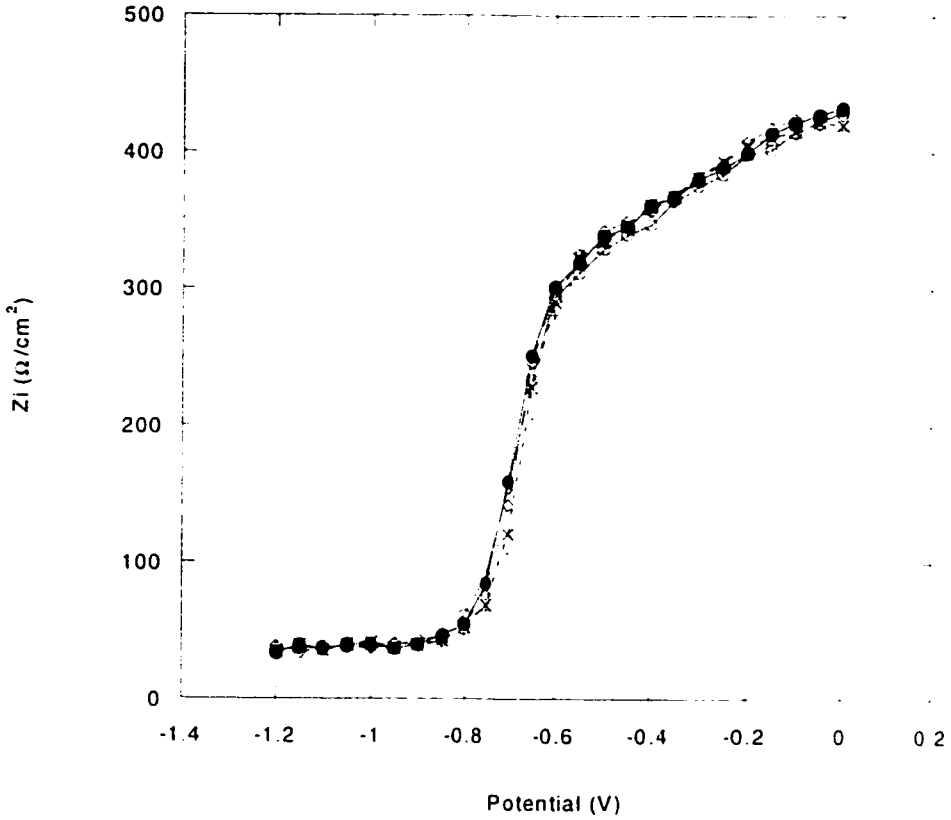

Figure 4.13 Determination of stability after 5 consecutive runs (o, •, ◇, x and + for Runs 1 – 5 respectively) on a functionalized substrate.

4.4.1.3 Impedance Before Etching

Figure 4.14 shows the impedance measurement of a substrate prior to etching. As illustrated, the impedance curve is essentially a straight line because the surface has not been functionalized and the thin oxide layer that is present may have holes in it. As a result the current is passed through the substrate and it behaves like a conductor. Once the substrate has been etched, the silicon's surface has a monolayer of hydrogen present and this layer provides a better electrical insulation to form an EIS structure.

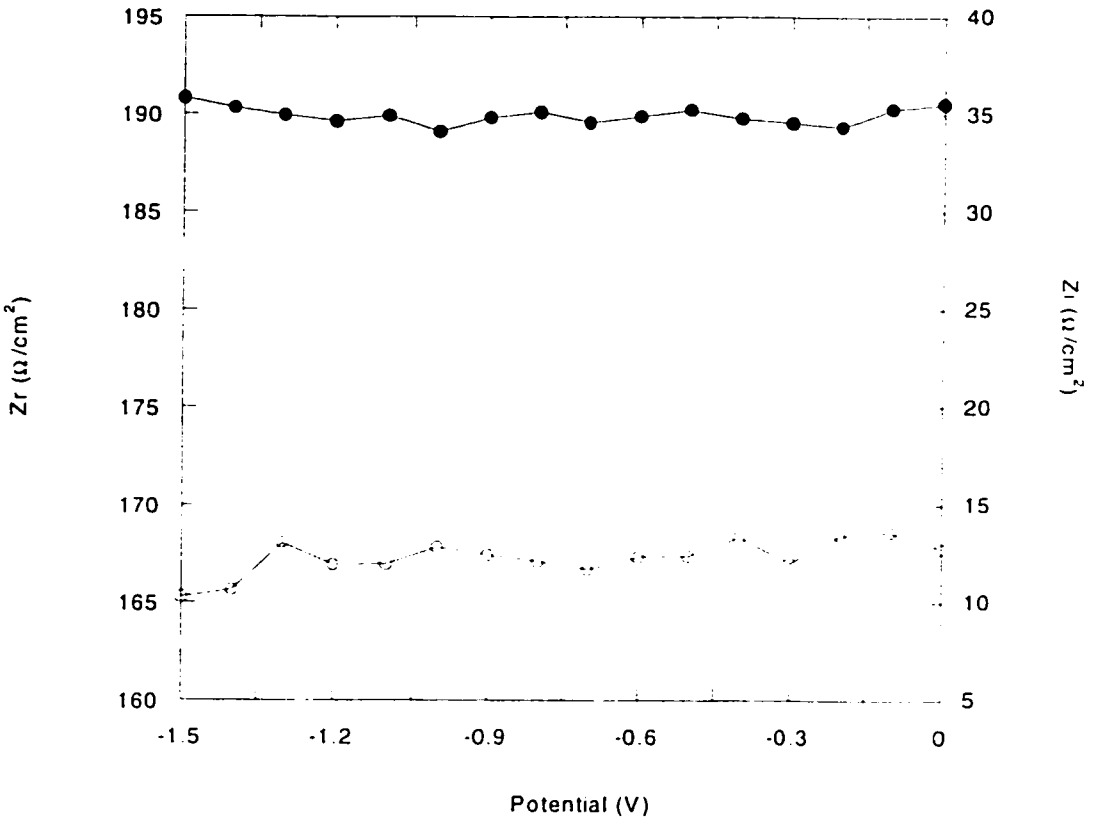

Figure 4.14 Impedance curves of the Z_i (•) and Z_r (o) components of a substrate prior to any modifications (prior to etching).

4.4.1.4 Reproducibility in the Preparation Stages

One of the most important features that leads to proper immobilization of the probe layer lies in the reproducibility in the preparation of the substrates. Figures 4.15 to 4.17 illustrate how good the reproducibility is for the preparation of a set of 4 substrates following the etching, functionalization and activation (treatment with glutaraldehyde) stages. There are slight variations in the reproducibility between the batches (a series of four substrates per batch) which were found to depend on many factors. These variations depend on the quality of the initial substrates before any modification, the evolution of gas from the electrochemical reduction of water during the functionalization process, and

also on the chemistry between the surface and the glutaraldehyde cross-linker. In most cases, the reproducibility following the etching process is very good (as in Figure 4.15), with an average V_{fb} (for 50 different substrates) at –0.90V ± 0.05.

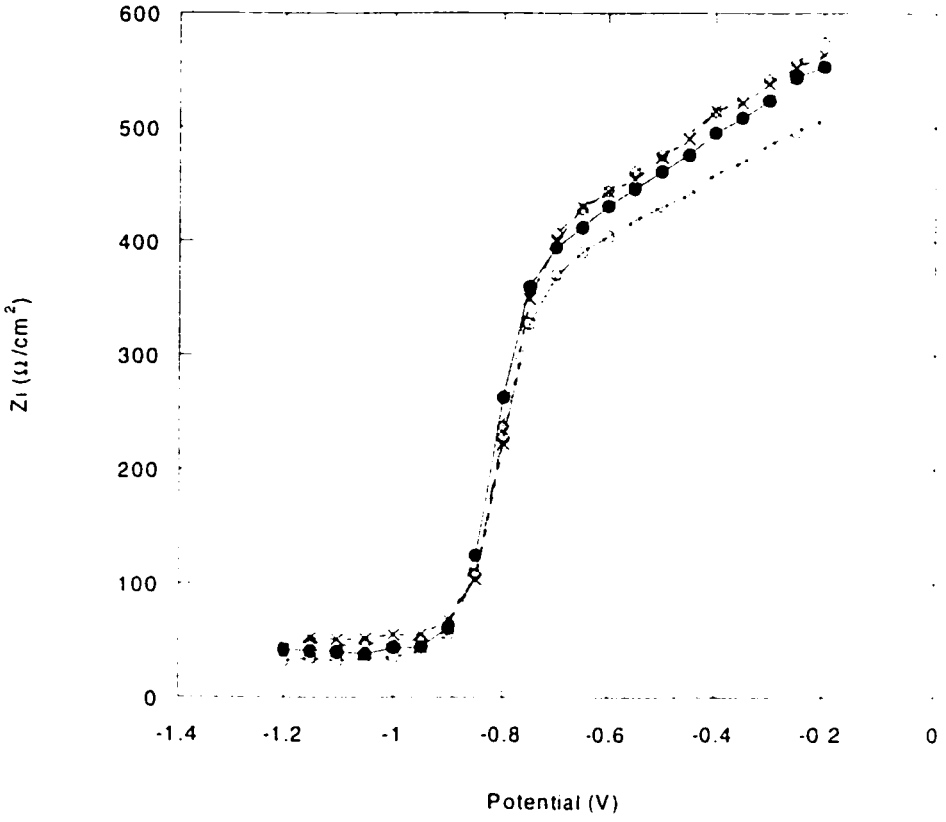

Figure 4.15 Reproducibility in the V_{fb} for 4 different etched substrates (o, •, ◇, and x respectively).

The reproducibility of the functionalized substrates (Figure 4.16, after reduction of nitro group into an amino group) within a batch was also found to be generally good with some exceptions. These may be due to the evolution of gas on the surface of the substrate during the initial functionalization (Section 4.1). The V_{fb} shift observed is approximately 20mV (for 50 substrates), thus giving an average V_{fb} of –0.88V ±0.07.

This V_{fb} value is similar to the value of the etched V_{fb} (–0.9V) because they both have same type of surface exposed to the electrolyte (NH_2 for reduction vs. Si-H for etched).

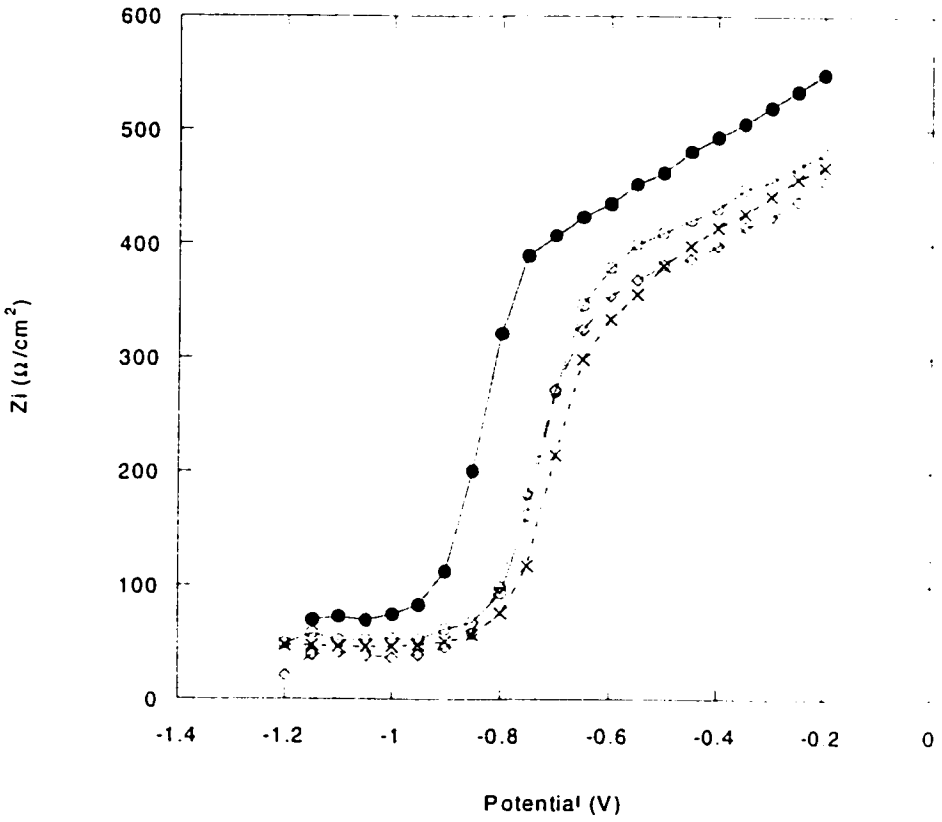

Figure 4.16 Variations in the V_{fb} in functionalized (after reduction of nitro groups into amino groups) substrates (o, •, ◇, and x respectively).

Following the functionalization of the substrates, they are then treated with glutaraldehyde in order to activate the surface. The glutaraldehyde acts as a cross linker between the amino groups on the surface of the substrate and that of the amino-linker on the oligonucleotide probe. As illustrated in Figure 4.17, the reproducibility at this stage is relatively good, even for substrate 2 (•), which was off by ~100mV in the previous stage (Figure 4.16). For this particular batch, the shift in the V_{fb} was 200mV ± 15.

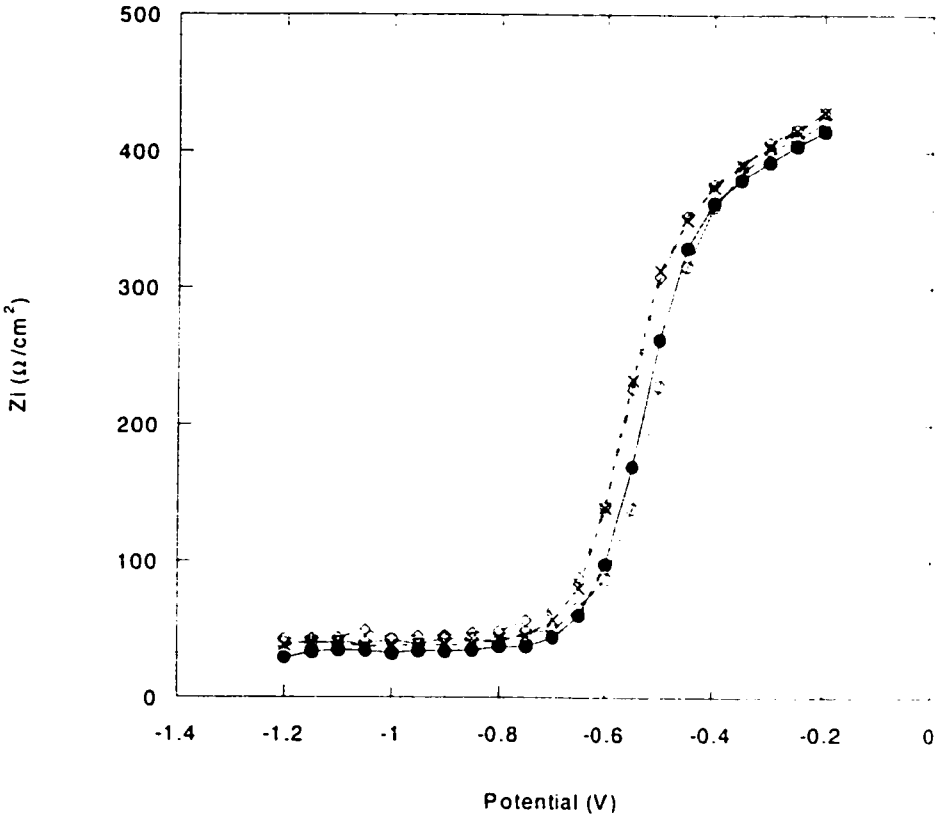

Figure 4.17 Reproducibility of substrates 1 – 4 (o, •, ◇, and x respectively) treated with glutaraldehyde.

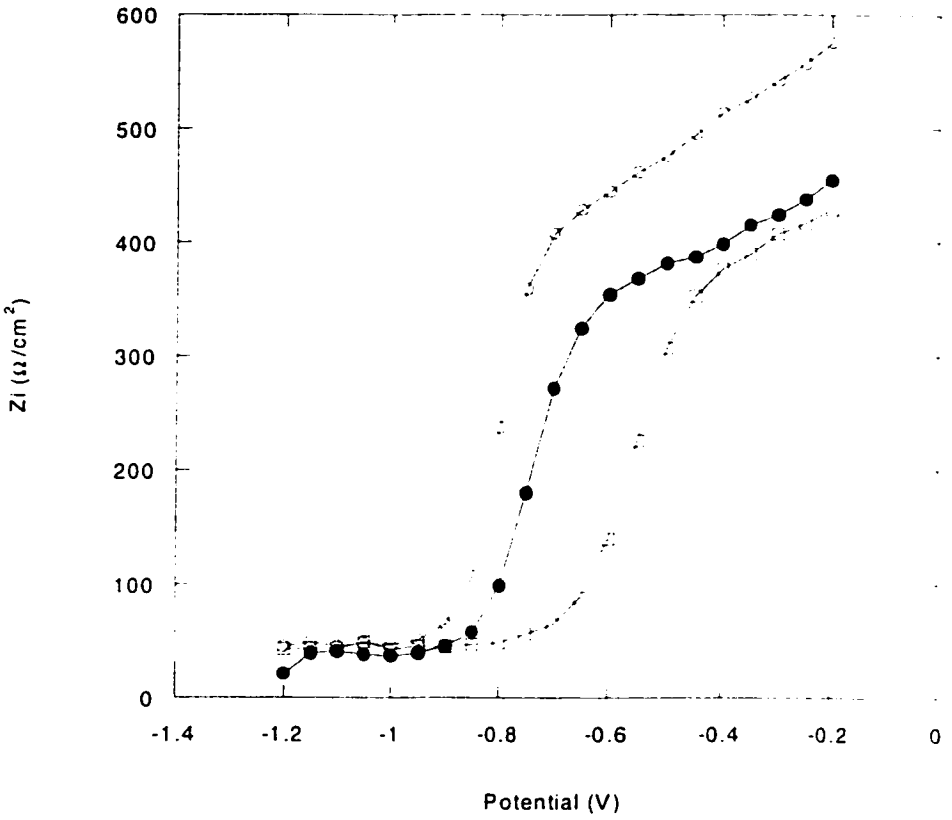

Figure 4.18 Impedance curves for each step in the preparation of substrate 3 (etched (o), functionalized (after NH_2) (•) and glutaraldehyde (□)).

Figure 4.18 shows how the impedance varies following the preparation steps of etching, functionalization with the diazonium (after reduction to an amino group), and the glutaraldehyde treatment for substrate 3 taken from Figures 4.15, 4.16 and 4.17. The V_{fb} was determined to be –0.89V, -0.86V and –0.68V following each step, respectively. As illustrated, there is a positive shift of 30mV between the etching and the functionalization (after reduction of the nitro group) steps. This small shift may be due to the presence of the hydrogen atoms of the amino group, which interacts with the electrolyte in a manner similar to the etched substrate that forms a hydrogen-terminated silicon layer. The average shift in the V_{fb} (for 50 substrates) between the functionalization (after reduction

into amino group) step and the glutaraldehyde treatment is approximately 150mV resulting in a V_{fb} at –0.74V ±0.10.

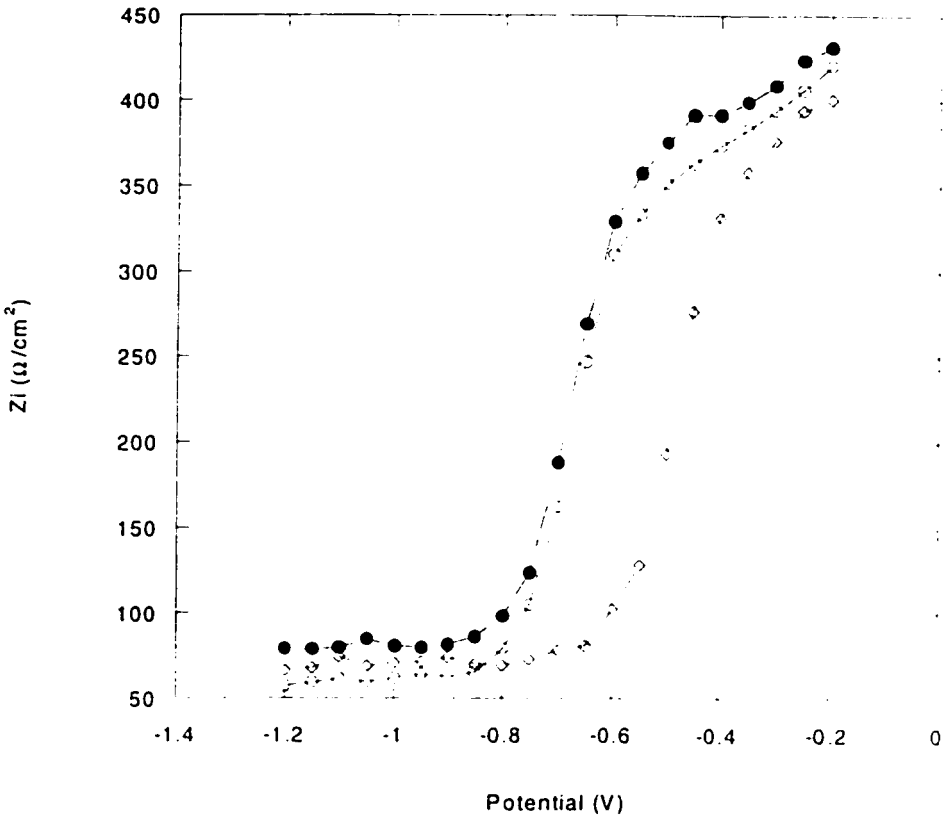

Figure 4.19 Impedance curves for a functionalized of the substrate on first day (o), the second day (•) and after activation of the substrate with glutaraldehyde (◊).

On an interesting note, Figure 4.19 illustrates the changes in the impedance curve when the substrate is treated with glutaraldehyde on a second day. The first curve (o) is the initial impedance curve of the functionalized substrate on day 1. The second curve (•) is the impedance curve of the same substrate on the second day to see if there were any changes when left overnight. In most cases, there is only a slight shift of 10mV or

less due the exposure to the environment. The third curve (◊) is after the treatment with glutaraldehyde and the shift in the V_{fb} is approximately 0.19V, which is in accordance with other substrates that are activated within the same day. It can be noted that the substrates are stable once they are functionalized and they can be activated the following day without too much difference in the flat-band potentials.

4.4.1.5 Immobilization of the Oligo(dT)$_{20}$ Probe Layer

Figure 4.20 shows the shift in the impedance between the glutaraldehyde treatment and that of a blank for the immobilization. The blank is basically the deposition of the 3mM $NaHCO_3$ solution (without any oligos) used in the immobilization step. There is generally a slight shift (0 to -40mV between batches) observed with the blank and this may be due to unspecific absorption of ions onto the semiconductor's surface. By knowing how much of a shift is produced by the blank, it can then be subtracted from that of the actual immobilization of the probe layer.

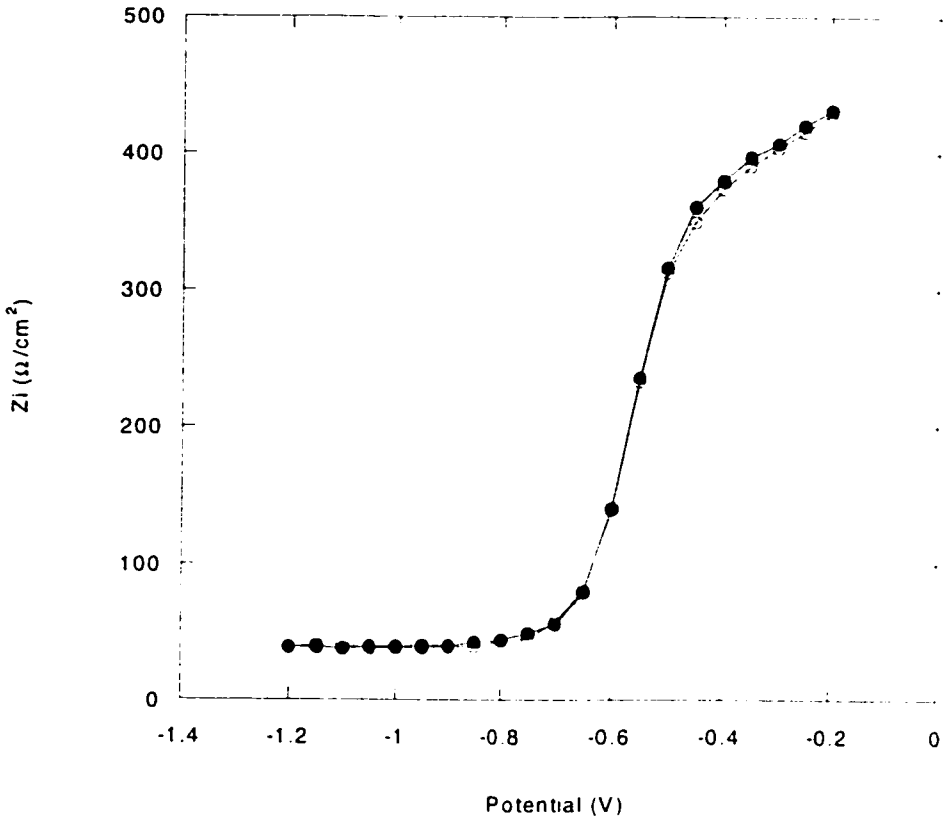

Figure 4.20 Impedance curve for the blank (o) (3mM $NaHCO_3$, no DNA) used in the immobilization of the probe layer following the glutaraldehyde treatment (•).

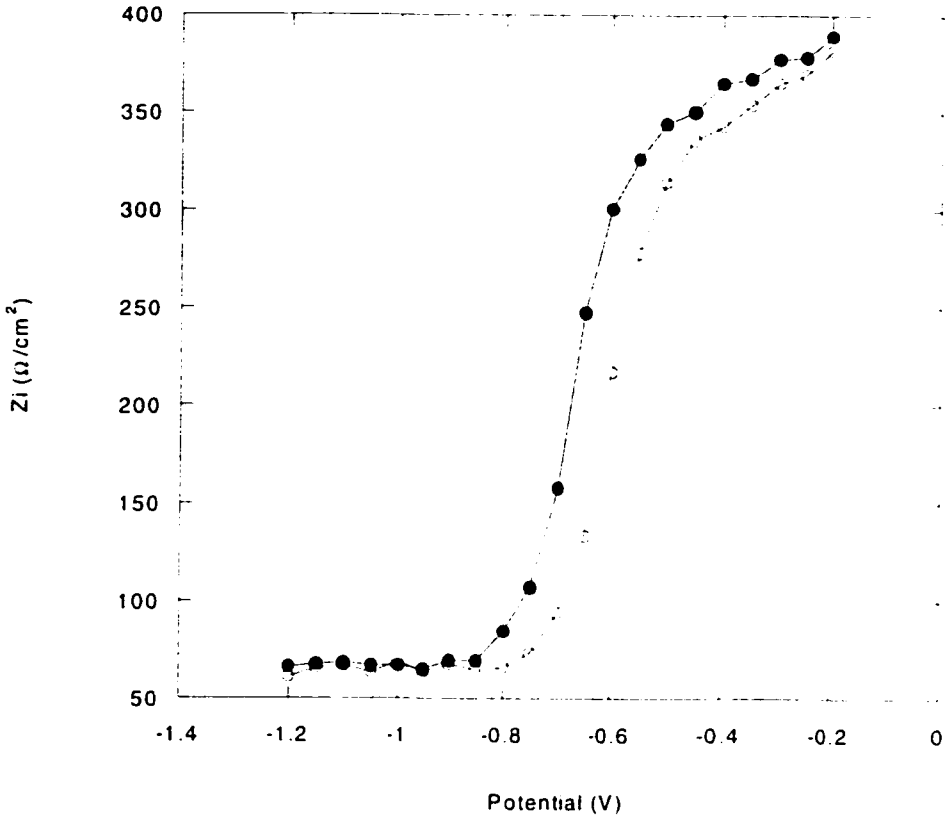

Figure 4.21 Immobilization of the oligo(dT)$_{20}$ (•) following glutaraldehyde treatment (o).

Figure 4.21 shows a -80mV shift (after subtraction of 0mV for the blank) upon the immobilization of the oligo(dT)$_{20}$ probe layer. It was observed that the longer the immobilization period was (1 hour vs. 15 minutes), the larger the impedance shift, which may indicate a denser concentration of the probe layer. The main disadvantage is that a denser probe layer would allow for less room for the complementary strand to come in and hybridize (Figure 4.23). Therefore, an immobilization time of 45 minutes was used since it provided good results for hybridization. Despite that, there is generally a negative shift in the V_{fb} due to the immobilization of the probe layer on the dielectric

surface which varies from –50 to -100mV between batches. On average, the V_{fb} is –0.74V ±0.07 (after subtraction of blank, -40mV) for 15 substrates.

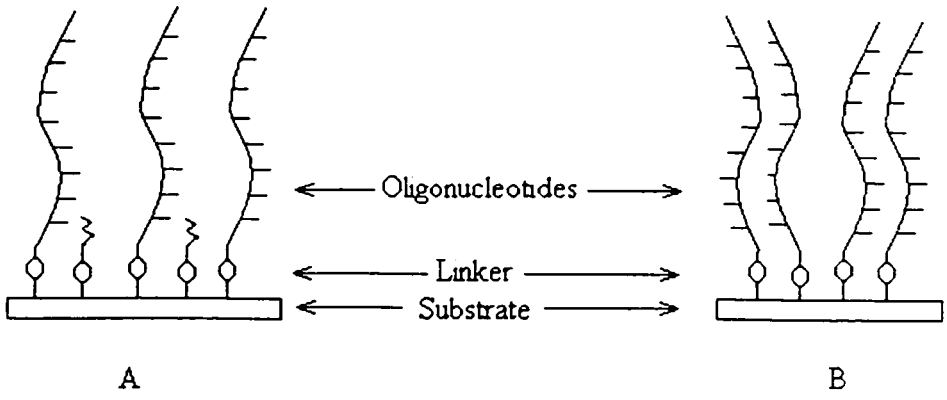

Figure 4.22 Illustration of the ideal immobilization (A) and possible outcomes (B).

4.4.1.6 Hybridization of Complemenatry Oligo(dA)$_{20}$

Following the immobilization of the probe layer, it is then hybridized with the complementary oligonucleotide sequence. Figure 4.23 illustrates the difference in the impedance for a blank used in the hybridization stage (a substrate immobilized with an oligo probe layer that is subsequently immersed in the hybridization solution without the complementary oligomer). It shows that there is a shift of 70mV ±10 due to the solution itself. Although a higher salt concentration (i.e. 1.0M NaCl, 15mM Tris-HCl, 0.01M PBS or 0.1M sodium citrate) would provide better hybridization conditions, this made determining whether the shift in the impedance was due to the hybridization event or the electrolytes more difficult. As a result, a lower concentration was used (1mM sodium citrate).

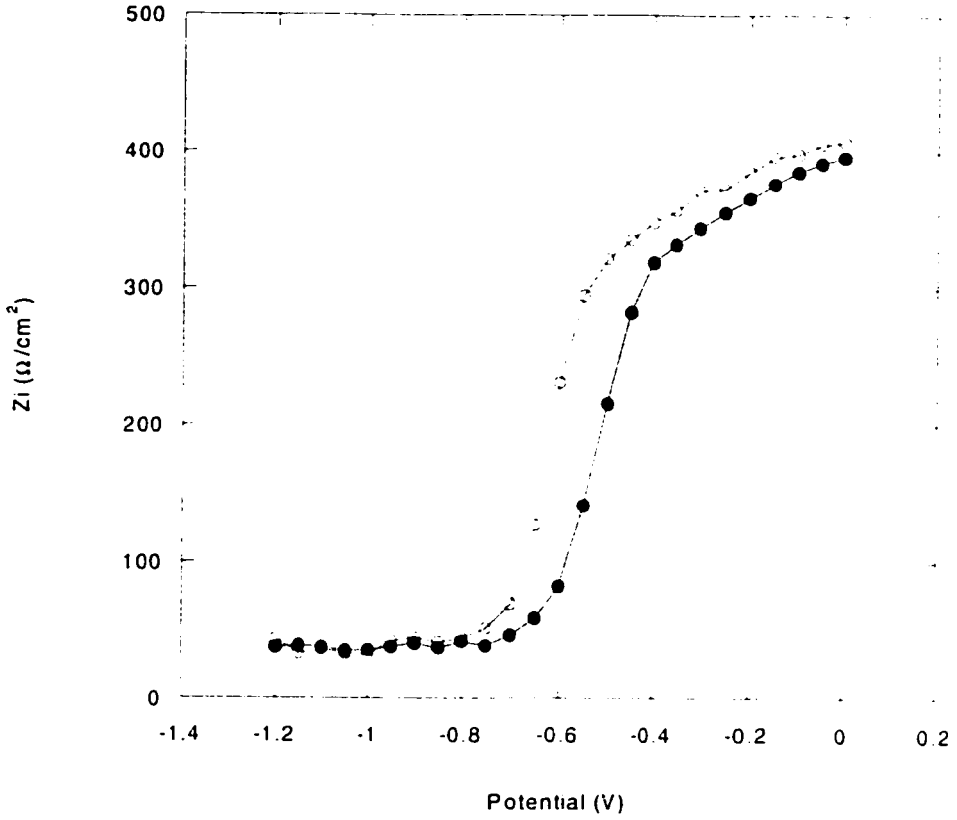

Figure 4.23 Substrate with an immobilized oligo(dT)$_{20}$ probe layer (•) was used as a blank (o) (0.001M sodium citrate, no DNA) in the hybridization.

Figure 4.24 illustrates the shifts due to the hybridization event between the immobilized oligo(dT)$_{20}$ probe layer and the complimentary oligo(dA)$_{20}$. In this case, there is a shift of 80mV (after the subtraction of the blank, 70mV) for the hybridization event. Overall however, the results for hybridization under these conditions showed poor reproducibility between batches with the flat band potential shifts varying between 50 and 150mV after subtraction of the blank.

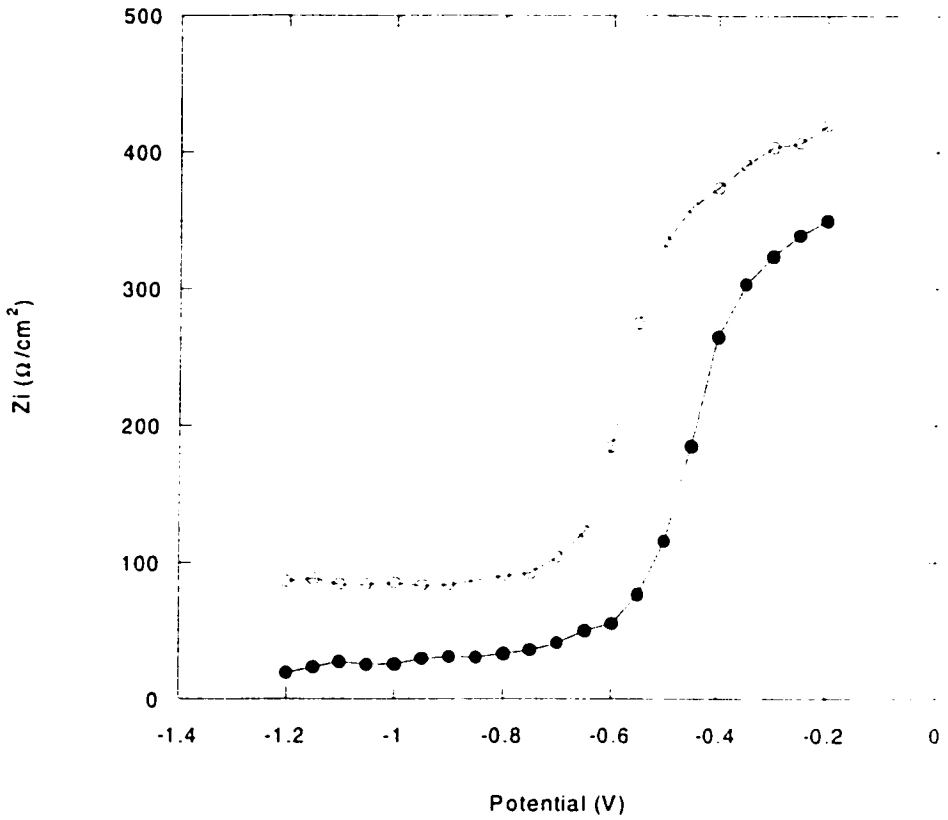

Figure 4.24 Shift in the impedance curve upon the hybridization of the oligo(dT)$_{20}$ probe layer (o) with complementary oligo(dA)$_{20}$ (•) nucleotide.

These variations in response may depend on how well the complementary strand can orient itself to hybridize with the probe layer as shown in Figure 4.26. Other factors to consider would the be desorption of the DNA from the probe's surface due to non-ideal (low salt concentration) hybridization conditions or the adsorption of the complementary strand onto multiple sites thus resulting in poor hybridization. However, it should be noted that when a good hybridization is obtained, the impedance shift is generally twice that of the shift for the immobilization of the probe layer with an average V_{fb} shift of 80mV ±10 for 10 different substrates.

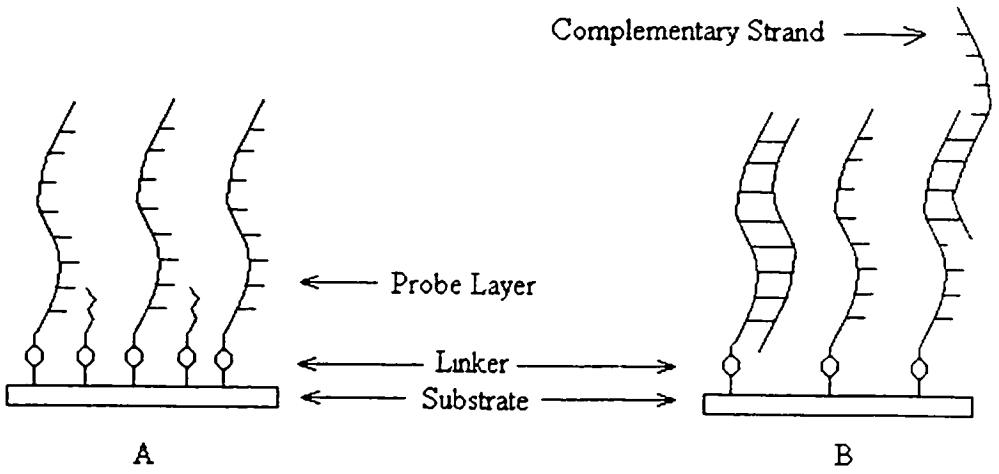

Figure 4.25 The ideal immobilized probe layer (A) with various hybridization (B) orientations.

4.4.1.7 Immobilization of Oligo(dA)$_{20}$ Probe Layer

As a comparison, an amino-linker oligo(dA)$_{20}$ was immobilized onto a substrate and subsequently hybridized with the complementary oligo(dT)$_{20}$, under the same reaction conditions, to determine how the structure of the nucleic acid would affect immobilization and subsequent hybridization. The blanks used for the immobilization and the hybridization stages for both these steps exhibit the same shifts in V_{fb} as previously described when the oligo(dT)$_{20}$ acts as the probe.

Figure 4.26 shows a shift of -40mV (after subtraction of the blank, 0mV) upon the immobilization of the amino-linked oligo(dA)$_{20}$ probe layer following the glutaraldehyde treatment. The larger shift observed for the immobilization of the oligo(dT)$_{20}$ probe layer compared to that of the oligo(dA)$_{20}$ may be attributed to the structure of the nucleic bases themselves. Recall from Figure 1.1 that the adenine base has an amino functional group attached to it while thymine does not. In the case of the amino-linked oligo(dA)$_{20}$, the oligonucelotide may not be immobilized properly on the surface. Instead of having the

oligo oriented in an orderly fashion by being attached to the surface through its amino linker, but the amino groups on the adenine base may also bind to the glutaraldehyde on the surface (i.e. laying flat or bound at multiple sites), thus affecting the amount of oligonucleotides immobilized onto the surface as a probe layer. There is generally a shift of -20 to -60mV between batches (after blank subtraction) for the immobilization of the oligo$(dA)_{20}$ probe layer. The average shift in the V_{fb} was found to be –50mV ±10 for 30 substrates.

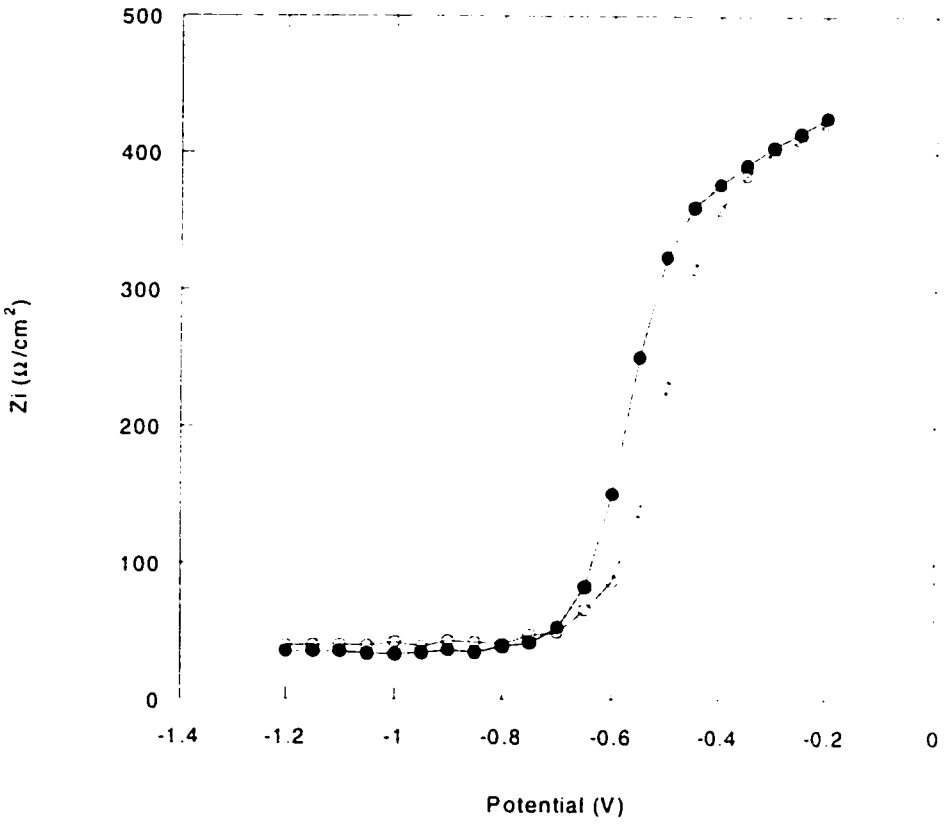

Figure 4.26 Impedance curve for the immobilization of the oligo$(dA)_{20}$ probe layer (•) after gluataraldehyde treatment (o).

4.4.1.8 Hybridization of the Complementary Oligo(dT)$_{20}$

Figure 4.27 illustrates the shift in the impedance curves following the hybridization of the complementary oligo(dT)$_{20}$ to the oligo(dA)$_{20}$ probe layer. In this case, there is a shift of 90mV (after subtraction of the blank). Due to the nature of the immobilization using this probe, the shifts in the immobilization of the oligo(dA)$_{20}$ probe layer also varies, but are generally smaller compared to that of the oligo(dT)$_{20}$ probe layer. However, upon the hybridization of the oligo(dA)$_{20}$ probe layer with its complementary strand (oligo(dT)$_{20}$), the shifts in the V_{fb} varies greatly from 60 to 200mV (after blank subtraction) between batches. The average shift in the V_{fb} was 70mV ±10 for 15 substrates.

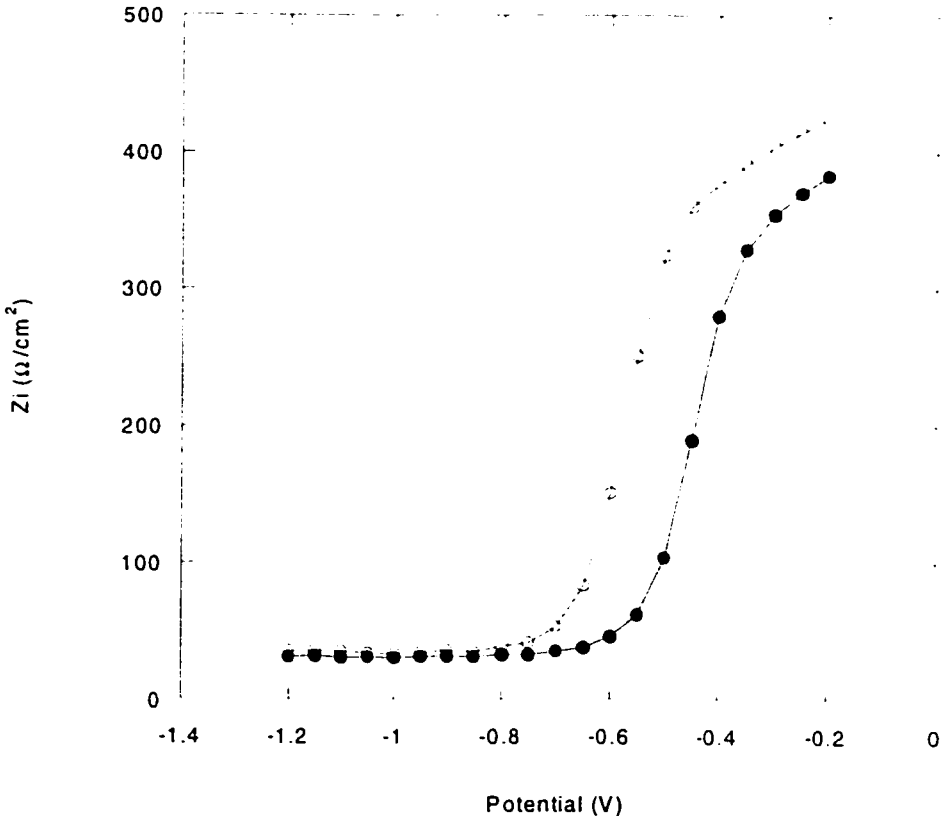

Figure 4.27 Shift in the impedance curve upon the hybridization of the oligo(dA)$_{20}$ probe layer (o) with complementary oligo(dT)$_{20}$ (•) nucleotide.

4.4.2 Preliminary Impedance Results for Si(111)

4.4.2.1 Comparison of Si(111) and Si(100)

As briefly discussed in Section 4.4.1, the orientation of the silicon crystal should have an effect on the impedance measurements. Figures 4.28 and 4.29 show a comparison between a Si(111) substrate and a Si(100) substrate. For the Si(111) substrate, the V_{fb} following the etching treatment occurs at a more positive potential, at approximately -0.58V ±0.07 compared to the –0.90V ±0.05 of the Si(100). Another difference lies in how much the V_{fb} of the Si(111) shifts following the initial functionalization of the substrate, in this case, approximately 0.16V compared to the 0.10V of the Si(100). Furthermore, the reduction of the nitro group into an amino group only shifts the V_{fb} –30mV towards the initial etched curve at –0.58V for the Si(111), thus giving a V_{fb} of –0.44V. In contrast, the reduction of the Si(100) substrates brings the V_{fb} towards the etched curve by –0.15V to a V_{fb} of –1.1V, which is similar to the V_{fb} of the etched curve (-0.90V). The larger shift in V_{fb} observed with the Si(111) substrates may be an indication of a denser layer of diazonium on its surface compared to Si(100) substrates.

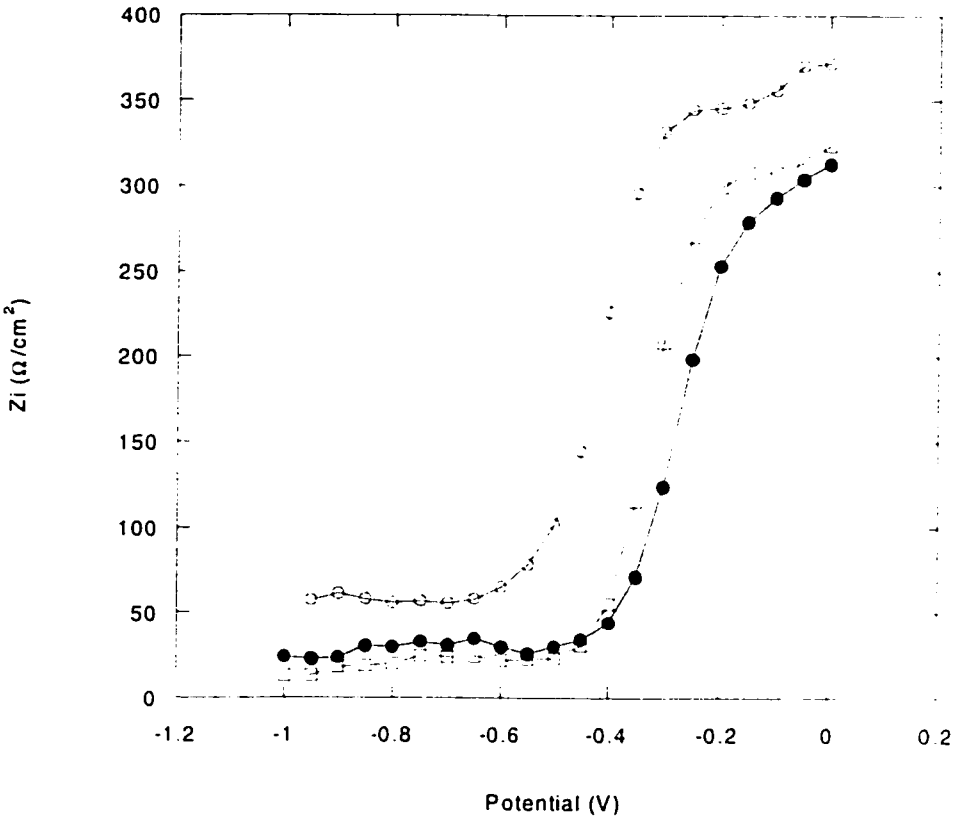

Figure 4.28 Shift in V_{fb} for the Si(111) substrate (etched (o), functionalized with 4-nitrobenzene (•) and reduction of nitro group into an amino group (□)).

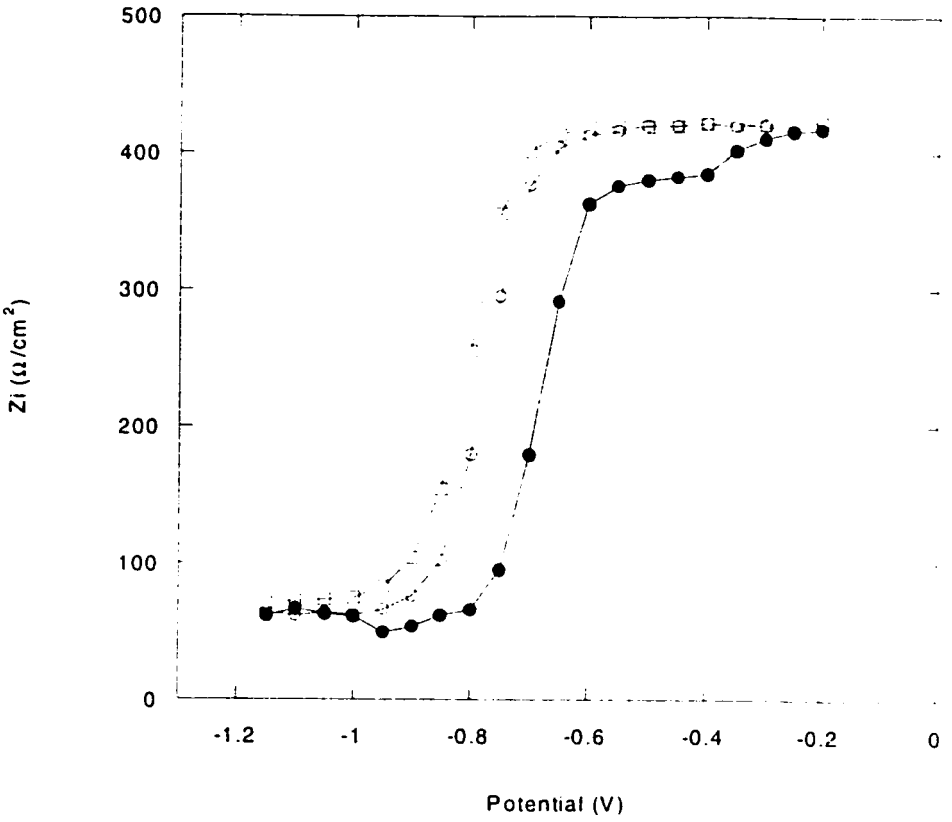

Figure 4.29 Shift in V_{fb} for the Si(100) substrates (etched (o), functionalized with 4-nitrobenzene (•) and reduction of nitro group into an amino group (□)).

4.4.2.2 Preparation of the Si(111) Substrates

The Si(111) substrates were prepared in the same manner as the Si(100) oriented substrates. Figure 4.30 shows a summary of the impedance curves obtained for the preparation of the substrates (i.e. etching, functionalization and reduction, and glutaraldehyde modifications). Between the etched and the functionalized substrate, there is a 150mV shift in the flat-band potential. Following the glutaraldehyde treatment, the shift is very small and only corresponds to 70mV. In most cases, there is only a small shift observed for the Si(111) substrates following the glutaraldehyde treatment. The average V_{fb} for 30 substrates were determined to be –0.58V ±0.07, -0.43V ± 0.05 and

-0.38V ±0.05 for the etched, functionalized (after reduction of nitro groups) and glutaraldehyde respectively.

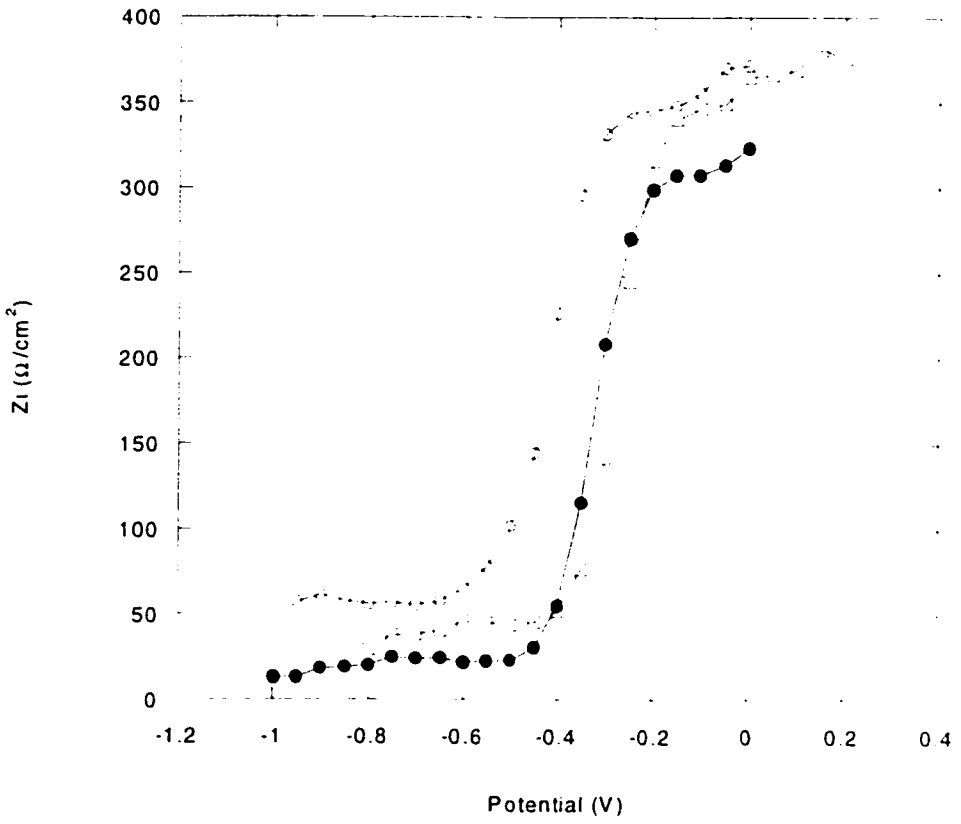

Figure 4.30 Shifts in the V_{fb} for the preparation stages (etched (o), functionalized (•) and glutaraldehyde treatment (□)).

4.4.2.3 Immobilization of the Oligo(dT)$_{20}$ Probe Layer onto Si(111)

Figure 4.31 represents a blank for the immobilization step. In this case, a substrate treated with glutaraldehyde has the oligo(dT)$_{20}$ immobilization solution (3mM $NaHCO_3$, no oligo(dA)$_{20}$) deposited on its surface. Following the immobilization period, the substrate was washed and the impedance measurement was taken. Like the Si(100), the impedance curve for the blank only shifts very slightly (about 1 to 5mV).

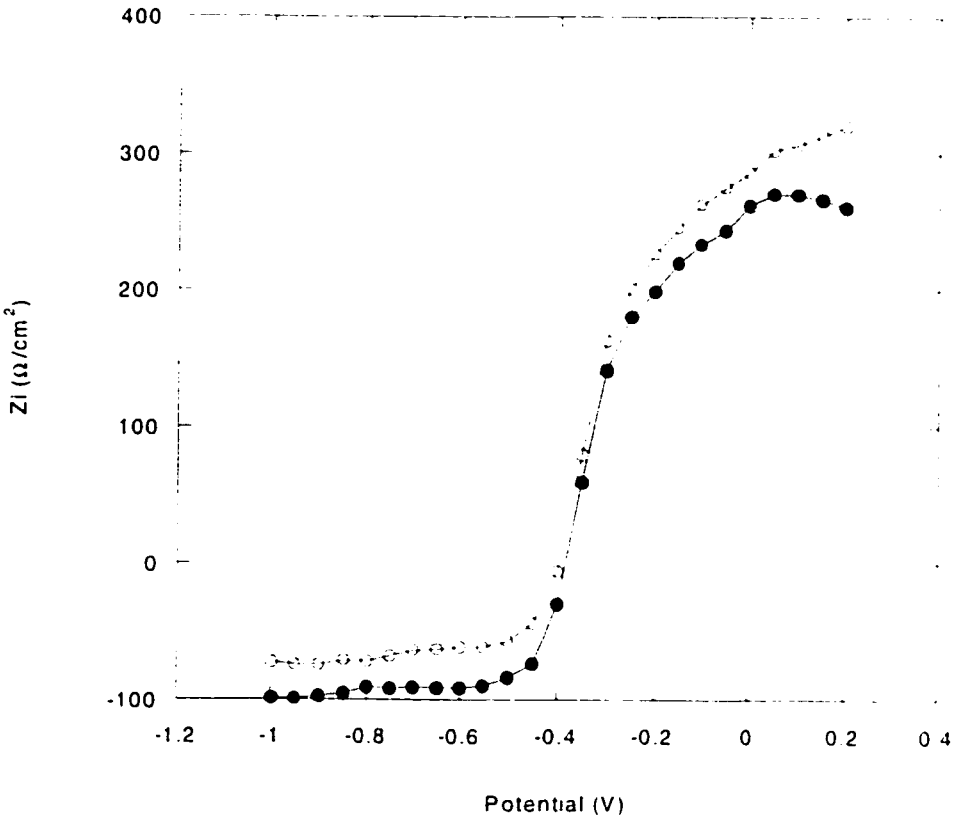

Figure 4.31 Impedance curve for the blank (3mM $NaHCO_3$, no DNA) used in the immobilization (o) following the glutaraldehyde treatment (•).

Figure 4.32 shows the impedance curve for the immobilization of the oligo(dT)$_{20}$ probe layer following the glutaraldehyde treatment. In this case, there is only a small shift of –15mV in the V_{fb} (after subtraction of the blank) which would indicate that the amount of probe immobilized is less than in the Si(100) case. The average shift in the V_{fb} was found to be 17mV ±5 for 15 substrates.

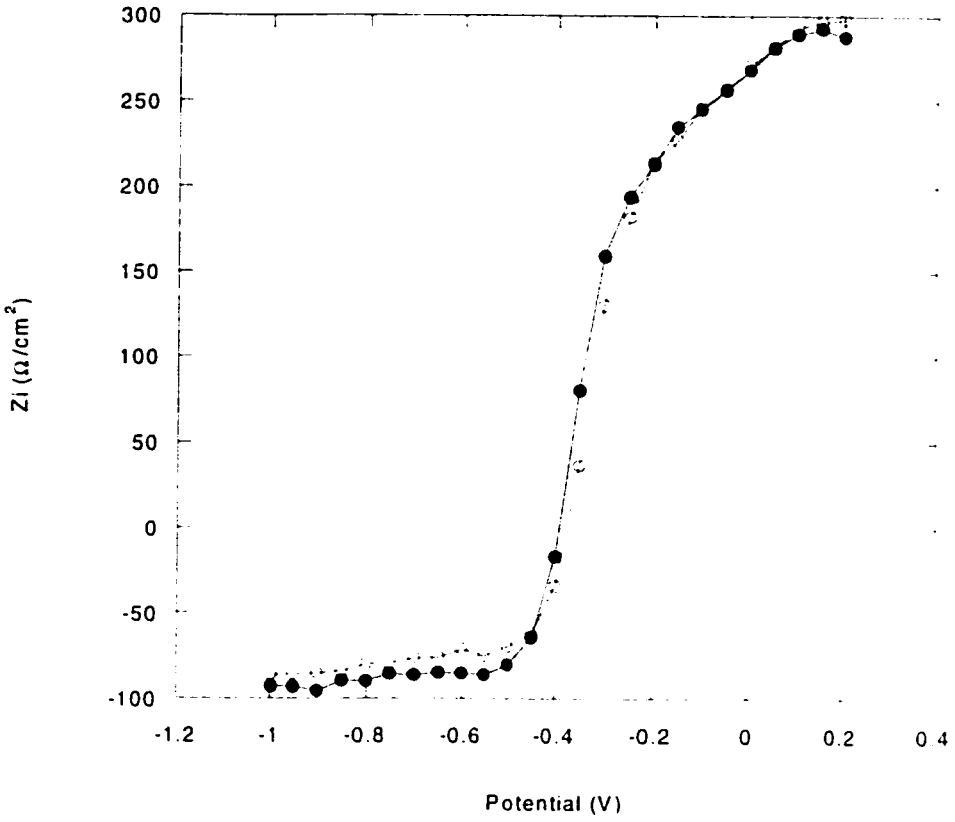

Figure 4.32 Immobilization of the oligo(dT)$_{20}$ (•) probe layer following glutaraldehyde treatment (o).

4.4.2.4 Hybridization of the Complementary Oligo(dA)$_{20}$

Figures 4.33 and 4.34 are the impedance curves for the hybridization blank and the hybridization of the complementary oligo(dA)$_{20}$ strand to the immobilized oligo(dT)$_{20}$ probe layer, respectively. As shown in Figure 4.33, the solution used for the hybridization event (1mM sodium citrate) shows little or no shift in the V_{fb}.

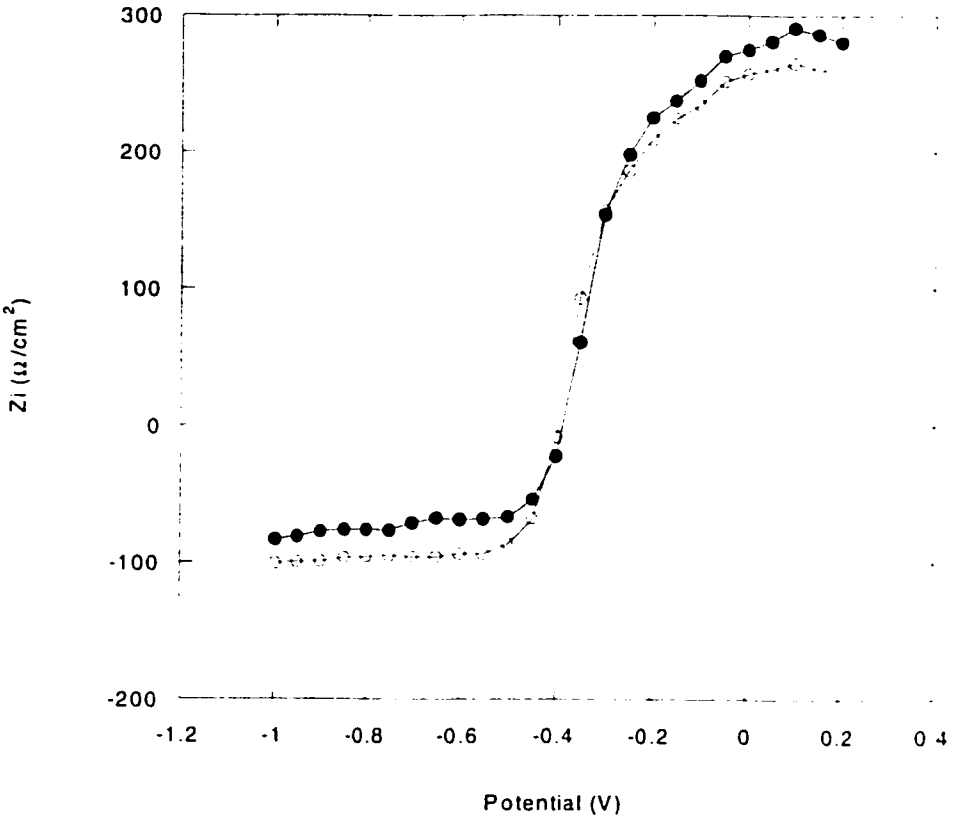

Figure 4.33 Immobilized oligo(dT)$_{20}$ probe layer (•) was used as a blank (0.001M sodium citrate, no DNA) in the hybridization solution (o).

Figure 4.34 shows the impedance curves for the hybridization of the immobilized oligo(dA)$_{20}$ probe layer with the complementary oligo(dT)$_{20}$ nucleotide sequence. In this case, there is a small shift of approximately 50mV. In general, shifts in the flat-band potentials for the hybridization of the Si(111) immobilized oligo(dT)$_{20}$ probe layer were small, at 45mV ±5 (for 10 substrates) compared to the 50 to 150mV (after subtraction of the blank) of the Si(100) substrates. This result is also in agreement with the fact that the immobilization of the probe layer on the Si(111) substrates is less efficient.

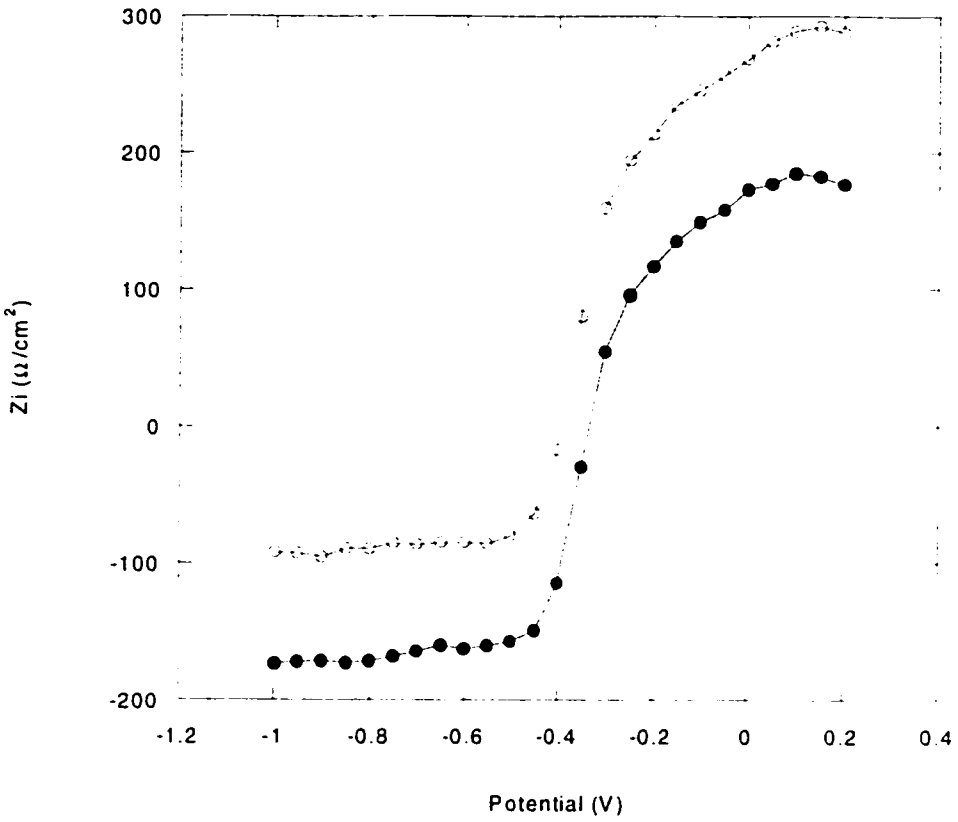

Figure 4.34 Impedance curve for the hybridization of the complementary oligo$(dA)_{20}$ (•) to the oligo$(dT)_{20}$ probe layer (o).

4.4.2.5 Immobilization of the Oligo$(dA)_{20}$ Probe Layer

The immobilization of the oligo$(dA)_{20}$ probe layer was also tested to determine its effectiveness. Upon immobilization of the oligo$(dA)_{20}$ probe layer following the glutaraldehyde treatment (Figure 4.35), there seems to be no shift observed as both curves overlap exactly.

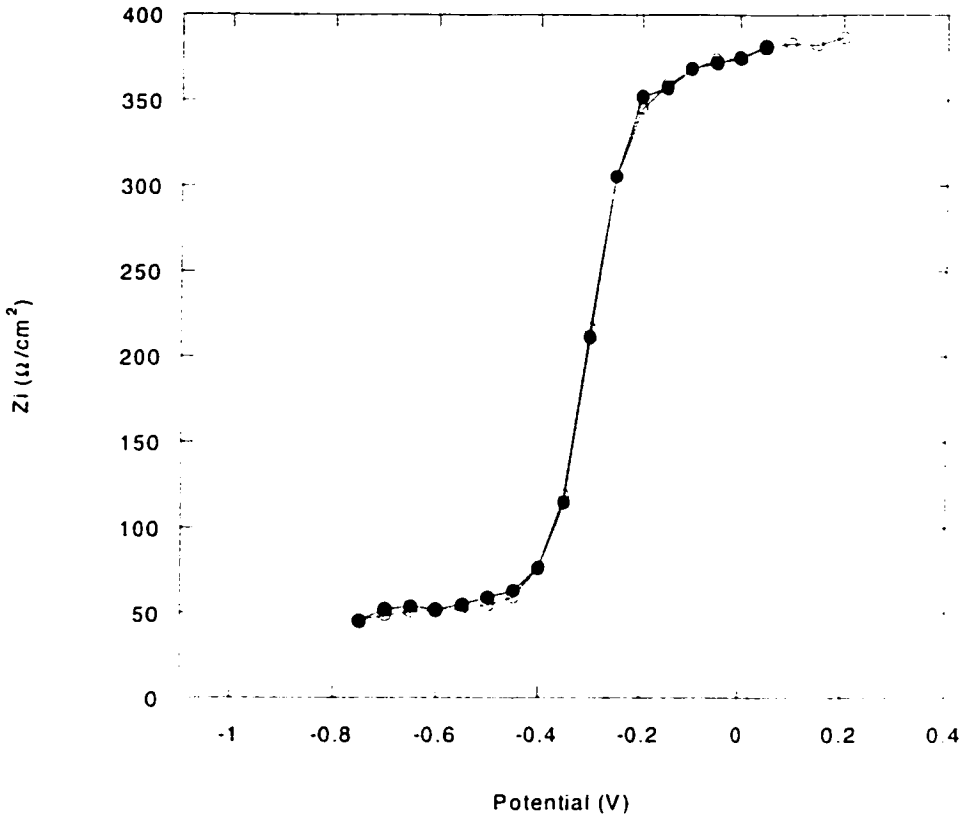

Figure 4.35 Impedance curve for the immobilization of the oligo(dA)$_{20}$ probe layer (•) after glutaraldehyde treatment (o).

4.4.2.6 Hybridization of the Complementary Oligo(dT)$_{20}$

Upon hybridization of the oligo(dA)$_{20}$ probe layer with the complementary oligo(dT)$_{20}$, there was only a slight shift of 30mV in the V_{fb} (Figure 4.36). Although there is a shift present, it can be assumed that this is due to non-specific adsorption of the oligo(dT)$_{20}$ onto the surface of the substrate since immobilization of the probe layer is apparently unsuccessful. In general, the shifts in the V_{fb} for the hybridization are very small (about 50mV or less after subtraction of a blank, 10 substrates) compared to the Si(100) substrates.

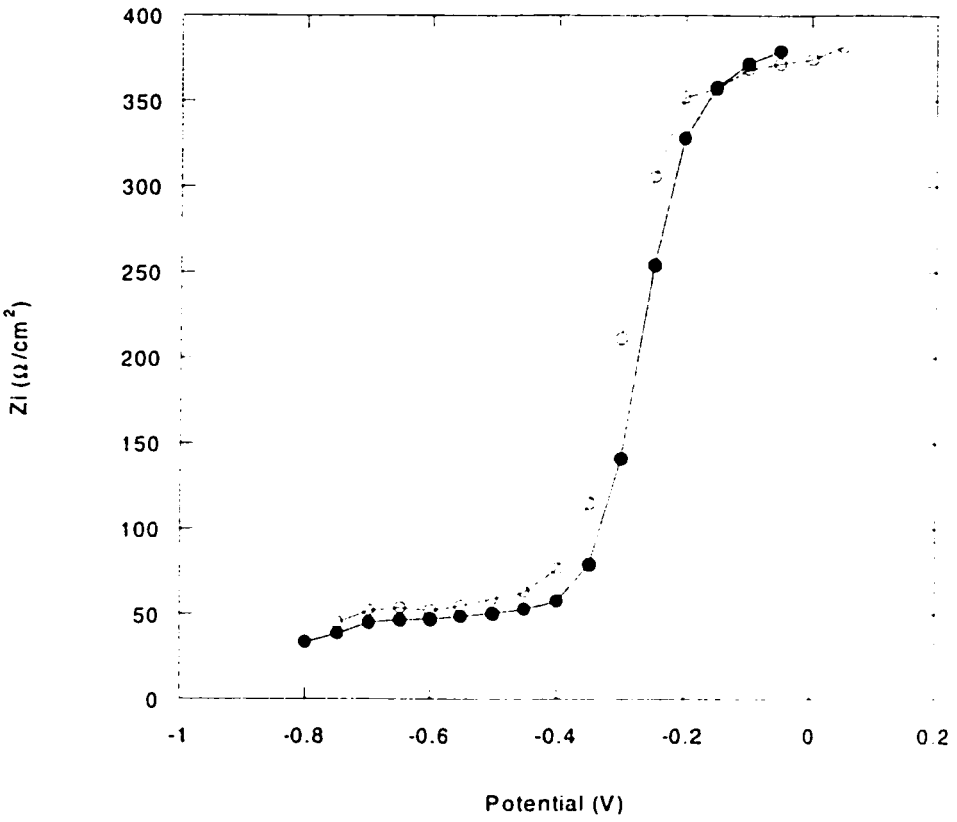

Figure 4.36 Impedance curve for the hybridization of the complementary oligo(dT)$_{20}$ (•) to the oligo(dA)$_{20}$ probe layer (o).

Based on these results, it can be inferred that the functionalization of the Si(100) appears to be more efficient for the immobilization of the probe layer. As a result, the shifts in the flat-band potentials of the Si(100) are more pronounced than the Si(111). The ideal experimental conditions for the Si(111) have yet to be determined.

4.5. Temperature Dependence of Impedance: T_m Measurements

The temperature dependence of impedance curves was used in an attempt to determine the melting temperature (T_m) of the oligodT-oligodA duplex used in these studies duplex. The melting point of a duplex can be calculated using the following empirical formula: [64-65]

$$T_m = \frac{[81.5(°C) + 16.6 \log M + 0.41(\% G + C) - 500}{n - 0.61 (\% \text{ formamide})}$$

where $M = [Na^+] + [DNA]$

n = number of oligonucleotide base pairs

and (%G + C) = represents the G and C content of the oligonucleotide sequence.

In the next two sections, all the temperature-impedance measurements show a linear increase for the 1800 seconds (or 20 minutes) before it stabilizes at the maximum temperature for an additional 900 seconds (or 15 minutes).

4.5.1 T_m Measurements for Immobilized Oligo$(dT)_{20}$ Probe Layer

Figures 4.37 to 4.39 are the impedance-temperature ramp graphs generated during the melting point analysis of an immobilized oligo$(dT)_{20}$ probe layer on Si(100) substrates. Both of these figures show a fairly stable impedance curve in relation to the temperature ramp because there are no complementary strands present in the electrolyte. Figure 4.37 the temperature-impedance curve for a blank used in the immobilization

stage (3mM $NaHCO_3$, no oligo$(dT)_{20}$). Since there are no oligonucleotides immobilized onto the surface, the impedance remains fairly constant (as shown by a relatively straight line).

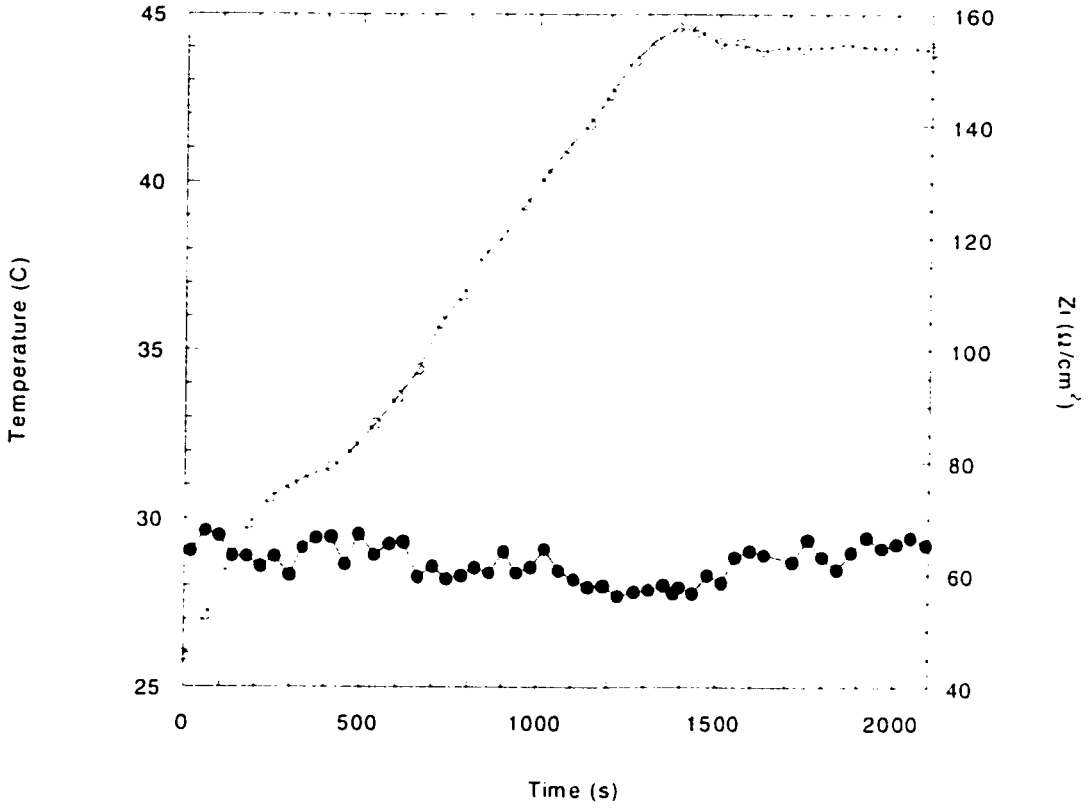

Figure 4.37 Temperature ramp (o) as a function of time for the impedance measurement of a blank immobilization (•).

Figure 4.38 represents the temperature-impedance curves of a substrate with the immobilized oligo$(dT)_{20}$ probe layer (no oligo$(dA)_{20}$ present in electrolyte). Since there is no complementary oligo$(dA)_{20}$ present in the sample, the impedance curve also exhibits a somewhat linear trend, although the data shows more fluctuation.

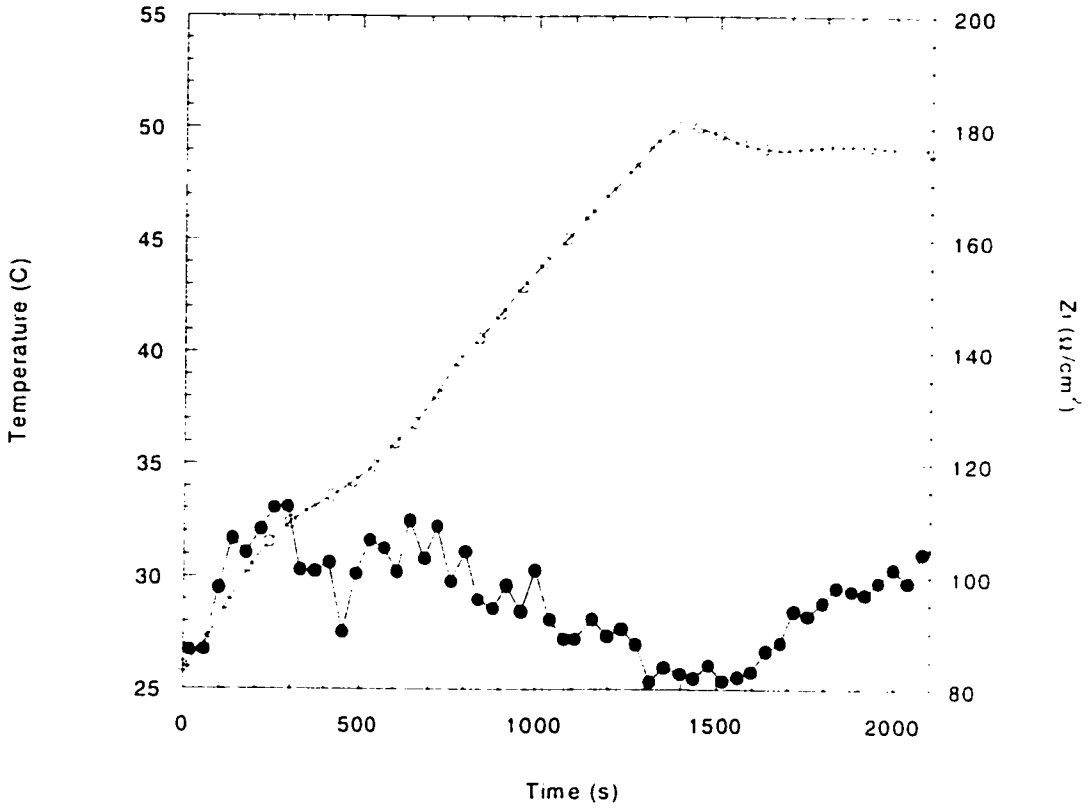

Figure 4.38 Temperature (o) – impedance (•) measurement as a function of time for an oligo(dT)$_{20}$ immobilized substrate.

Figure 4.39 shows the temperature-impedance curve for an oligo(dT)$_{20}$ immobilized probe layer that is hybridized with oligo(dA)$_{20}$. Initially, the drop in the impedance is rapid (in the first 100 seconds) and then it decreases gradually until it stabilizes (starting at 400 seconds). The point at which the impedance measurements first plateaus occurs at 31°C which coincides with the theoretical melting point of the 31.2°C for dT:dA duplex.

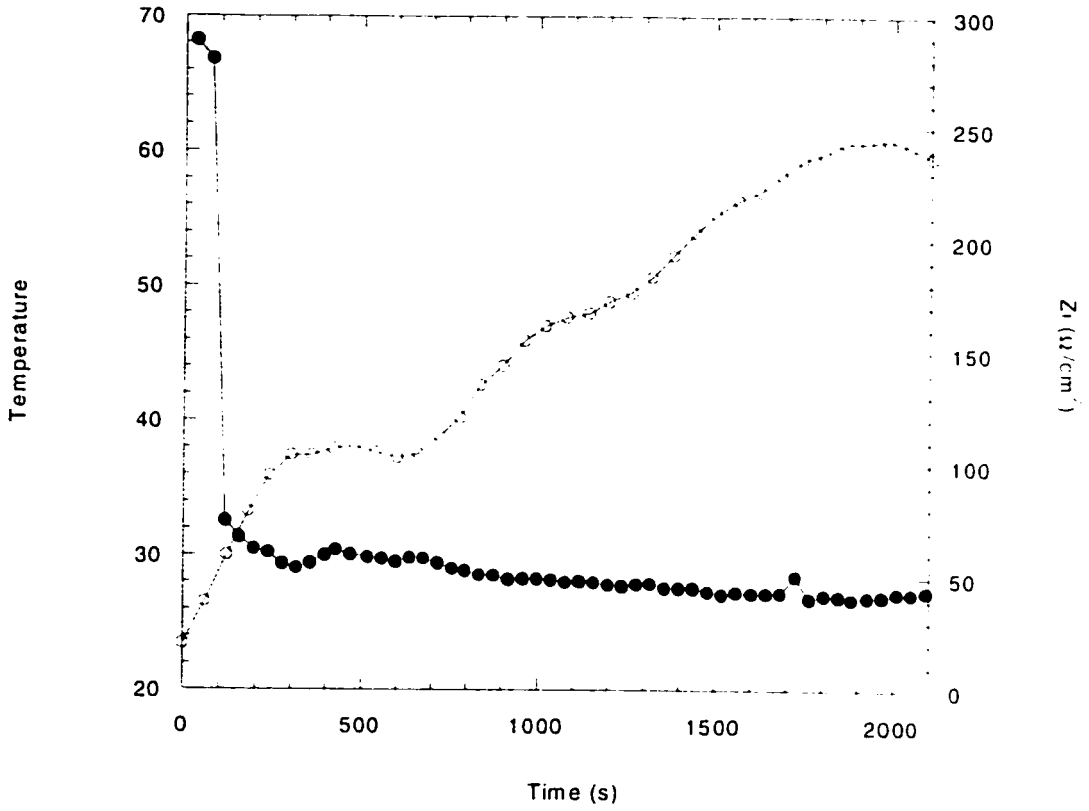

Figure 4.39 Temperature (o) – impedance (•) measurement as a function of time for an immobilized oligo(dT)$_{20}$ probe layer hybridized with oligo(dA)$_{20}$.

Figure 4.40 illustrates the changes in the impedance measurement throughout the T_m measurements. The initial impedance curve at –0.70V corresponds to the immobilized oligo(dT)$_{20}$ hybridized with oligo(dA)$_{20}$. The second impedance curve at –0.73V is the V_{fb} which corresponds to the circulation of the electrolyte. The third impedance curve at –0.71V corresponds to the flat-band potential after the T_m measurements were completed. This difference in shift between the initial measurement at –0.70V and the final one at –0.71V is 10mV.

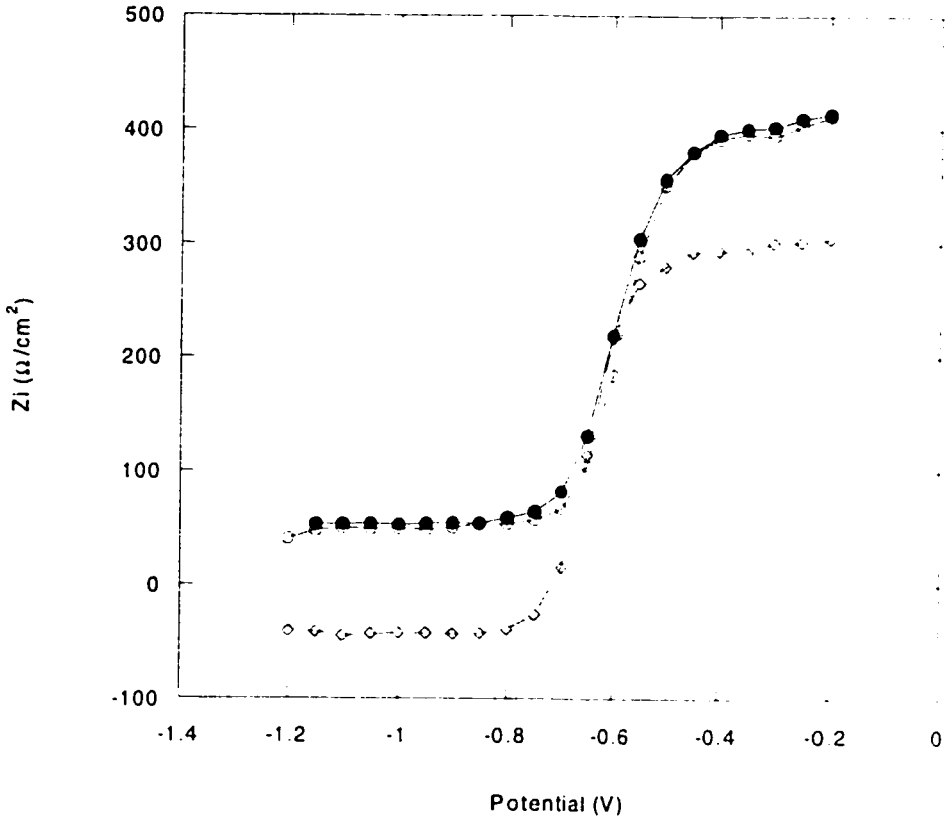

Figure 4.40 **Impedance curves for immobilized oligo(dT)$_{20}$ probe layer hybridized with the oligo(dA)$_{20}$ (o), fluid circulation (●) and after the completion of the T_m measurement (◊).**

4.5.2 T_m Measurements for Immobilized Oligo(dA)$_{20}$ Probe Layer

Temperature-impedance measurements were also performed on the substrates with the immobilized oligo(dA)$_{20}$ probe layer. The blank (3mM $NaHCO_3$ solution) used for the immobilization has the same profile as that for the immobilization of the oligo(dT)$_{20}$ probe layer (see Figure 4.37). Figure 4.41 represents the temperature-impedance measurement for a substrate with the immobilized oligo(dA)$_{20}$ probe layer. As in Figure 4.38 (oligo(dT)$_{20}$ probe layer), the impedance is relatively stable as the temperature ramp proceeds.

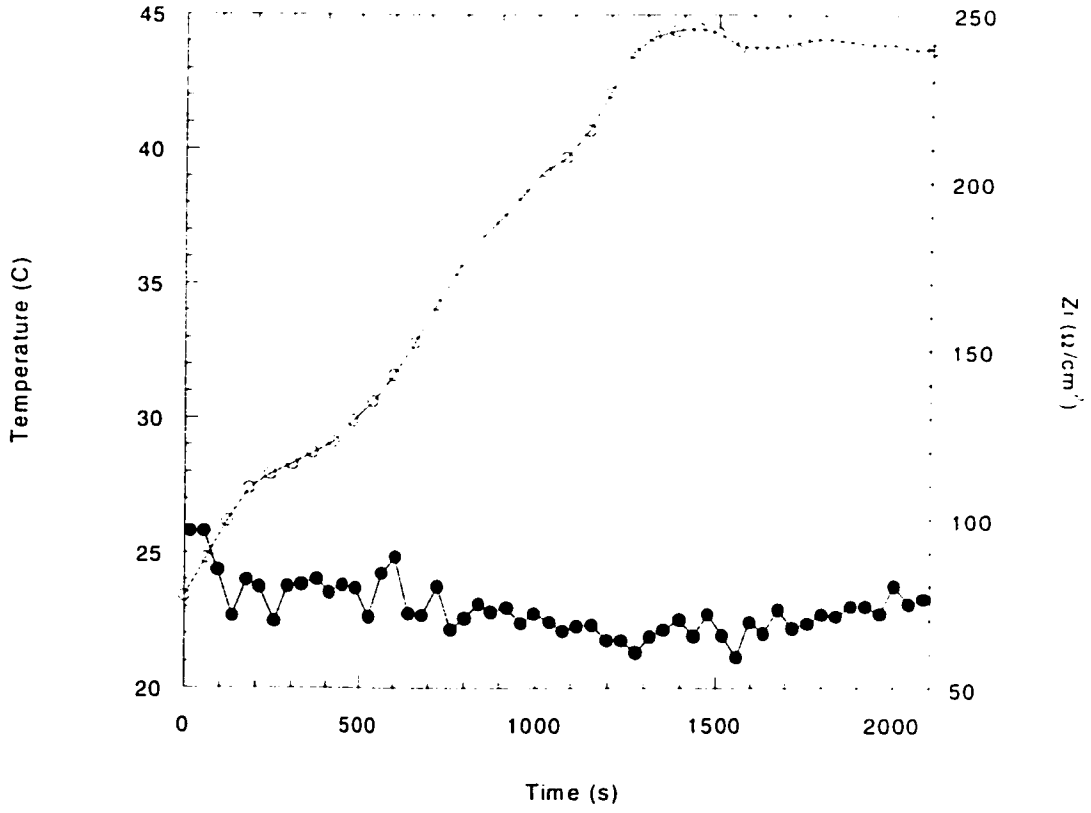

Figure 4.41 Temperature ramp (o) as a function of time for an oligo(dA)$_{20}$ immobilized substrate (●).

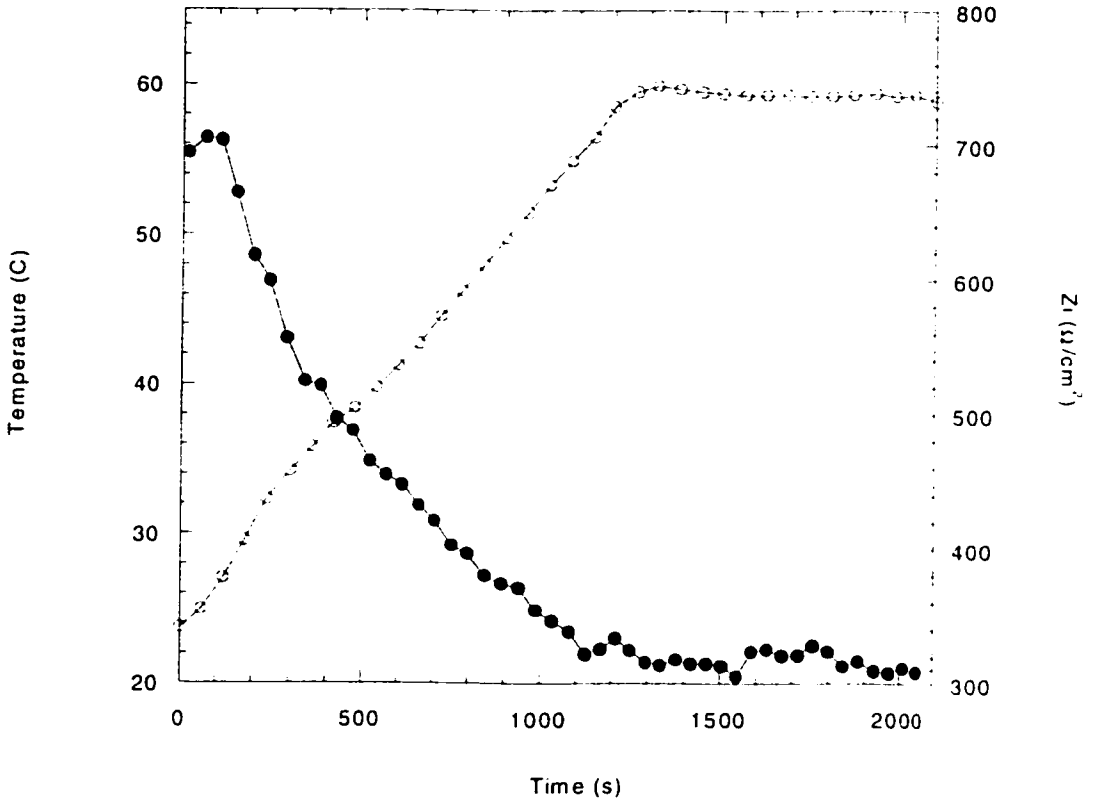

Figure 4.42 The temperature (o) - impedance (•) measurement as a function of time for an oligo(dA)$_{20}$ immobilized probe layer hybridized with oligo(dT)$_{20}$.

Figure 4.42 is the temperature-impedance measurement for the hybridization of the oligo(dT)$_{20}$ to the immobilized oligo(dA)$_{20}$ probe layer. In the first 100 seconds, there is a very small plateau in the impedance measurement and this may be the adsorption of the oligo(dT)$_{20}$ onto the surface of the substrate. Following this plateau, the impedance gradually decreases for another 1000 seconds before it stabilizes again. This gradual decrease gives a melting temperature at 54°C, which is significantly higher than the theoretical melting point (31.2°C).

The effect of non-specific adsorption was previously investigated by immersing a substrate immobilized with the oligo(dT)$_{20}$ probe layer into a solution containing the non-

complementary oligo$(dG)_{20}$. It was determined that about 30% of the signal in the impedance measurement was attributed to non-specific adsorption of the oligo$(dG)_{20}$.[65]

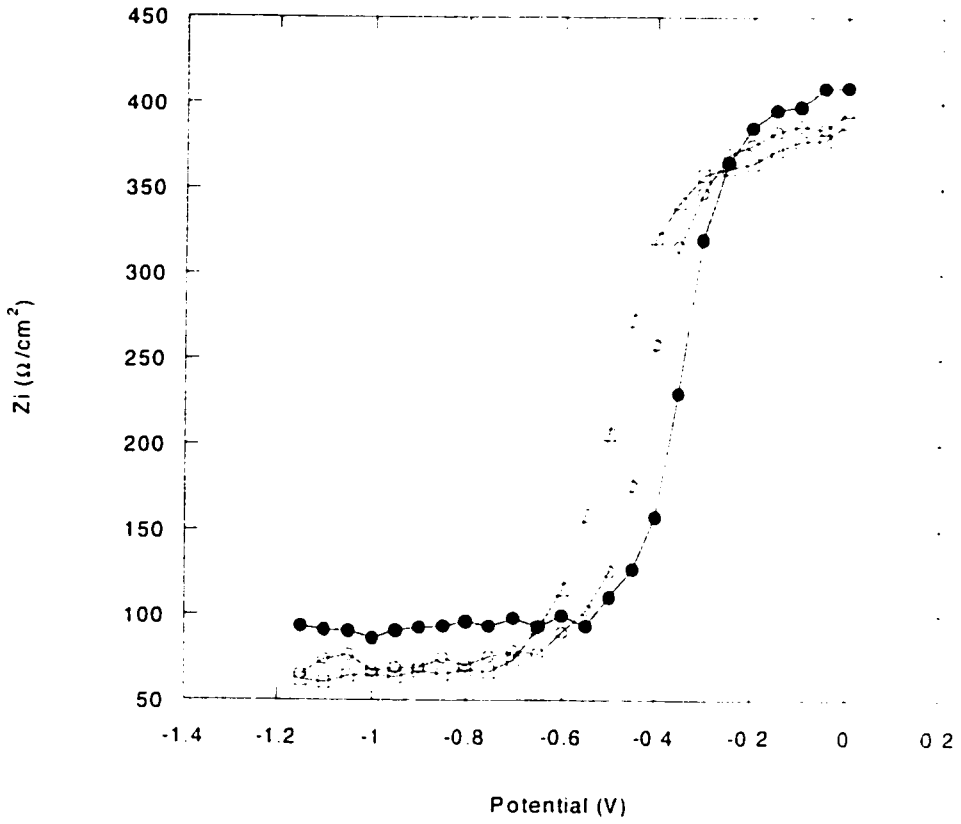

Figure 4.43 Impedance curves for immobilized oligo$(dA)_{20}$ probe layer hybridized with the oligo$(dT)_{20}$ (o), fluid circulation (•) and after the completion of the T_m measurement (□).

Figure 4.43 illustrates the changes in the impedance measurement throughout the T_m measurements. The initial impedance curve at –0.58V corresponds to the immobilized oligo$(dA)_{20}$ hybridized with oligo$(dT)_{20}$. The flat-band potential then shifts to –0.50V during upon fluid circulation. The last impedance curve shifts to –0.70V following the completion of the T_m measurements. The difference in shift between the initial measurement at –0.58V and the final one at –0.70V is 120mV which also

corresponds to the shift observed upon the hybridization. Although the T_m measurement shows that hybridization does occur, the quality it is not as good compared to that of the immobilized oligo$(dT)_{20}$ probe layer.

5. Conclusions and Future Work

5.1 Immobilization of Oligo(dT)$_{20}$ Probe Layer vs. Oligo(dA)$_{20}$

The main objective of this thesis was to develop a DNA biosensor using a silicon transducer. A novel approach to functionalization of the substrates used a diazonium moiety in order to create a well-order immobilized probe layer. This method proved that the functionalization of the silicon substrates using a diazonium moiety is rapid and gives reproducible results (up to the immobilization stage). The immobilization of the probe layer (oligo(dT)$_{20}$ or oligo(dA)$_{20}$) results in shifts of –50 to –100mV while hybridization of the complementary strand to the probe layer always gives a positive shift in the V_{fb} which is twice as large the shift of the V_{fb} of the immobilization. The temperature-impedance (T_m) measurements also showed that there was hybridization between the probe layer and the complementary strand as indicated by the measured T_m of 31°C, which is in good agreement with the calculated value. However, the impedance and T_m measurement results shows that immobilization of the oligo(dT)$_{20}$ as the probe layer more efficient that the oligo(dA)$_{20}$ for hybridization purposes.

5.2 Si(100) vs. Si(111) Oriented Substrates

A comparison between the Si(100) and Si(111) oriented substrates showed that the Si(100) was better suited for the procedure outlined in this study. The preliminary impedance results may indicate that functionalization of the Si(111) substrates leads to a denser probe layer, however, the immobilization of the oligomers showed a very small shift of -17mV . The ideal experimental conditions in this case have yet to be determined.

5.3 Suggestions for Future Research

Although the results from this study are promising, much work remains to be done in this matter. Future research would include the following:

1) Quantification through ^{32}P labeling to determine the amount of DNA immobilized onto the substrate and the amount hybridized (as fluorescence measurements were unsuccessful),
2) Determining how to prevent nonspecific adsorption of ions from the electrolyte onto the probe's surface,
3) Finding the ideal conditions for the immobilization of the a probe layer on the Si(111) substrates,
4) Using a guanidine-cytosine system or a mixed DNA sequence to determine how much of an effect it would have on the impedance measurements,
5) Functionalization with other types of diazonium salts.

References

1. Balakin, K.V., Korshun, V.A, Mikhalev, I.I, Maleev, G.V, Malakhov, A.D, Prokhorenko, I.A., Berlin, Y.A., *Biosensors & Bioelectronics*, 13, 1998, 771-778.

2. Pérez-Luna, V.H., Yang, S., Rabinovich, E.M., Buranda, T., Sklar, L.A., Hampton, P.D., Lopez, G.P., *Biosensors & Bioelectronics*, 17, 2002, 71-78.

3. Fotin, A.V., Drobyshev, A.L., Proudnikov, D.Y., Perove, A.N., Mirzabekov, A.D, *Nucleic Acids Research*, 26, 1998, 1515-1521.

4. Cloarec, J.P, Deligianis, N., Martin, J.R., Lawrence, I., Souteyrand, E., Polychronakos, C., Lawrence, M.F., *Biosensors & Bioelectronics*, 17, 2002, 405-412.

5. Rogers, K.R., Apostol, A., Madsen, S.J., Spencer, C.W., *Analytica Chimica Acta*, 444, 2001, 51-60.

6. Slavik, R., Homola, J., Brynda, E., *Biosensors & Bioelectronics*, 17, 2002, 591-595.

7. Piunno, P.A.E., Watterson, J., Wust, C.C., Krull, U.J., *Analytica Chimica Acta*, 400, 1999, 73-89.

8. Nelson, B.P., Grimsrud, T.E., Liles, M.R., Goodman, R.M., Corn, R.M., *Analytical Chemistry*, 2001, 73, 1-7.

9. Sawata, S., Kai, E., Ikebukuro, K., Iida, T., Honda, T., Karube, I., *Biosensors & Bioselectronics*, 14, 1999, 397-404.

10. Babacan, S., Pivarnik, P., Letcher, S., Rand, A.G., *Biosensors & Bioelectronics*, 15, 2000, 615-621.

11. Zhou, X.C., Huang, L.Q., Li, S.F.Y., *Biosensors & Bioelectronics*, 16, 2001, 85-95.

12. Su, X., *Biochemical and Biophysical Research Communications*, 290, 2002, 962-966.

13. Kurowski, A., Schultze, J.W., Lüth, H., Schöning, M.J., *Sensors and Acutators B: Chemical*, 83 (2002) 123-128.

14. Zhao, Y.A., Pang, D.W., Hu, S., Wang, Z.L., Cheng, J.K., Qi, Y.P., Dai, H.P., Mao, B.W., Tian, Z.Q., Luo, J., Lin, Z.H., *Analytica Chimica Acta*, 388, 1999, 93-101.

15. Brynda, E., Houska, J., Skvor, J., Ramsden, J.J., *Biosensors & Bioelectronics*, 13, 1998, 165-172.

16. Wang, J., *Biosensors & Bioelectronics*, 13, 1998, 757-762.

17. Verneulen, L.A., Smith, K., Wang, J., *Electrochimica Acta*, 45, 1999, 1007-1014.

18. Chrisey, L.A., Lee, G.U, O'Ferrall, E., *Nucleic Acids Research*, 24, 1996, 3031-3039

19. Barness, Y., Gershevitz, O., Sekar, M., Sukenik, C., *Langmuir*, 2000, 16, 247-251.

20. Joos, B., Kuster, H., Cone, R., *Analytical Biochemistryl*, 247, 1997, 96-101.

21. Rogers, Y.H., Jiang-Baucom, P, Huan, Z.J., Bogdanov, V., Anderson, S., Boyce-Jacino, M.T., *Analytical Biochemistry*, 266, 1999, 23-30.

22. Yang, M., Kong, R.Y.C., Kazmi, N., Leung, A.K.C., *Chemistry Letters*, 3, 1998, 257-258.

23. Takahashi, K., Seio, K., Sekine, M., Hino, O., Esashi, M, *Sensors and Actuators B*, 83, 2002, 67-76.

24. Williams, R.A., Blanche, H.W., *Biosensors & Bioelectronics*, 9, 1994, 159-167.

25. Singh, A.K., Flounders, A.W., Volponi, J.V., Ashley, C.S., Wally, K., Schoeniger, J.S., *Biosensors & Bioelectronics*, 14, 1999, 703-713.

26. Mishima, Y., Motonaka, J., Maruyama, K., Minagawa, K., Ikeda, S., *Sensors and Actuators B: Chemical*, 65, 2000, 340-342.

27. Strother, T., Cai, W., Zhao, X., Hamers, R., Smith, L.M., *Journal of American Chemical Society*, 122, 2000, 1205-1209.

28. Strother, T., Hamers, R.J., Smith, L.M., *Nucleic Acids Research*, 28, 2000, 3535-3541.

29. Ushizawa, K., Sato, Y., Mitsumori, T., Machinami, T., Ueda, T., Ando, T., *Chemical Physics Letters*, 351, 2002, 105-108.

30. Bergerson, W.F., Mulder, J.A., Hsung, R.P., Zhu, X.Y., *Journal of American Chemical Society*, 121, 1999, 454-455.

31. Vo-Dinh, T., *Sensors and Acutators B: Chemical*, 51, 1998, 52-59.

32. Zhang, S., Wright, G., Yang, Y., *Biosensors & Bioelectronics*, 15, 2000, 273-282.

33. Berney, H., West, J., Haefele, E., Alderman, J., Lane, W., Collins, J.K., *Sensors and Actuators B: Chemical*, 68, 2000 100-108.

34. Thévenot, D.R., Toth, K., Durst, R.A., Wilson, G.S., *Biosensors & Bioelectronics*, 16, 2001, 121-131.

35. Pividori, M.I., Merkoçi, A., Alegret, S., *Biosensors & Bioelectronics*, 15, 2000, 291-303.

36. Marrazza, G., Chianella, I., Mascini, M., *Biosensors & Bioelectronics*, 14, 1999, 43-51.

37. Paleček, E., Fojta, M., Tomschik, M., Wang, J., *Biosensors & Bioelectronics*, 13, 1998, 621-628.

38. Moser, I., Schalkhammer, T., Pittner, F., Urban, G., *Biosensors & Bioelectronics*, 12, 1997, 729-737.

39. Wang, J., Cai, X., Rivas, G., Shiaishi, H., Dontha, N., *Biosensors & Bioelectronics*, 12, 1997, 587-599.

40. Wang, J., Palecek, E., Nielson, P.E., Rivas, G., Cai, X., Shiraishi, H., Dontha, N., Luo, D., Farias, P.A.M., *Journal of American Chemical Society*, 118, 1996, 7667-7670.

41. Campbell, N.A., Biology, 3rd Ed., The Benjamin/Cummings Publishing Company, California, 1993. p.87, 303-306.

42. Chang, R., Chemistry, 5th Ed., McGraw Hill, New Jersey, 1994. p.986-989, 817-819.

43. Cloarec, J.P., Martin, J.R., Polychronakos, C., Lawrence, I., Lawrence, M.F., Souteyrand, E., *Sensors and Actuators B: Chemical*, 58, 1999, 394-398.

44. Souteyrand, E., Cloarec, J.P., Martin, J.R., Wilson, C., Lawrence, I., Mikkelsen, S., Lawrence, M.F., *Journal of Physical Chemistry* B, 101, 1997, 2980-2985.

45. Wilson, C.J., Detection of Specific DNA Sequences by Electrochemical Impedance Measurements Using Si/SiO_2 Substrates. Thesis. August 1994.

46. Deligiannis, N., DNA Detection System of Homo-Oligomers by Electochemical Impedance and Quantification Through Radiolabeling. Thesis. March 2000.

47. Macanovic, A, Marquette, C., Polychronakos, C., Lawrence, M.F., *Unpublished data.* 2002.

48. Lawrence, M.F., Chemistry 638/498X: Physical Chemistry of Solid-State Electronic Materials, Class Notes, Winter 2002.

49. Skoog,, D.A., Holler, F.J., Nieman, T.A., Principles of Instrument Analysis, 5th Ed., Saunders College Publishing, USA, 1998, p. 30-35, 538-539, 412-413.

50. Deng, Z., Cinquino, M., Lawrence, M.F., *Journal of Materials Research*, 6, 1991, 1293-1299.

51. Fisher, A.C., Oxford Chemistry Primers, Vol. 6: Electrode Dynamics, Oxford University Press, 1996, p. 31-32.

52. de Villeneuve, C.H., Pinso, J., Bernard, M.C., Allongue, P., *Journal of Physical Chemistry: B*, 101, 1997, 2415-2420.

53. Allongue, P., Delamar, M., Desbat, B., Fagebaume, O., Hitmi, R., Pinson, J., Savéant, J.M., *Journal of American Chemical Society*, 119, 1997, 201-207.

54. Allongue, P., Kieling, V., Gerischer, H., *Electrochimica Acta*, 40, 1995, 1353-1360.

55. Allongue, P., de Villeneuve, C.H., Morin, S., Boukherroub, R., Wayner, D.D.M., *Electrochimica Acta*, 45, 2000, 4591-4598.

56. Harris, D.C., Quantitative Chemical Analysis, 4th Ed., W.H. Freeman and Company, New York, 1995. Appendix H AP39.

57. Ghosh, P.K., Introduction to Photoelectron Spectroscopy, Vol.67, John Wiley & Sons Inc., USA, 1983, p. 2-23.

58. Carlson, T.A., Photoelectron and Auger Spectroscopy, Plenum Press, New York, 1975, p.65-73.

59. www.lasurface.com

60. Colthup, N.B., Daly, L.H., Wiberley, S.E., Introduction to Infrared and Raman Spectroscopy, 2nd Ed., Academic Press, New York, 1975, p.240-243, 338-343.

61. Pavia, D.L., Lampman, G.M., Kriz, G.S. Introduction to Spectroscopy, 2nd Ed., Saunders College Publishing, USA, 1996.

62. Ingle, J.D., Crouch, S.R., Spectrochemical Analysis, Prentice-Hall Inc., New Jersey, 1988.

63. Sze, S.M., Physics of Semiconductor Devices. John Wiley & Sons, USA., 1981. p.10, 386.

64. Kricka, L.J. Ed., Nonisotopic DNA Probe Techniques. Academic Press, Inc. California, 1992. p.69.

65. Marquette, C.A., Lawrence, I., Polychronakos, C., Lawrence, M.F., *Talanta*, 56, 2002, 763-768.